N°d'ordre NNT : 2019LYSEI116

THESE de DOCTORAT DE L'UNIVERSITE DE LYON
opérée au sein de
INSA Lyon
En cotutelle internationale avec
Università la Sapienza di Roma

Ecole Doctorale N° ED165
Ecole Doctorale Mécanique, Energétique, Génie Civil et acoustique

Spécialité / discipline de doctorat :
Biomécanique

Soutenue publiquement le 06/12/2019, par :
Lina Zouggari

BIOMECHANICAL BEHAVIOR OF CAROTID ATHEROSCLEROSIS: A NUMERICAL APPROACH

Devant le jury composé de :

DEPLANO Valérie	Directrice de Recherche CNRS	Ecole centrale de Marseille	Rapporteure
TICHY John	Professeur des universités	Rensselaer Polytechnic Institute	Rapporteur
BOU-SAID Benyebka	Professeur des universités	INSA Lyon	Directeur de thèse
CULLA Antonio	Ricercatore	Università la Sapienza di Roma	Directeur de thèse
LERMUSIAUX Patrick	Professeur	Centre Hospitalier Universitaire de Lyon	Invité
MASSI Francesco	Professore associato	Università la Sapienza di Roma	Invité

Département FEDORA – INSA Lyon - Ecoles Doctorales – Quinquennal 2016-2020

SIGLE	ECOLE DOCTORALE	NOM ET COORDONNEES DU RESPONSABLE
CHIMIE	**CHIMIE DE LYON** http://www.edchimie-lyon.fr Sec. : Renée EL MELHEM Bât. Blaise PASCAL, 3e étage secretariat@edchimie-lyon.fr INSA : R. GOURDON	**M. Stéphane DANIELE** Institut de recherches sur la catalyse et l'environnement de Lyon IRCELYON-UMR 5256 Équipe CDFA 2 Avenue Albert EINSTEIN 69 626 Villeurbanne CEDEX directeur@edchimie-lyon.fr
E.E.A.	**ÉLECTRONIQUE, ÉLECTROTECHNIQUE, AUTOMATIQUE** http://edeea.ec-lyon.fr Sec. : M.C. HAVGOUDOUKIAN ecole-doctorale.eea@ec-lyon.fr	**M. Gérard SCORLETTI** École Centrale de Lyon 36 Avenue Guy DE COLLONGUE 69 134 Écully Tél : 04.72.18.60.97 Fax 04.78.43.37.17 gerard.scorletti@ec-lyon.fr
E2M2	**ÉVOLUTION, ÉCOSYSTÈME, MICROBIOLOGIE, MODÉLISATION** http://e2m2.universite-lyon.fr Sec. : Sylvie ROBERJOT Bât. Atrium, UCB Lyon 1 Tél : 04.72.44.83.62 INSA : H. CHARLES secretariat.e2m2@univ-lyon1.fr	**M. Philippe NORMAND** UMR 5557 Lab. d'Ecologie Microbienne Université Claude Bernard Lyon 1 Bâtiment Mendel 43, boulevard du 11 Novembre 1918 69 622 Villeurbanne CEDEX philippe.normand@univ-lyon1.fr
EDISS	**INTERDISCIPLINAIRE SCIENCES-SANTÉ** http://www.ediss-lyon.fr Sec. : Sylvie ROBERJOT Bât. Atrium, UCB Lyon 1 Tél : 04.72.44.83.62 INSA : M. LAGARDE secretariat.ediss@univ-lyon1.fr	**Mme Sylvie RICARD-BLUM** Institut de Chimie et Biochimie Moléculaires et Supramoléculaires (ICBMS) - UMR 5246 CNRS - Université Lyon 1 Bâtiment Curien - 3ème étage Nord 43 Boulevard du 11 novembre 1918 69622 Villeurbanne Cedex Tel : +33(0)4 72 44 82 32 sylvie.ricard-blum@univ-lyon1.fr
INFOMATHS	**INFORMATIQUE ET MATHÉMATIQUES** http://edinfomaths.universite-lyon.fr Sec. : Renée EL MELHEM Bât. Blaise PASCAL, 3e étage Tél : 04.72.43.80.46 infomaths@univ-lyon1.fr	**M. Hamamache KHEDDOUCI** Bât. Nautibus 43, Boulevard du 11 novembre 1918 69 622 Villeurbanne Cedex France Tel : 04.72.44.83.69 hamamache.kheddouci@univ-lyon1.fr
Matériaux	**MATÉRIAUX DE LYON** http://ed34.universite-lyon.fr Sec. : Stéphanie CAUVIN Tél : 04.72.43.71.70 Bât. Direction ed.materiaux@insa-lyon.fr	**M. Jean-Yves BUFFIÈRE** INSA de Lyon MATEIS - Bât. Saint-Exupéry 7 Avenue Jean CAPELLE 69 621 Villeurbanne CEDEX Tél : 04.72.43.71.70 Fax : 04.72.43.85.28 jean-yves.buffiere@insa-lyon.fr
MEGA	**MÉCANIQUE, ÉNERGÉTIQUE, GÉNIE CIVIL, ACOUSTIQUE** http://edmega.universite-lyon.fr Sec. : Stéphanie CAUVIN Tél : 04.72.43.71.70 Bât. Direction mega@insa-lyon.fr	**M. Jocelyn BONJOUR** INSA de Lyon Laboratoire CETHIL Bâtiment Sadi-Carnot 9, rue de la Physique 69 621 Villeurbanne CEDEX jocelyn.bonjour@insa-lyon.fr
ScSo	**ScSo*** http://ed483.univ-lyon2.fr Sec. : Véronique GUICHARD INSA : J.Y. TOUSSAINT Tél : 04.78.69.72.76 veronique.cervantes@univ-lyon2.fr	**M. Christian MONTES** Université Lyon 2 86 Rue Pasteur 69 365 Lyon CEDEX 07 christian.montes@univ-lyon2.fr

*ScSo : Histoire, Géographie, Aménagement, Urbanisme, Archéologie, Science politique, Sociologie, Anthropologie

Résumé

Introduction et positionnement scientifique de la thèse

L'athérosclérose est une maladie qui atteint le système vasculaire. Elle se manifeste par la formation d'une plaque d'athérome au niveau de la couche intima de tissu artérielle causant la rigidification et la paroi. La majorité des décès cardiovasculaire en Europe sont une conséquence de cette pathologie. En effet, une plaque d'athérome non stable, qu'on appelle aussi vulnérable, peut évoluer vers un stade avancé appelé sténose ou la lumière artérielle est réduite à un tel niveau que le sang ne peut plus irriguer les organes en aval. Dans le cas où la formation de la plaque a lieu au niveau des artères coronaires, il s'agit d'un risque d'arrêt cardiaque. Une autre conséquence de la présence d'une plaque dans le système vasculaire est sa possibilité de rupture et donc le relâchement de débris qui, transporté par le flux sanguin, sont capables d'obstruer les plus petits vaisseaux au niveau du cerveau causant des accidents cérébraux et par conséquent paralysie ou mort cérébrale.

Le processus de formation de la plaque est très long et renforcé par la présence de substances telles que la nicotine ou Cholestérol LDL dans le sang. Quand ces substances s'introduisent dans le tissu artériel, elles peuvent causer une réaction inflammatoire en chaine provoquant la génération et l'évolution de l'athérome. En général, l'athérosclérose est une maladie asymptomatique, ceci rend son diagnostic difficile au premiers stades. En effet, le diagnostic s'effectue suite à un malaise ou urgence médicale à l'aide d'outils d'imagerie médicale tels que IRM ou Echo-doppler.

Pour toutes les raisons invoquées précédemment, cette pathologie ne cesse de susciter la curiosité de la communauté scientifique dans le but de la comprendre tout d'abord les phénomènes qui conduisent à l'occurrence et au développement de cette maladie ainsi que d'améliorer diagnostic et le traitement.

Dans ce sens, notre projet consiste à étudier les phénomènes mécaniques qui accompagnent la présence de la plaque au niveau de la bifurcation carotidienne, un site fréquent de formation d'athéromes. Afin d'effectuer cela, nous évaluons le comportement du fluide et de la structure artérielle par les méthodes volumes finis et éléments finis. Dans un premier temps, nous étudions la dynamique du sang pour des modèles simplifiés et réels

avec et sans plaque. Ensuite, nous nous intéressons à l'effet de la déformation de la paroi sur l'hémodynamique. Finalement, nous étudions la réponse vibratoire de la structure artérielle afin de vérifier l'effet la présence de la plaque sur la déformation de la carotide.

Méthodologie

Modèles géométriques

Deux types de modèles géométriques ont été étudiés représentés dans Fig. 1 : Une géométrie simplifié réalisé sur CREO avec et sans plaque ainsi qu'une géométrie spécifique au patient obtenue par reconstruction d'images à partir de scans IRM à l'aide du logicielle SCANIP (Simplware Inc.). Dans les deux cas, la paroi artérielle est modélisée par l'ajout d'une couche uniforme d'une épaisseur de 1mm.

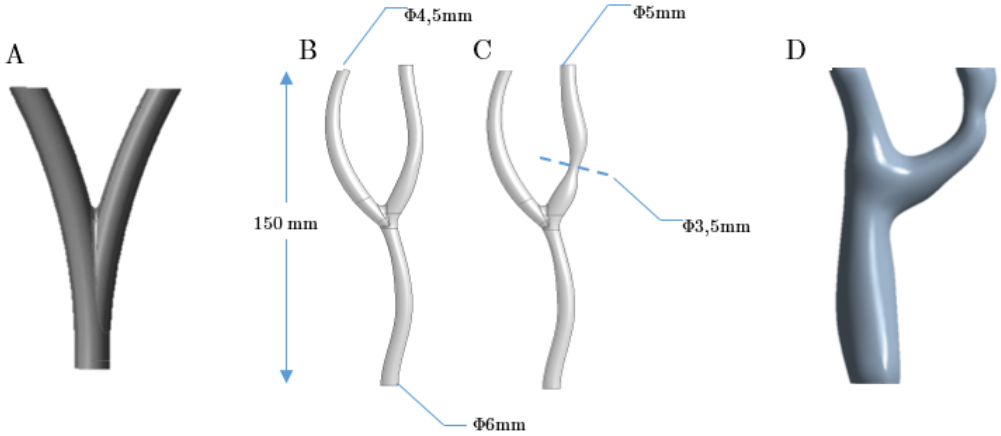

Fig. 1 : Différents modèles géométriques pour la bifurcation carotidienne

Modélisation du sang

Le sang est considéré comme un fluide non compressible dont la densité est égale à $1060 kg/m^3$. La loi Carreau a été choisi pour décrire la viscosité du fluide selon la formule ci-dessous

$$\mu = \mu_\infty + (\mu_0 - \mu_\infty)(1 + \lambda(\dot{\gamma})^2)^{\frac{n-1}{2}}$$

Où

μ : *Viscosité dynamique*

μ_∞ : *Viscosité à haut taux de cisailement*

μ_0 : *Viscosité à faible taux de cisailement*

n : *Index puissance*

Conditions aux limites

Après une mesure de flux par IRM à contraste de phases (Fig. 2), une condition en vitesse distribuée paraboliquement a été imposée à l'entrée.

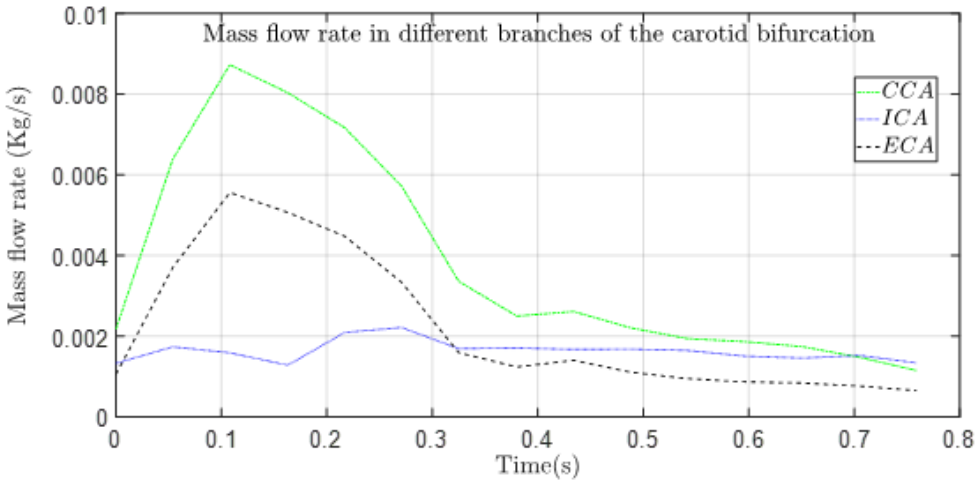

Fig. 2 : Débit massique au niveau des 3 branches de la bifurcation carotidienne

Quant aux conditions aux sorties, 3 configurations ont été étudiées. Dans un premier temps, une pression constante de 13 kPa a été appliquée en sortie. La deuxième configuration consiste à appliquer une pression qui varie linéairement entre les valeurs de pression diastolique et systolique. Ensuite, les deux configurations précédentes ont été comparées au modèle couplé 3D-0D pour les simulations à parois rigides.

Modélisation de l'artère

La paroi artérielle d'une densité 1160kg/m3 est considérée incompressible et anisotrope. Par ailleurs, afin de décrire le comportement du tissu artériel, la loi de comportement décrite par le modèle Mooney-Rivlin à 5 paramètres ci-dessous a été utilisée

$$W = \sum_{i+j\leq 2} C_{ij}(In_i - 3)^i.(In_j - 3)^j$$

où W est la fonction de densité d'énergie de déformation, (In_i, In_j) les invariants du tenseur gauche de Cauchy-Green et C_{ij} des constantes propres au matériau dont les valeurs correspondantes sont résumées dans le tableau ci-dessous.

Paramètre	C_{10}	C_{01}	C_{20}	C_{02}	C_{11}
Valeur (kPa)	50.445	30.491	40	120	10

L'artère a été fixée au niveau de l'entrée et sorties et un support élastique de 0.001N/mm3 a été appliquée à la paroi externe de l'artère afin de tenir en compte le tissu adjacent.

Simulation de l'hémodynamique à parois rigides

Tout d'abord en évaluant l'effet de plusieurs paramètres de modélisation du fluide à travers des simulations basées sur la méthode des volumes finis sur FLUENT, le profil de pression en sortie influence les résultats obtenus en termes de distribution de la contrainte pariétale et flux qui passent à travers des deux branches de la carotide comparée à l'influence la loi comportementale du fluide ou à la distribution de la vitesse du sang au niveau de la section d'entrée. En effet, dans les grandes artères, le sang acquiert un comportement Newtonien et la longueur de l'artère carotide commune permet au flux de se stabiliser enlevant l'effet de la distribution imposée à l'entrée.

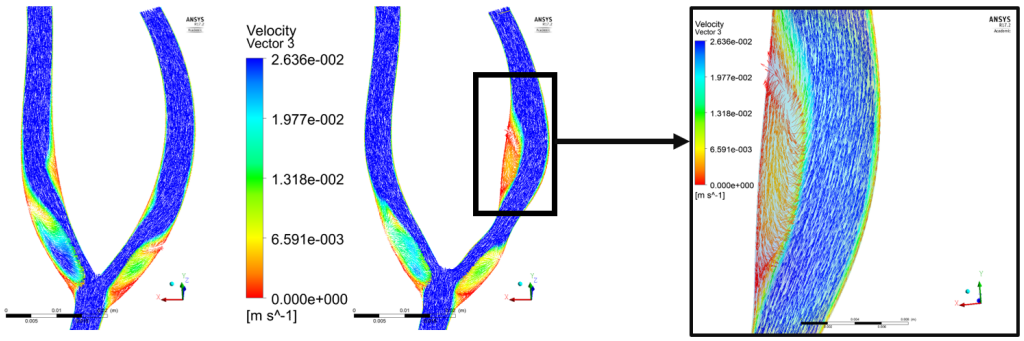

Fig. 3 : Streamlines de vitesse dans un section plane de la carotide avec et sans plaque

En analysant les résultats obtenus, la plaque cause une augmentation de la contrainte pariétale au niveau de l'athérome et une baisse de ce paramètre dans la région en aval. L'observation de l'évolution dans le temps de la contrainte pariétale montre la présence d'une composante oscillatoire importante dans la région après-plaque due aux zones de recirculation. Cette contrainte pariétale faible et oscillante se traduit par un temps de

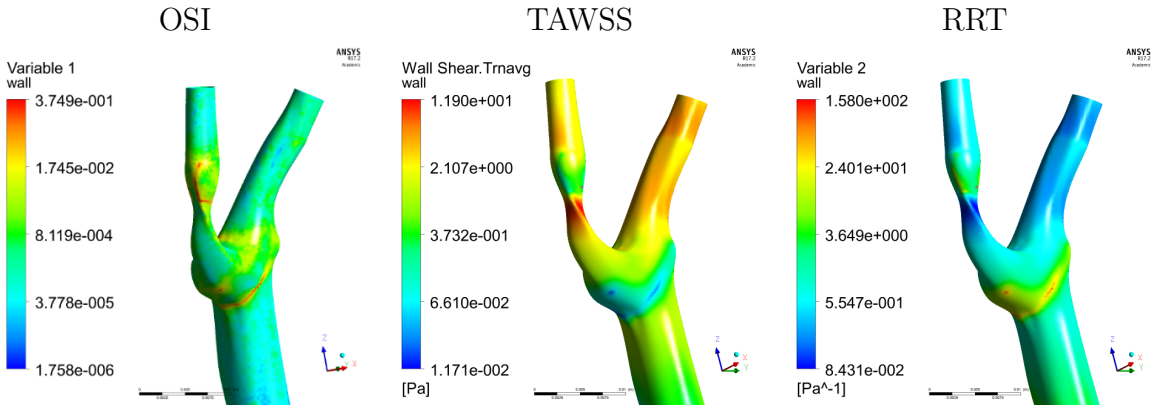

Fig. 4: Distribution des grandeurs moyennées à proximité de la paroi pour le cas de carotide avec plaque

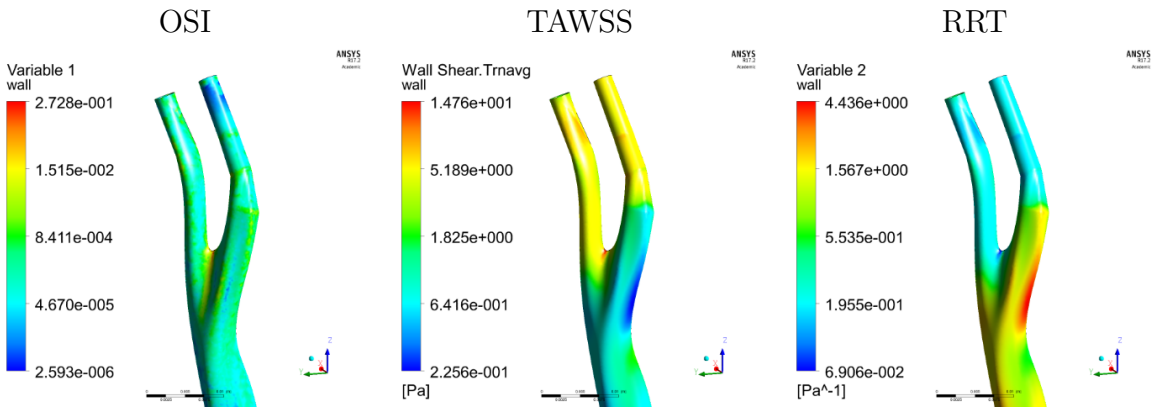

Fig. 5: Distribution des grandeurs moyennées à proximité de la paroi pour le cas de carotide sans plaque

résidence élevé qui peut être en cause de dépôt de particules et par conséquent la croissance de la plaque (voir Fig. 4 et Fig. 5).

Les valeurs de la contrainte pariétale obtenues par cette méthode sont très élevées par rapport à celle mesurée par IRM-4D. Ceci peut être expliquée par l'effet de changement de volume qui n'est pas pris en compte dans les calculs sous l'hypothèse de paroi rigide. Pour remédier à cela, nous effectuons les mêmes simulations en considérant une paroi déformable.

Interaction fluide-structure de la bifurcation carotidienne

Afin d'évaluer l'effet de la déformation artérielle sur la dynamique du sang, le couplage fort entre le domaine fluide et structural a été établi dans ANSYS pour les géométries simplifiées ainsi qu'une étude de faisabilité dans le cas de géométrie spécifique au patient. Les phénomènes observés pour les modèles simplifiés à parois rigides liés à la présence de la plaque subsistent, i.e. séparation du flux, perturbation du flux au niveaux de la

région après plaque sous forme de zones de recirculation et l'altération des valeurs de la contrainte pariétale par rapport au modèle sans plaque. Néanmoins, la déformation de la paroi conduit à la baisse de la vitesse du flux et par conséquent des valeurs des contraintes pariétales qui se rapprochent plus de celle obtenues par IRM de flux. Par ailleurs, d'un point de vue structurale, l'analyse vibratoire de la structure précontrainte montre l'apparition de formes modales à basses fréquences liés à la concentration de masse engendrée par la présence de la plaque (Voir Fig. 6).

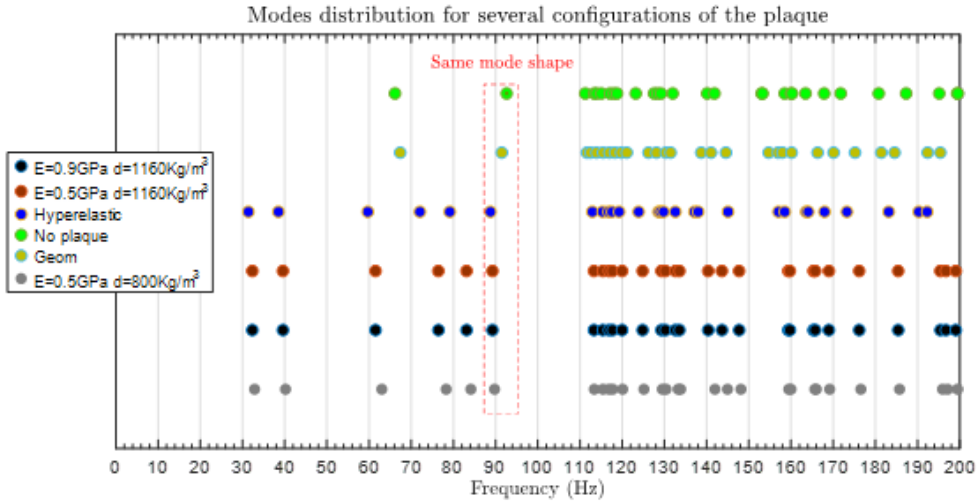

Fig. 6 : Distribution des fréquences modales pour différents cas de carotide

Pour conclure, d'un côté, les modèles MFN sont bien capables de capturer les phénomènes liés au fluide mais les valeurs de contraintes pariétales obtenus par cette méthode sont très élevées. D'autre part, les modèles couplés donnent une appréciation plus correcte du comportement du sang or ils sont moins stables et plus couteux en termes de temps et moyens de calculs. L'analyse vibratoire montre la possibilité de détection de la présence de la plaque par analyse du déplacement de la carotide cette hypothèse reste à confirmer par des compagnes expérimentales.

Sommario

Introduzione e inquadramento scientifico della tesi

L'aterosclerosi è una malattia che colpisce il sistema vascolare. Si manifesta con la formazione di una placca di ateroma nella tonaca intima del tessuto arterioso che causa l'irrigidimento della parete. La maggior parte delle morti cardiovascolari in Europa è una conseguenza di questa patologia, infatti, una placca ateromatosa instabile, detta anche vulnerabile, può progredire fino a uno stadio avanzato, chiamato stenosi, dove il lumen arterioso si riduce a un livello tale che il sangue non è più in grado di irrigare gli organi a valle. Nel caso in cui la formazione della placca si verifichi nelle arterie coronarie, vi è il rischio di arresto cardiaco.

Un'altra conseguenza della presenza di una placca nel sistema vascolare è la sua possibilità di rottura con conseguente rilascio di detriti che, trasportati dal flusso sanguigno, possono ostruire i vasi più piccoli del cervello causando danni cerebrali con conseguente paralisi o morte cerebrale. Il processo di formazione della placca è molto lungo ed è favorito dalla presenza di sostanze come la nicotina o il colesterolo LDL nel sangue. Quando queste sostanze vengono introdotte nel tessuto arterioso, possono causare una reazione infiammatoria a catena che causa la generazione e l'evoluzione dell'ateroma. In generale, l'aterosclerosi è una malattia asintomatica, questo ne rende difficile la diagnosi nelle prime fasi, infatti generalmente la diagnosi viene fatta utilizzando strumenti di imaging medicale come la risonanza magnetica o eco-doppler in seguito a un malessere o emergenza medica.

Per tutte le ragioni sopra menzionate, questa patologia continua a suscitare la curiosità della comunità scientifica al fine di comprendere i fenomeni che portano alla comparsa e allo sviluppo di questa malattia, nonché a migliorarne la diagnosi e il trattamento.

In questo senso, il nostro progetto consiste nello studio dei fenomeni meccanici che accompagnano la presenza della placca a livello della biforcazione carotidea che è dimostrato essere un frequente sito di formazione di ateroma. Per fare ciò, è stato valutato il comportamento del fluido e della struttura arteriosa mediante metodi ai volumi finiti e agli elementi finiti. In primo luogo, è stato studiata la dinamica del sangue per modelli semplificati e reali con e senza placca. Quindi è stato analizzato l'effetto della deformazione della parete sull'emodinamica. Infine, utilizzando la risposta vibratoria della struttura arteriosa

è stato verificato l'effetto della presenza della placca sulla deformazione carotidea.

Metodologia Modelli geometrici

Sono stati studiati due differenti modelli geometrici: una geometria semplificata realizzata utilizzando CREO con e senza placca e una geometria specifica del paziente ottenuta mediante ricostruzione di immagini da scansioni MRI utilizzando il software SCANIP (Simplware Inc.). In entrambi i casi, la parete arteriosa è stata modellata aggiungendo uno strato solido uniforme dello spessore di 1 mm.

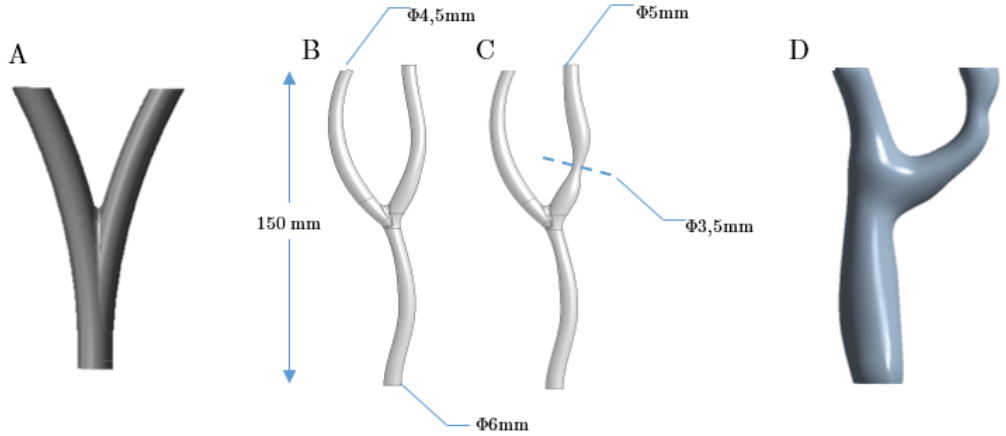

Fig. 1 : Diversi modelli geometrici per la biforcazione carotidea

Modellazione del sangue

Il sangue è stato considerato come un fluido non comprimibile con una densità di 1060 kg / m3. Per descrivere la viscosità del fluido è stata utilizzata la legge di Carreau di cui segue la formulazione

$$\mu = \mu_\infty + (\mu_0 - \mu_\infty)Ö(1 + \lambda(\dot{\gamma})^2)^{\frac{n-1}{2}}$$

Où

- μ : *Viscosità dinamica*
- μ_∞ : *Viscosità con elevata velocità di taglio*
- μ_0 : *Viscosità a bassa velocità di taglio*
- n : *Indice di potenza*

Condizioni al contorno

Considerando la misurazione del flusso effettuata mediante l'analisi MRI a contrasto, è

stata imposta una condizione di velocità all'ingresso.

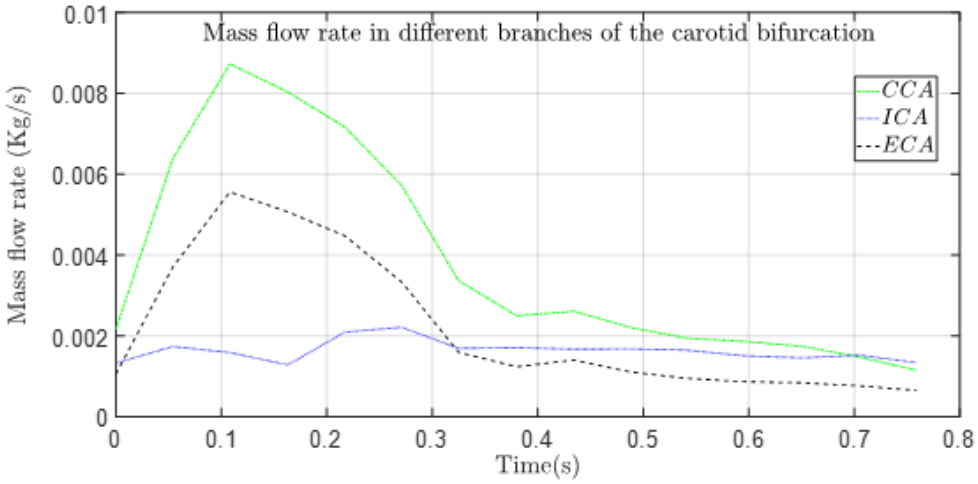

Fig. 2 : Flusso di massa sui 3 rami della biforcazione carotidea

Per quanto riguarda le condizioni alle uscite, sono state studiate 3 differenti configurazioni. Inizialmente, all'uscita è stata applicata una pressione costante di 13 kPa, successivamente è stata presa in considerazione una configurazione nella quale è stata applicata una pressione il cui valore varia linearmente tra i valori di pressione diastolica e sistolica. Quindi, le due configurazioni precedenti sono state confrontate con il modello accoppiato 3D-0D per le simulazioni con parete rigide.

Modellizzazione dell'arteria

La parete arteriosa è stata modellata come incomprimibile e anisotropa con una densità di $1160 kg/m^3$. Inoltre, per descrivere il comportamento del tessuto arterioso, è stata utilizzata la legge costitutiva iperelastica descritta dal modello Mooney-Rivlin con 5 parametri che ha la formulazione seguente.

$$W = \sum_{i+j \leq 2} C_{ij} (In_i - 3)^i . (In_j - 3)^j$$

Dove W è la funzione di densità di energia di deformazione, (In_i, In_j) gli invarianti del tensore sinistro di Cauchy-Green e C_{ij} sono costanti specifiche del materiale i cui valori sono riepilogati nella tabella seguente.

Parametri	C_{10}	C_{01}	C_{20}	C_{02}	C_{11}
Valori (kPa)	50.445	30.491	40	120	10

Simulazione di emodinamica della parete rigida

Valutando l'effetto di diversi parametri di modellazione del fluido mediante simulazioni basate sul metodo del volume finito, effettuate utilizzando il software FLUENT, si è notato come il profilo di pressione in uscita abbia un influenza maggiore sui risultati ottenuti in termini di distribuzione dello stress parietale e del flusso in entrambi i rami della carotide rispetto all'influenza della legge comportamentale del fluido e alla distribuzione della velocità del sangue alla sezione di ingresso. Infatti, nelle grandi arterie, il sangue acquisisce un comportamento newtoniano e la lunghezza dell'arteria carotide comune consente al flusso di stabilizzarsi, rimuovendo l'effetto della distribuzione imposta all'ingresso.

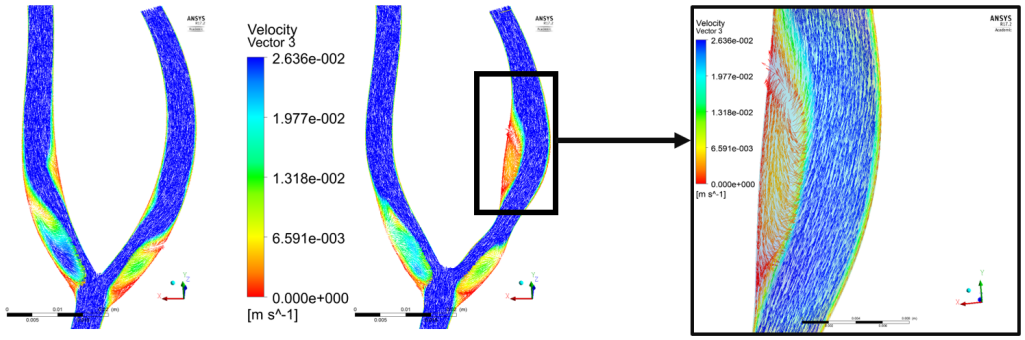

Fig. 3 : Linee de velocità in una sezione piana della carotide con e senza placca

Analizzando i risultati ottenuti, si nota come la placca provoca un aumento dello stress parietale a livello di ateroma e una diminuzione di questo nella regione a valle dell'ateroma stesso. L'osservazione dell'evoluzione nel tempo dello stress parietale mostra la presenza di una significativa componente oscillatoria nella regione postplacca dovuta alla presenza di zone di ricircolazione. Questa sollecitazione parietale di piccola ampiezza e oscillante si traduce in un elevato tempo di permanenza che può essere responsabile della deposizione di particelle e quindi della crescita della placca.

I valori dello stress parietale ottenuti con questo metodo sono molto elevati rispetto a quelli misurati con MRI-4D. Questo può essere spiegato dall'effetto di variazione del volume che non è stato preso in considerazione nei calcoli effettuati sotto l'ipotesi di parete rigida. Per

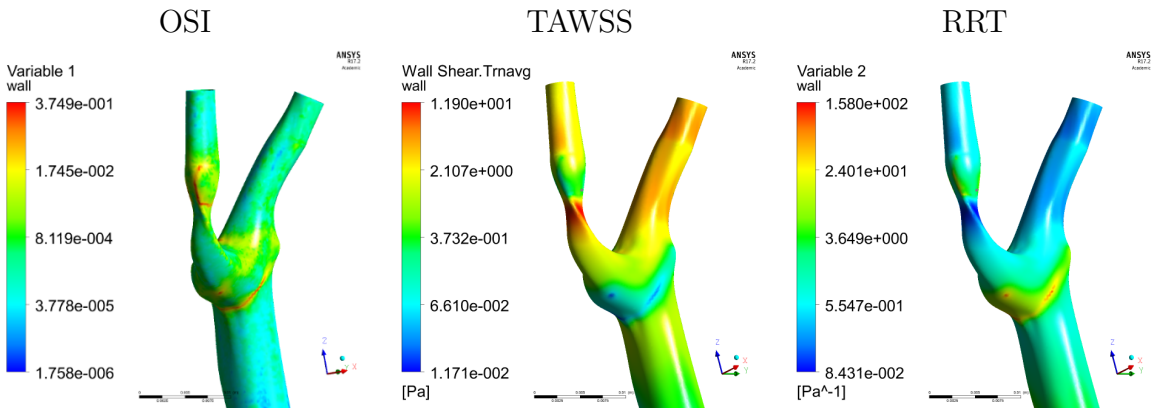

Fig. 4: Distribuzione di grandezze medie vicino al muro per il caso di carotide con placca

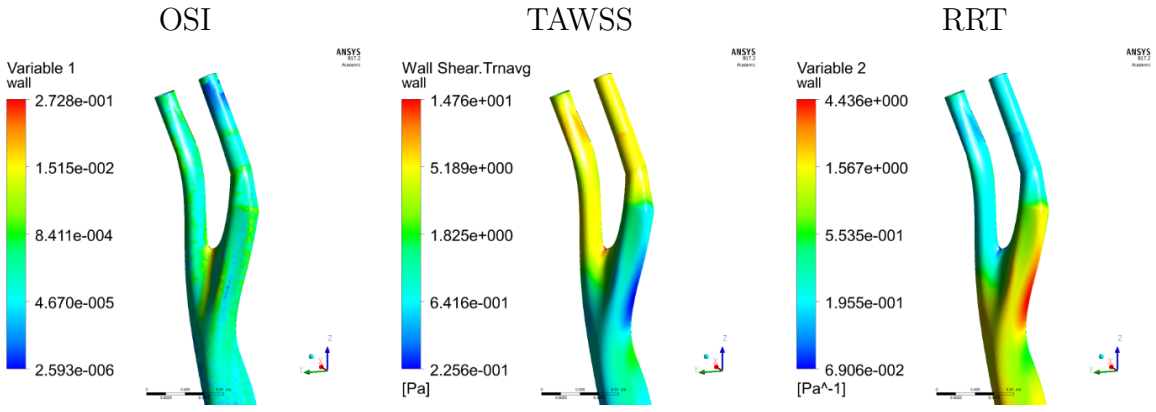

Fig. 4: Distribuzione di grandezze medie vicino al muro per il caso di carotide senza placca

rimediare, sono state eseguite le stesse simulazioni considerando la parete deformabile.

Interazione fluido-struttura della biforcazione carotidea

Al fine di valutare l'effetto della deformazione dell'arteria sulla dinamica del sangue, è stato realizzato un modello, utilizzando il software ANSYS, nel quale il dominio del fluido e la struttura sono stati considerati in "accoppiamento forte" per le geometrie semplificate ed uno studio di fattibilità nel caso di geometria specifica del paziente. Anche in questo caso è possibile notare i fenomeni osservati per i modelli semplificati a parete rigida dovuti alla presenza della placca, ossia la separazione del flusso, il disturbo del flusso a livello della regione dopo la placca sotto forma di zone di ricircolazione e l'alterazione dei valori dello stress parietale rispetto al modello senza placca. Tuttavia, la deformazione della parete porta alla diminuzione della velocità del flusso e di conseguenza dei valori delle tensioni parietali che sono più vicine a quelle ottenute dal flusso MRI.

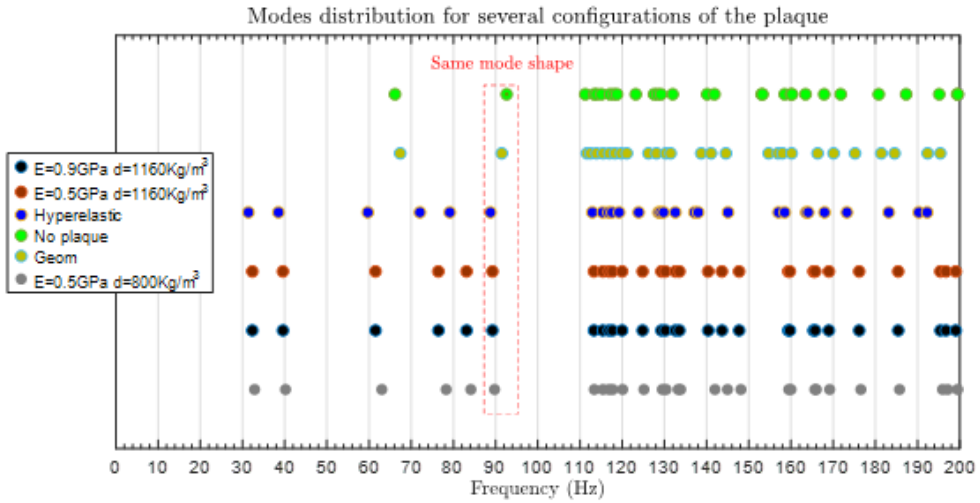

Fig. 6 : Distribuzione delle frequenze modali per diversi casi di carotide

Inoltre, da un punto di vista strutturale, l'analisi vibratoria della struttura precompressa mostra l'aspetto di forme modali a basse frequenze legate alla concentrazione di massa dovuta dalla presenza della placca.

In conclusione, da un lato, i modelli MFN sono in grado di catturare fenomeni legati ai fluidi, ma i valori di stress parietali ottenuti con questo metodo sono molto alti. D'altra parte, i modelli accoppiati, che descrivono in maniera più fedele il comportamento del sangue, sono meno stabili e più costosi in termini di costo computazionale. L'analisi vibratoria mostra la possibilità di rilevare la presenza della placca mediante analisi di

spostamento carotideo, che deve essere confermata da compagnie di misura sperimentali.

Acknowledgements

This project was funded by the university of Rome la Sapienza.

I would like to thank my supervisor Benyebka Bou-Said for giving me the opportunity to pursue my PhD, and his compassion he has shown during the past three years Furthermore, I would also like to express my deep gratitude to my supportive supervisor, Antonio Culla, for his availability and humility. Last but not the least, I would like to thank Francesco Massi, my co-director in Italy, for his precision and engagement.

I would also like to acknowledge the thesis committee, Pr. Valérie Deplano and Pr. John Tichy, the experts who were kindly accepted to referee this research project. Without their intelligent and heartfelt participation and input, the validation survey could not have been well done.

I give all thanks to Pr. Patrick Lermusiaux, Pr. Antoine Millon, Pr. Loic Boussel and Dr. Monica Sigovan for their availability and heartfelt participation to this project.

I wish to appreciate the contribution of various people to this project; those who were truly encouraging and helping me to get the most out of my talents and skills. Specifically speaking, the members of our office both in France and Italy who had been helpful with their valuable scientific support.

Finally, I would like to thank the administration staff in both universities of Lyon (INSA LYON) and Rome (La Sapienza) for running the administrations so well! I'm glad I didn't have to be worried about the details of the paper works during the past three years thanks to the responsibility of the staff for resolving the issues.

List of Abbreviations

CA Carotid Artery

CVA Cardiovascular Accident

ECA External Carotid Artery

HWSS High Wall Shear Stress

ICA Internal Carotid Artery

LDL Low-Density Lipoprotein

LWSS Law Wall Shear Stress

MRI Magnetic Resonance Imaging

OSI Oscillating Shear Index

RRT Relative Residency Time

SEDF Strain Energy Density Function

WSS Wall Shear Stress

Contents

List of Tables

List of Figures

General introduction

Advancement in health science have participated in improving the quality of human life condition. This translated to longer longevity and thus the rise in cardiovascular disease cases that are correlated with advancement in age. On the other hand, the change in human dietary habits and the sedentary lifestyle are worsening the circumstances. This alarming situation led to a global interest in understanding the human cardiovascular system from a multidisciplinary point of view for the purpose of accelerating the diagnosis and enhancing the quality of treatments.

Particularly, atherosclerosis acquires a special attention due its high mortality rate and the deterioration in life quality they cause. In particular, the carotid artery is one of the most common locations of atherosclerosis plaque buildup. Carotid atherosclerosis disease doesn't suddenly occur, it generally takes years for a plaque to form through a complex process including several factors (age, diet, biochemistry and biomechanics, etc.) and is generally diagnosed in advanced stages when the occlusion is severe (over 50%). This led to higher interest in understanding the disease before it becomes a surgical emergency.

The present thesis is focused on the numerical modeling of the mechanical behavior of the carotid artery. In fact, computational methods allow for the investigation of phenomena taking place in this artery which can be an indicator of the health status of the patient. The main objective of the present work is evaluating the effect of the plaque presence on the arterial response through the development of a numerical model able to simulate the behavior of the carotid artery and analyzing the blood flow and the structural response of the artery.

To do this, both CFD and FSI simulations were conducted on idealized and patient-specific geometries. The distribution of velocity and WSS between healthy and diseased cases showed that the plaque presence causes a disturbance in the flow. Low wall shear stress was observed in the after-plaque area which might cause plaque growth.

On the other hand, the analysis of the modal response of the arterial structure with and without plaque demonstrated the appearance of modal frequencies correlated with the mass concentration due to the plaque formation and can become after calibration a relevant indicator for evaluating the severity of the plaque.

Chapter 1

State of the art: biomechanics of carotid atherosclerosis

In this chapter, we describe the anatomical context of carotid atherosclerosis with an as well as available treatments. We also present an overview of the major biomechanical approaches in studying cardiovascular related problematics. Finally, we specify the main objectives of this work.

1.1 Carotid atherosclerosis

1.1.1 Atherosclerosis definition, causes and risk factors

In 1940, Felix Marchand suggested the word 'Atherosclerosis', which comes from the Greek words athero (gruel) and sclerosis (hardness) to name the disease characterized by the thickening and stiffening of the arterial wall called plaque formation [1] . Atherosclerosis usually affects large to medium sized arteries. Researchers continue to look for the causes of atherosclerosis and the reasons that can lead the artery to damage and the plaque to the rupture [2][3]. Nevertheless, some general prevalent factors can be observed in the affected population such as smoking, high cholesterol levels, high blood pressure and hyperglycemia[4]. In 2014, 37.1% deaths in Europe resulted from diseases of the circulatory system often due to atherosclerosis. According to the European Cardiovascular Disease Statistics 2017 [5], cardiovascular diseases (CVDs) costs €210 billion to the EU28 each year. The distribution of this costs is shown in Figure 1.1 below.

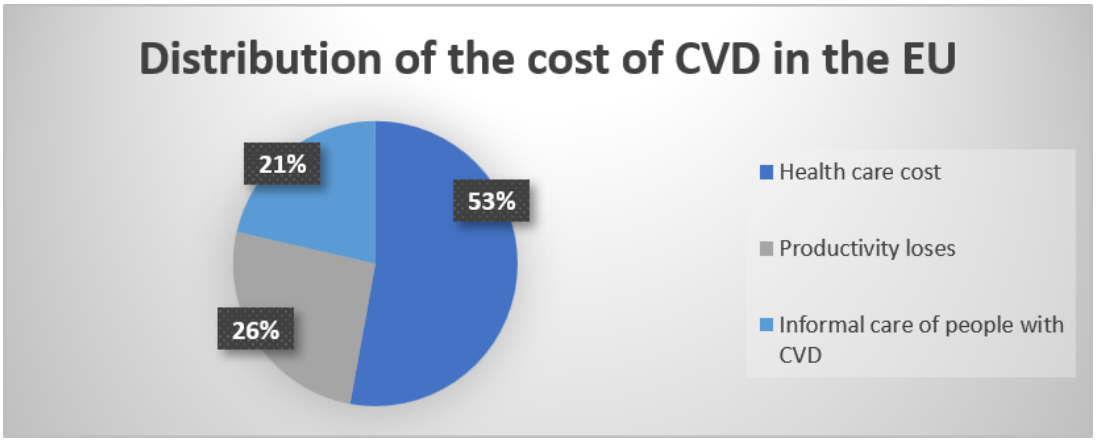

Figure 1.1: *Distribution of the cost of CVD in the EU*

1.1.2 The mechanisms of formation of the plaque

In the presence of this disease, the basic structure of arteries is altered by the accumulation of tissue in the intima [6]. Atherosclerosis is an inflammatory response favored

by circulating oxidized LDL, known as 'bad cholesterol' [7]. The process of formation of atherosclerosis plaques as illustrated in Figure 1.2 is the following:

- **Endothelial cell injury**

  Due to constant exposition to the circulation the endothelial layer can be damaged. The physical force, exerted on the internal wall of arteries and increased in the case of hypertension is believed to play a major role in initiating the process of plaque formation by injuring the endothelial cells.

- **LDL deposition**

  After the endothelial injury he toxin present in the blood, such as LDL, can infiltrate the arterial wall towards the intima. The LDL becomes oxidized and thus inflammatory.

- **Inflammatory reaction**

  The new LDL cells attract monocytes causing a chain of inflammatory reaction within the arterial wall. When the white cells ingest the LDL they are transformed into foam cells and later on into plaques

- **Fibrous cap formation**

  Smooth muscle cells migrate to the surface creating a fibrous cap. When this Cap is thick the plaque is stable otherwise the inflammatory reaction can continue until the full blockage of the artery or rupture of the cap causing a thrombosis or migration of debris through the circulation.

1.1.3 Anatomical consideration of the carotid bifurcation

The carotid artery is a major blood vessel that transport the blood to the brain, neck and face [9][10]. The human has two CAs, left CA originating from the aortic arch and right CA which is a terminal branch of the brachiocephalic trunk. Each CA has two branches

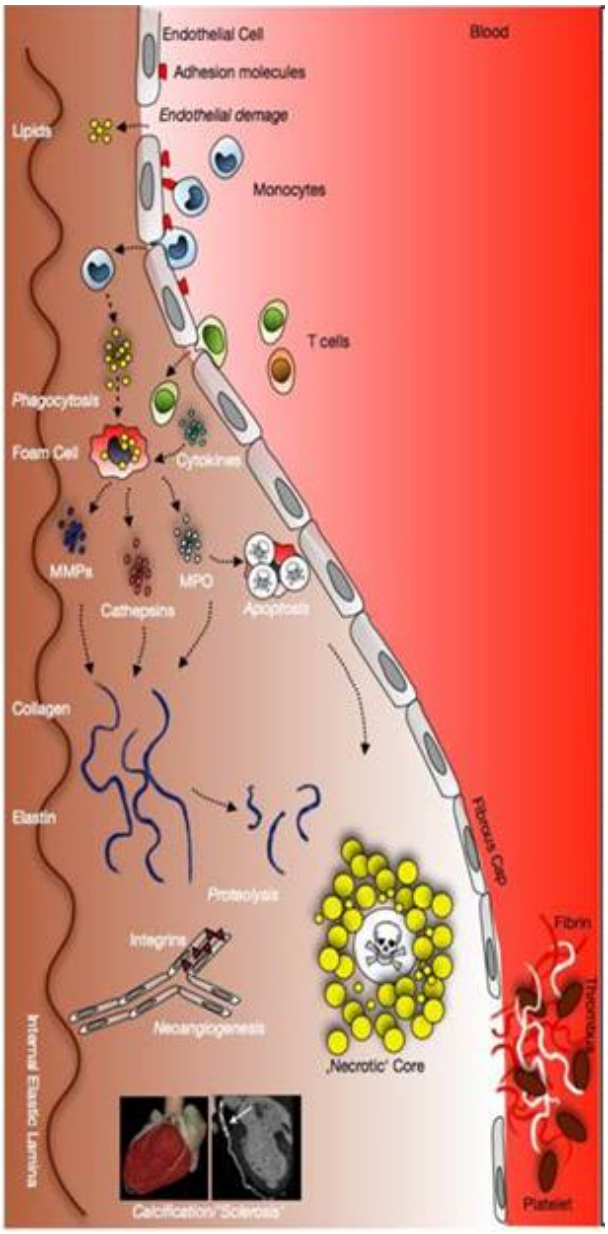

Figure 1.2: *Steps of formation of atherosclerosis plaque [8]*

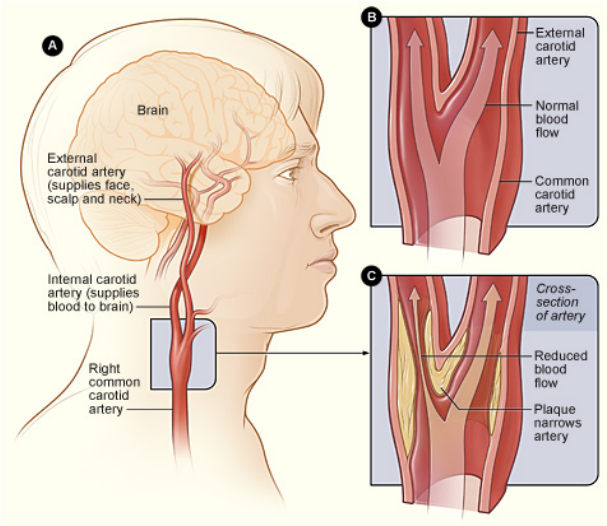

Figure 1.3: *Right Carotid artery A. Anatomical position of the right CA B. Normal CA C. CA with atherosclerosis plaque [11]*

	Female	Male
Systolic blood pressure(mmHg)	132.3±22.5	135.7±23.1
Diastolic blood pressure(mmHg)	69.1±13.0	71.9±14.1
CCA diameter(mm)	6.10±0.80	6.52±0.98
ICA diameter(mm)	4.66±0.78	5.11±0.87

Table 1.1: *General specifications about the carotid artery [12]*

as shown in Figure 1.3, where the ECA transporting the blood to the neck and face and the ICA, supplying the brain, are detailed.

Table 1.1 presents the usual values of blood pressure and diameters of CCA and ICA as reported in a study by Ruan et al. [12]. The downstream organs supplied by the ICA branches are very active and consume a great amount of oxygen per unit time, which explains the difference between the blood flow volume going through the ICA and ECA respectively.

1.1.4 Diagnosis and imaging techniques

Due to its geometry and location near the aorta, carotid artery is a common location for plaques to build-up. Furthermore, being the blood supplier of the brain, carotid atherosclerosis is one of the major causes of ischemic strokes. Yet, this condition is

usually asymptomatic; it is diagnosed at late stages when symptoms become apparent, as in the case of stroke, retinal infarction, weakness or paresthesia of the face, etc.

Exams such as electrocardiogram or Echo-Doppler allow for a preliminary evaluation of the critically of the plaque by measuring its thickness. If the occlusion is over 60%, an angiography or MRI exams are required to analyze the effect of the occlusion on the vascularization of the brain and other organs.

1.1.5 Treatment of carotid atherosclerosis

After evaluating the percentage of stenosis, considering its symptomatic or asymptomatic character, as well as other criteria (e.g. morphology of the plaque, age, cardiac condition, etc.), the choice of treatment can be made.

- **Medical treatment**

In addition to prevention from cardiovascular risk factors such as physical activity, smoking cessation and pressure control, platelet anticoagulant treatment is indicated in the case of low to medium occlusions that do not require a surgical intervention.

- **surgical treatment**

When the occlusion is over 60%, or the plaque is considered vulnerable i.e. able to rupture or to create complications, a surgical intervention called endarterectomy is considered. The procedure consists of a total ablation of the atheroma and the intima and media tissue attached to it. The intervention is long (one hour and a half to 3 hours) and delicate, it is operated under general anesthesia. The procedure is detailed in Figure 1.4.

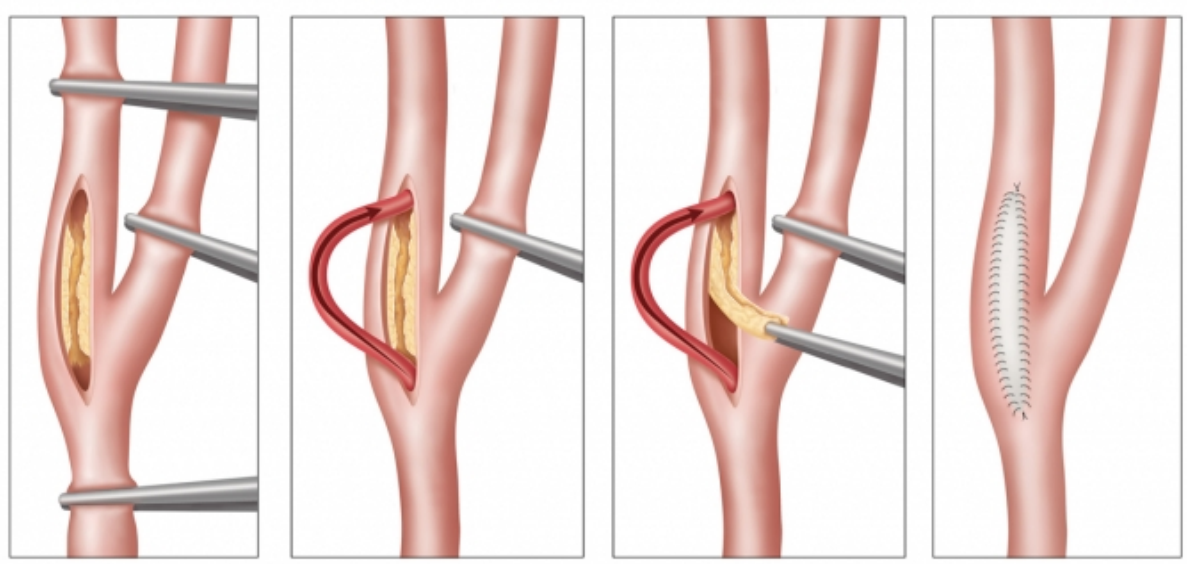

Figure 1.4: *Endarterectomy procedure. 1- Isolation of the carotid artery for the vasculature and making an incision. 2- Creating a provisional shunt. 3- Removal of the plaque. 4- Repairing the artery with stiches or a graft or making a bypass [13]*

This procedure has, in general, good results, but it presents some risks during the intervention: peripheral nervous lesions, AVC's and accidents due to anesthesia. The post operatory complications include cervical hematoma, and AVC's generally caused by cerebral embolism, not to mention the risk of restenosis.

- **Carotid angioplasty with stent**

Angioplasty is indicated mostly when the patient is at risk or when there is a chirurgical contraindication after a multidisciplinary concertation (cardiovascular surgeon, cardiologist, anesthetist, neurologist etc.). However, the risks of complication of the endovascular procedure, although different from the direct surgery, are still statistically equivalent to the endarterectomy ones [14].

The procedure, as presented in Figure 1.5 [15], is carried out in an operating room containing vascular radiology material and under local anesthesia. A catheter, equipped with a protection filter, to limit the risk of embolism during the procedure, is inserted through the femoral artery. A dilatation balloon is utilized to crush the plaque against the arterial wall and then a metallic stent is deployed.

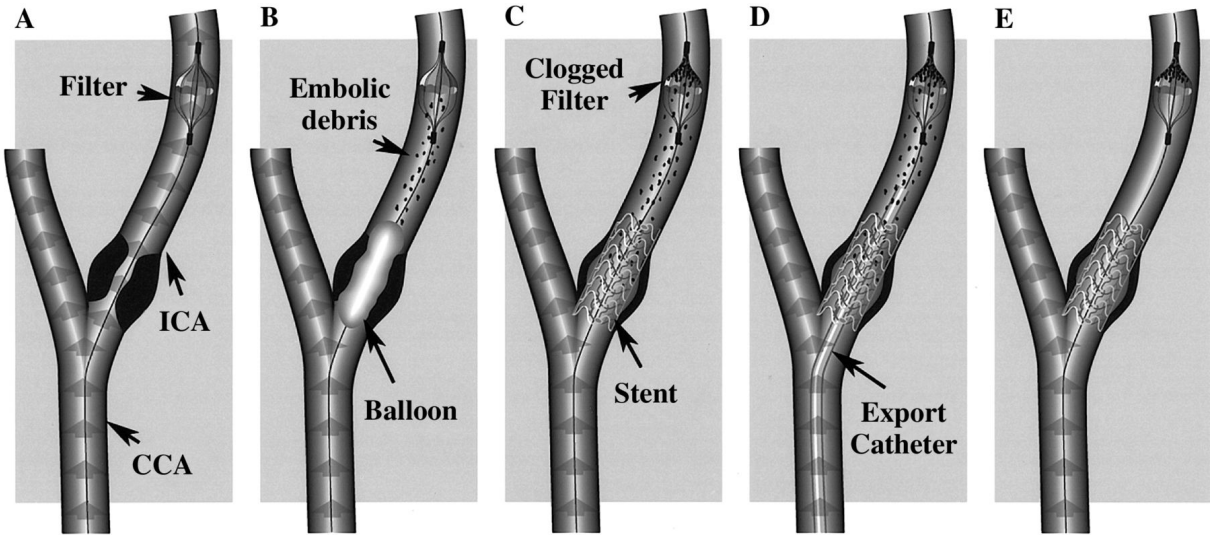

Figure 1.5: *Carotid angioplasty procedure [15]*

1.1.6 Mechanisms of plaque growth and remodeling

One aspect of atherosclerosis plaque growth can be explained by silent cycles of healing and rupturing of the fibrous cap. In fact, to cover the rupture, fibrous matrices along with collagen fibers and extracellular spaces are formed but can be a location of further ruptures and thus thrombosis which rewinds the cycle. This silent mechanism is observed in many cases of sudden death[16].

Regions of arteries with developing plaque might undergo a positive remodeling that normalizes the shear in the artery and preserve the lumen diameter. It is interesting to note that compared to inward growth where the WSS is higher due to the shrinkage of the diameter, LWSS present in the outward can be corelated with higher intake of lipid material and thus the presence of larger necrotic cores[17].

When the positive remodeling cannot compensate the plaque presence, a phenomenon that occurs when the lesion exceeds 40% of the arterial area, the further plaque enlargement reduces the lumen diameter enhancing the significance of the hemodynamic factors in the plaque growth[18].

Effect of endothelial shear stress

In healthy arteries, high wall shear stress is considered athero-protective. However, in the

case where an unstable plaque is present, high WSS may lead to further fragilization of the plaque. Following the radial deformation of the plaque during a cardiac cycle

Gijsen FJH et al. have noted that areas with higher strain are in proximity with high shear stress regions [19]. In fact, exposure to high WSS leads to diminution of fibrous components and increases the burden of necrotic core and dense calcium which are indicators of plaque vulnerability[20].

1.1.7 Clinical positioning of the research project

Since the affected population has, generally, a relatively advanced age, physicians are often in a situation where they need to make the decision of prescribing, or not, a surgical treatment to a vulnerable patient; a decision that needs to be based on the stability of the plaque. Moreover, and despite the availability of multiple treatment procedures, the mortality rate due to complications of atherosclerosis plaque are still high. This is largely due to the unavailability of a tool able to explain the behavior of a diseased artery.

Blood vessels are constantly exposed to a complex interaction between blood flows and the artery walls, that influence the initiation and growth of atherosclerosis plaques. Plaque rupture, on the other hand, is influenced by an interaction between biological and mechanical factors. It is important to understand those phenomena to prescribe efficient therapeutic strategies that promote plaque stabilization and prevent complications.

In the last decades, many developments have been made to meet this purpose, especially with the emergence of new imagery technics that enabled patient specific analysis. Nevertheless, more multidisciplinary studies should take place to offer global comprehension of these complex cases.

Within this context, this work aims to the development of a numerical tool for analyzing the blood flows/artery walls interactions and for investigating newer diagnostic approaches to verify the presence and severity of a plaque. In fact, since the arterial structure is in motion under the effect of blood pressure it is possible that the plaque presence alters the

blood flow distribution and the arterial response. With this in mind, both the fluid and the structural domain of the artery are analyzed to investigate the possibility of detecting atherosclerosis presence in peripheral tissue through new diagnosis methods.

1.2 Biomechanics of arteries

1.2.1 Mechanical properties of the arterial wall

1.2.1.1 Arterial wall structure

To understand the mechanical properties of the arterial wall, it is important to account for its anatomical composition. Generally, blood vessels have a circular section with a varying wall thickness. The ratio of the wall thickness to the diameter of the wall is of the order of 0,1.

The arterial wall, as presented in the figure below (from: Novogen.com) is composed of three concentric layers:

- Tunica intima: Consists of a single thin layer (0,5 µm) of endothelial cells. It is connected to the median layer through connective tissue composed of collagen fibers.
- Tunica media: it consists of several concentric layers of elastin separated by thin fibers of collagen and elastin layers. It is generally the thickest layer of the artery wall. Soft muscular tissue and elastic fibers are obliquely oriented regarding to the center axis of the artery.
- Tunica adventitia: consists of loose tissue containing both collagen and elastin fibers.

The structure of the vessels depends on the role they play: large vessels which role is distributing the blood, have a conductive behavior. They are mainly composed of elastin,

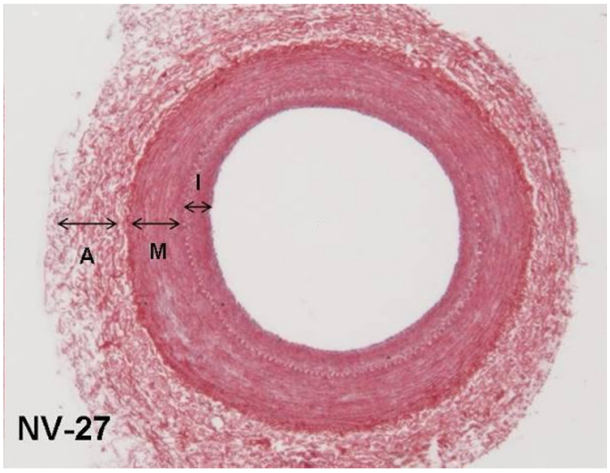

Figure 1.6: *Arterial layers. L: Lumen, I: Intima, M: Media, A: Adventitia (Novogen.com)*

allowing a variable continuous flow. To put it in another way, during systole the flow is a result of the contraction of the heart while during the diastole the flow is maintained by the elastic pressure of the vessels. On the other hand, small arteries cause a drop of the velocity due to their resistance to the circulation. The veins are mainly composed of muscular tissue allowing blood to return to the heart.

Mechanical characteristics of arterial wall

For understanding and modelling the behavior of anatomical or diseased arteries, whether to explain phenomena taking place in the circulatory system or to be able to prescribe adequate treatment for patients, it is necessary to know the mechanical properties of blood vessels in order to model them correctly.

- **Anisotropy**

The presence of oriented long chains of collagen makes the arteries behave in an anisotropic way. Patel and Fry(1969) were the first to discuss the anisotropy of arterial wall in dogs [21]. Cox and co-workers explained how the arteries are stiffer in the circumferential direction compared to the axial one [22]. The arterial tissue can be defined as transverse isotropic material where the three directional stresses produce only normal strains [23]. Holzapfel and Ogden, on the other hand, considered the arterial wall as an orthotropic material [24][25], even if it is usually considered isotropic when anisotropy is low or in

cases of low pressure variations (Peterson 1960).

- **Nonlinear elasticity**

Arteries exhibit a non-linear stress-strain response [26][27]. An important characteristic of soft tissues is that they exhibit high strain when exposed to low stress values, and show a stiffer response at higher stress levels [25].

Many Strain Energy Density Functions (SEDF) are used in the literature to describe the arterial tissue; the review of Holzapfel et al. is a comparative study between the major 3D constitutive models [26]. Material constants of these equations need to be determined through mechanical testing and, even if the constitutive models are very different from each other, it is still possible to fit them to the same experimental results, due to the large number of parameters [28]. Hence, the results obtained should always be observed carefully verifying the range of applicability of the fitted model.

- **Compressibility**

Arterial tissue is nearly incompressible according to the tests of [29], where they observed 1% change in arterial wall volume when the tissue is submitted to 10kPa radial compression. This observation led to a wide assumption of incompressibility of the wall by researchers in the field.

1.2.1.2 Atherosclerosis plaque characterization

Atherosclerosis plaques are complex tissues[30]. They can be classified into: Calcified, fibrous, necrotic or mixed tissues[31]. This leads to a difference in behaviour compared to a healthy artery. Diseased vessels exhibit higher compressibility[32] and a viscoelastic behavior when exposed to constant compressive loads[33].

During the plaque formation, the changes in the arterial wall occurs in the intimal layer which transforms to a thicker layer mainly containing smooth muscle cells, collagen and lipids. Various studies focused on examining the mechanical properties of atherosclerotic

intimal tissu due to the difficulty in separating the plaque from the intimal layer.

The mechanical properties of the plaque have been evaluated through tensile test[34][35][36][37][38][39][40] and compression tests[41][42][43][44][39][45][46][47].

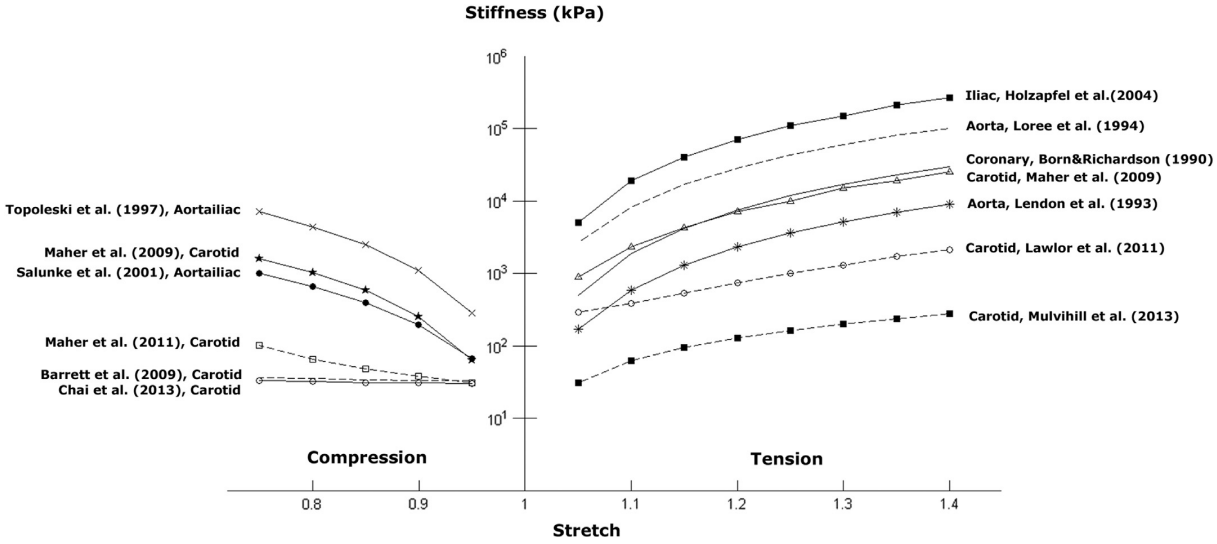

Figure 1.7: *Tangential stiffness values from the data reported in the reviewed papers [48]*

From the comparision of these studies , see Figure 1.7 , Akyildiz et al. concluded that[48]:

- The plaque has a non linear behavior
- Large variation in stiffness within atherosclerotic tissue have been observed
- The available data doesn't allow for differentiating the origine of the plaque (iliac, coronary or carotid, etc.)
- Extension stiffness is higher than compression stiffness.

Although numerous post-mortem experimental studies have been performed to obtain the mechanical properties of atherosclerosis. The patient dependency,the localization of the plaque and difference in plaque type create a great discrepancy in the obtained results. This reinforces the need of more documented experiments and underlines the importance of patient specific data when evaluating bio-mechanical quantities.

1.2.2 Modeling blood flow

Computational hemodynamics is the computer simulation of blood flows within blood vessels. It is an emerging research field that uses the computational simulations to answer biomedical engineering problematics [49]. The blood flows described by the Navier-Stokes equations can be modeled using CFD.

Blood is a non-Newtonian fluid, where viscosity depends on the plasma, the protein content, the hematocrit, the temperature, the diameter of the vessel, the shear rate [50], etc. Blood flows in the circulatory system have generally a periodic behavior, with a periodic variation of pressure and velocity. Pressure and velocity profiles with respect to time are altered with aging and diseases.

1.2.2.1 Rheology of blood flow

The Newtonian hypothesis of blood, which consists in taking a constant dynamic viscosity , can be considered as valid in large vessels [51], where we observe high shear rate, which is the case for carotid bifurcation. However, this assumption is questionable when we are interested in near-wall quantities; near-wall regions experience low shear rate due to the low velocities. Consequently, it is necessary to consider the non-Newtonian behavior of blood [52].

All the non-Newtonian time-independent models for blood viscosity show a shear-thinning behavior. In their work, Vijayaratnam et al. have summarized a large number of rheological models, as presented in Figure 1.8. The power law, Casson and Carreau-Yasuda models are the most commonly used non-Newtonian models [53].

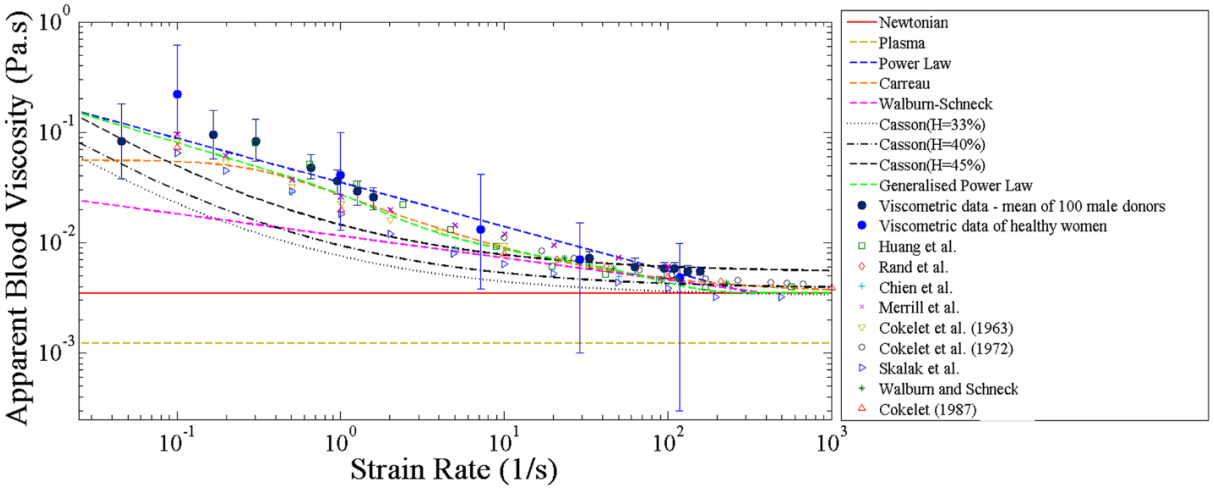

Figure 1.8: *Different blood rheological models and experimental measurements [53]*

Other than the generalized Newtonian models, more elaborated theories consider the microstructure of the blood and the interaction between its constituents. They can be used to describe the viscoelastic behavior of blood, e.g. the non-linear differential models as well as diluted and concentrated network theories and more recently the MPTT model [54].

1.2.2.2 Near wall quantities of interest

Several patterns can be considered when studying disturbed flows, such as recirculation areas and stagnation zones, which play an important role in altering the arterial tissue.

- **Wall shear stress**

Studies on fluid dynamics show that the flow and the WSS are disturbed near to the carotid bifurcation [55], which may cause endothelial dysfunction [56]. LWSS has a significant role in inducing arterial damage and plaque instability, due to the increase of residual time and therefore platelets and macrophage probability of adhesion to the arterial wall [57]. Moreover, it seems that chronic exposure to high WSS causes an atheroprotective phenotype [58] and, probably, a remodeling phenomenon. Investigations should be carried out to confirm this hypothesis.

- **Oscillating Shear Index**

The oscillatory nature of WSS is examined through the OSI, which was defined by [59]. It has values ranging from 0 to 0.5, where regions with high OSI (> 0.1) are considered of high risk of plaque formation [60][61].

1.2.3 Measuring WSS

In-vivo Blood-related variables can be obtained using non-invasive techniques such as Magnetic Resonance Imaging (MRI) [62][63][64], Particle Image Velocimetry (PIV) and μPIV [65] [66].

The case of MRI

Assuming that the dynamic blood viscosity is knows, the WSS can be determined by multiplying the spacial gradient of blood velocities near and perpendicular to the wall by the dynamic viscosity of the blood. Nevertheless, MRI can underestimation the WSS due to the low resolution of the scanning, particularly in the case of large population studies where the accuracy is lowered to gain time[67][68].

These techniques have had a great improvement during the past decade but they still are expensive and difficult to use on each patient. Nonetheless, they present a very good validation method for numerical approaches.

1.2.4 State of the art on numerical models for carotid artery

Several CFD analyses have been carried out considering idealized geometries [69] or more complicated geometries, obtained using medical imagery [70][71][72]. These studies have provided a great number of information about the circulatory system, but the assumption of rigid walls overestimates the WSS compared to flexible walls[73].

Few studies have established 3D FSI numerical models for diseased carotid arteries. A study performed by Tang et al. in 2004, was the first attempt to investigate the effect of material properties in stress distribution in an atherosclerosis plaque, using a 3D FSI

model [74]. Li et al. examined the critically of the fibrous cap thickness by simulating the interaction between blood flow and a stenosed artery, under the assumption of Newtonian flow in a simplified geometry [75]. Recent studies continue exploring the effect of modeling parameters on the results observed in vascular numerical simulations. The inlet and outlet boundary conditions, the viscosity law for the fluid as well as the constitutive law for the arterial wall have been discussed by several authors [35][76][52][77][78].

In a study conducted by Richardson et al., the authors evaluated the internal stress distribution in multiple lesions using finite elements method. They concluded that the stress concentration was observed at the fibrous cap explained by the inability of the lipid core to bear high mechanical stresses [79]. With the same purpose Cheng et al. evaluated the difference between the stress distribution between ruptured and unruptured fibrous caps and concluded that ruptured fibrous caps presented higher stress concentrations and thus more ability of re-rupturing [80]. To summarize, the accumulation of lipids in the lesion that leads to the increase of the internal stresses combined with the weakening of the fibrous cap and elevated blood pressure leads to plaque rupture.

In the recent past, coupling between the blood flow and carotid wall has also been investigated for more realistic artery geometries. Gao et al. have evaluated the stress distribution in a plaque located in the carotid artery through one way (weak) coupling between the blood and the arterial structure [81][82]. Other authors have conducted two ways (strong) coupling, but have used simplifying considerations about the boundary conditions of the fluid [83][84], considering a Newtonian behavior of the fluid [85] or with simplified geometries [86]. More recently, Fluid structure interaction techniques have been used in the study of blood behavior in healthy and diseased carotid artery [87] [88] [89], these studies showed the correlation between areas of the flow disruption and locations conducive to develop atherosclerosis.

1.2.5 Research objectives:

Despite the advances in the bio-medical field, there are still many limitations in patient specific representation of blood flow and artery behavior. Conventional markers (i.e. degree of stenosis and plaque burden) are not enough to provide an answer to the stability of the plaque. However, with the availability of patient specific data, thanks to the advancement in imaging techniques, a great opportunity to comprehend phenomena taking place in the human body is available. The chance to understand diseases and to offer earlier diagnosis can be concretized by an improved numerical modelling of carotid atherosclerosis.

Nowadays, only few studies have investigated the fluid/structure interaction in the carotid artery and usually by using simplifying assumptions as mentioned before [90][91]. This project is focused on building a numerical model of the CA able to predict the behavior of this artery both in presence and in absence of atherosclerosis plaques, considering patient specific data. The potential presence of new markers, which can characterize the atherosclerosis of the carotid artery, are as well investigated.

The main objectives of the present work are the following:

- To develop both CFD and FSI models for biomechanical analysis of the carotid artery on a commercial software (ANSYS);
- To study the effect of the plaque presence in the CA, using idealized geometrical models;
- To evaluate the distribution of stresses in the arterial wall;
- To compare the results obtained using CFD and FSI methods, both by the one-way and the two-ways coupling approaches.
- To study the applicability of the previous numerical methods for patient-specific cases.

- To verify the presence, and the retrievability by simulation, of new markers of the stenosis stability trough the frequency signature response of the artery.

At this aim, the model developing will follow a step-by-step approach, starting from simplified geometries in CFD simulation, up to patient specific geometries in FSI.

Chapter 2

Numerical approach for modeling blood flow in the carotid artery

This chapter presents the general approach, used here, for computing the mechanical behavior of the carotid artery. The constitutive models for the fluid and the mechanical properties of the structural parts, as well as the boundary conditions used are presented in detail.

A description of the specific methods for solving the fluid and the structural domains and the coupling between the two domains is detailed.

2.1 Introduction

The human body is a complex system where physiological, chemical and mechanical phenomenon take place and it is very important for physicians to procure an understanding of these factors. Since its development, finite element method has been used to analyze complex structures and retrieve the stress and motion fields in fluid and solid mechanics. Recently, this tool has proven having a great potential in the cardiovascular field. The role of cardiovascular computational modeling is to evaluate in-vivo physiological properties, such as arterial pressure and organ irrigation. This is very important in the clinical diagnosis of cardiovascular pathologies. The second major role is to predict the occurrence of these pathologies and assess the choice of therapeutic procedures.

In this study a computational model based on finite element and finite volume methods has been built to describe carotid artery behavior through the implementation of a simulation tool that succeeds in delivering patient-specific CA mechanical behavior. The development of the numerical model has been attained through a series of strategical steps from the geometrical modeling to the definition of the material properties and boundary conditions.

2.2 Geometrical models and mesh generation

2.2.1 Idealized geometries

With the aim of studying the influence of the main geometrical factors, geometries were modeled using the commercial CAD software CREO. A geometry with 6mm diameter and 30° bifurcation was first modeled (Figure 2.1 A). Then, in order to account for the main geometrical features of a real carotid geometry, e.g. the curvature and the corresponding diameters of the different branches, the fluid domain of the healthy CA is a representation of a carotid bifurcation with an inlet diameter of 6mm, Internal Carotid Artery (ICA) 5mm and the External Carotid Artery (ECA) 4.5mm (Figure 2.1 B). To

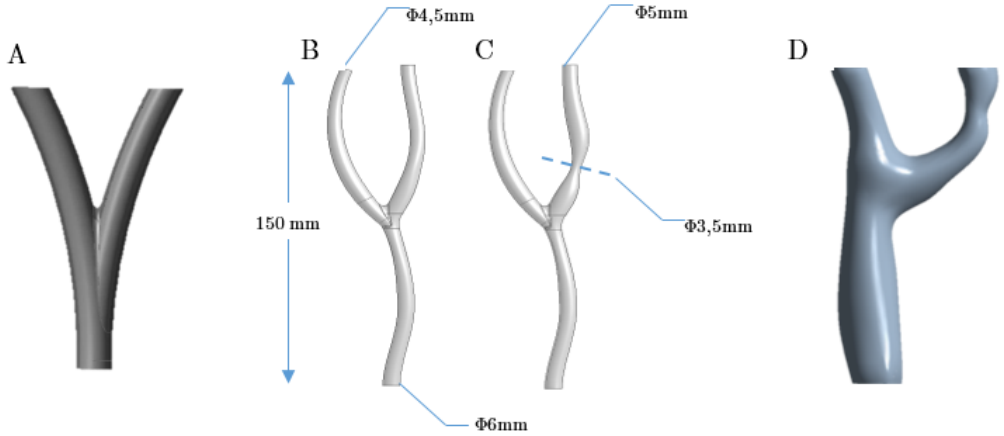

Figure 2.1: *Geometry models: A: Idealized Geometry, B:simplified geometry without plaque, C: simplified geometry with plaque, D: Patient specific geometry*

model the presence of the plaque, a diameter narrowing of 30% at the internal CA has been introduced (Figure 2.1 C).

2.2.2 Patient-specific geometrical models

Since the geometrical features highly affect the mechanical behavior of arteries and knowing the importance of the patient specific data in the mechanical analysis when dealing with the vascular biomechanical field, it is necessary to verify the applicability of the computational model in a patient specific case.

In the simplified geometry, the diameter of the inlet section is set to 6mm. the length of the CCA branch is 90 mm and the distance between the bifurcation and outlet sections is 60 mm .

MRI images of patients with atherosclerosis plaque located at the ECA were recovered from the Edouard Herriot Hospital-Lyon and one geometry was segmented and smoothed using the SCANIP (Simpleware Inc.) software. The inlet section was slightly modified to ensure a circular shape (Figure 2.1 D), to apply parabolic boundary condition to ensure an established flow state.

2.3 Computational fluid modeling

Computational fluid dynamics is based on the numerical approximation of the solution of the partial differential equations, the Navier-Stokes equations, which describe the relation between pressure, velocity, temperature and density in a fluid in motion, including the effect of viscosity on the flow. An accurate resolution of the fluid flow is achieved by the right modelling of the problem, i.e. properties of the fluid, geometry of the domain and boundary conditions.

2.3.1 Constitutive model of the fluid domain

As mentioned in the previous chapter, the blood in large arteries shows a Newtonian behavior. Nevertheless, in order to compute correctly the shear stress in low shear areas of the fluid domain, it is necessary to consider the low shear viscosity. At this aim, the viscosity law should meet the right properties in high and low shear. The well-known Carreau model is defined in a way that enables the capture both the high and law shear viscosity properties.

In this work, blood was described as a Carreau model, where the parameters were obtained experimentally by Cho and Kensey [92]. Moreover, CFD results has been compared with different models, where the blood was considered Newtonian or where the viscosity was described according to the Casson model [93]. A summary of the model parameters is presented in the Table 2 .

2.3.2 Inlet Boundary Conditions

2.3.2.1 4D MRI data acquisition

Magnetic Resonance Imagery(MRI) flux is a technique based on grey scale phase contrast evaluation . This is founded on the analysis of protons and neutrons response to an added

Viscosity Model	Parameters	Nomenclature
Newtonian	$\mu = 0.0035 Pa.s$	μ : Dynamic Viscosity
Carreau $\mu = \mu_\infty + (\mu_0 - \mu_\infty) * (1 + \lambda(\dot{\gamma})^2)^{\frac{n-1}{2}}$	$\mu_\infty = 0.0035 Pa.s$ $\mu_0 = 0.056 Pa.s$ $\lambda = 3.313 s$ $n = 0.3568$	μ_∞ : Viscosity at high shear μ_0 : Viscosity at low shear n : Power index λ : Time constant
Casson $\sqrt{\tau} = \sqrt{\tau_c} + \sqrt{\mu_c} * \sqrt{\dot{\gamma}}$	$\mu_c = 0.00414 Pa.s$ $\tau_c = 0.0038 Pa$	μ_c : Critical viscosity τ_c : Yield stress

Table 2.1: *Parameters of the used viscosity models*

energy in an electromagnetic field and it is used to obtain information about the blood flow quantities [94].

PC-MRI measurements were realized by Professor Loic Boussel head of Radiology department at the Croix-Rousse hospital, on a male patient, in order to recover in-vivo velocity profiles, in the carotid artery, throughout the cardiac cycle. The measures were conducted in three sections of interest: CCA, ECA and ICA. The acquisition timeframe is 0.05s ±0.005, which is the minimum acquisition time available.

In the figure below, the flow profiles, obtained by the 4-D MRI data, are shown. established flow state.

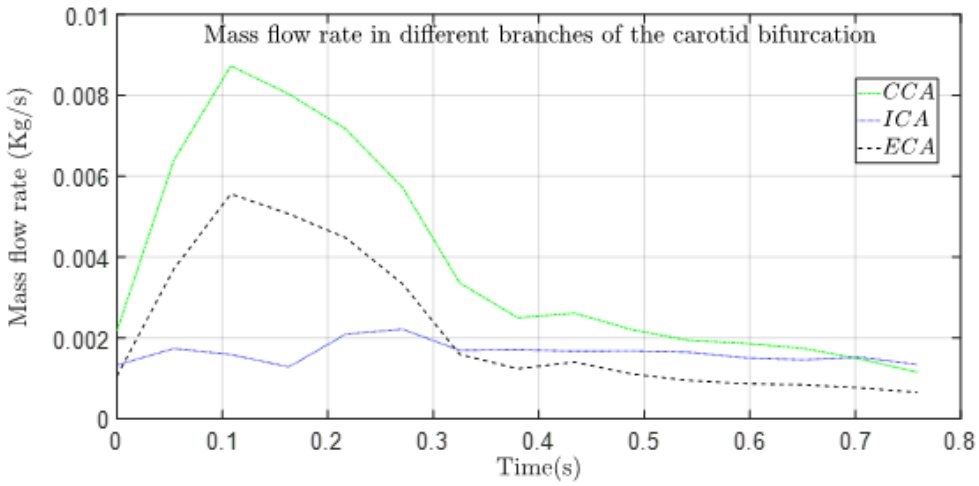

Figure 2.2: *Mass flow rate through CCA, ECA and ICA branches recovered from 4D MRI Scan during a cardiac cycle*

2.3.2.2 Velocity distributions in the inlet section

The Womersley-number (α) is a dimensionless number used to describe the dominance of viscous or inertial forces in a pulsatile flow and, with that, the shape of the velocity distribution in a section of a fluid domain. This is calculated using the formula [95][96] (eq 2.1):

$$\alpha = R\sqrt{\frac{\omega\rho}{\mu}} \tag{2.1}$$

where:

R	:	Radius of the pipe
ω	:	First harmonic of the pulsatile pressure
ρ	:	Density of the fluid
μ	:	Dynamic viscosity of the fluid

The higher the , the more dominant the inertial forces, which leads to a flattened distribution of the velocity in a section of the pipe, as we can see in the figure below:

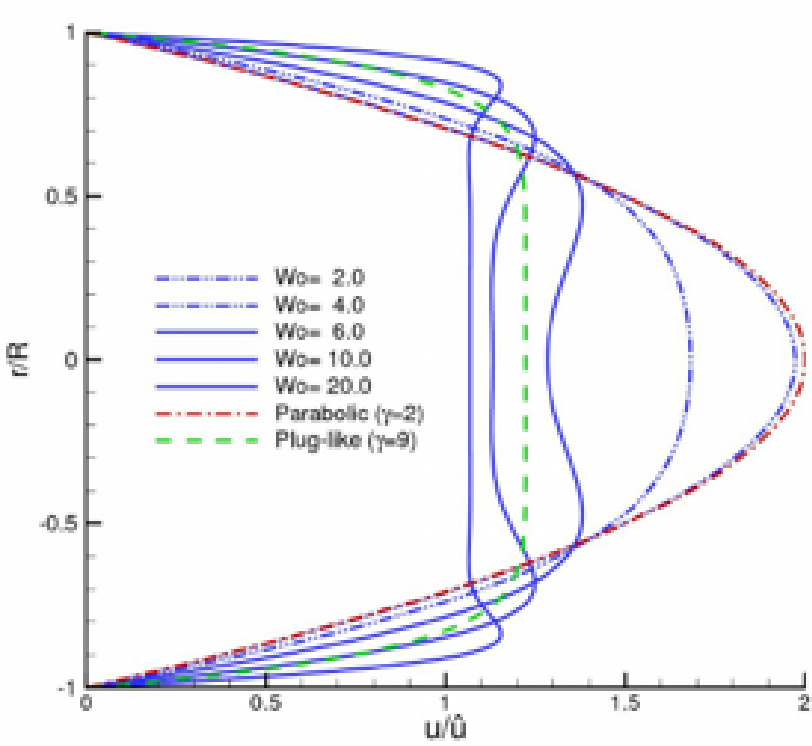

Figure 2.3: *Representation of velocity distributions of transient flow with diverse Womersley numbers in comparison with parabolic and plug-like distributions [97]*

The Womersley number in the CCA is around 4.2, which results in an almost parabolic profile, as represented in Figure 2.3. Moreover, Campbell et al [98] concluded that a parabolic inlet velocity leads to more accurate mean WSS and OSI values. They also found that CFD calculations in the CA are much more sensitive to the geometry and the velocity profiles in time, with respect to the velocity distribution at the inlet boundaries.

From the Mass flow rate data presented in Figure 2.2, the maximum velocity at the center of the artery is obtained considering a parabolic distribution, resulting in the following expression (eq 2.2):

$$V_{max} = \frac{2Q}{Sd} \tag{2.2}$$

where:

V_{max}	:	Maximum velocity
Q	:	Mass flow rate
S	:	Area of the inlect section where the velocity is applied
d	:	Blood density

2.3.3 Outlet boundary conditions

2.3.3.1 Lumped Windkessel model

There are many ways to represent the outlet boundary condition, in the hemodynamic computational context, while dealing with a transient flow.

The presence of bifurcations and the high deformability of the arterial wall lead to an attenuation of the wave flow amplitude . In fact, the elasticity of the artery allows for the transformation of the pulsatile flow into a continuous one. This phenomenon is very noticeable while following the Pulse Wave from large to small arteries. A class of methods, such as 3D models, coupling 3D-1D models and 3D-0D models, have been developed to consider the effects of the resistance and the compliance of the downstream vasculature and solve the boundary condition problem.

The lumped three-elements Windkessel (WK3), also known as RCR, is a 0D type outlet BC. It is used to describe the behavior of the downstream vasculature by analogy with an electrical circuit composed of a Resistance Z in arrangement with a capacitance C and a distal resistance R (see Figure 2.4). The three parameters have a physiological meaning:

Z	:	Local inertia and compliance of the artery of interest
C	:	Arterial capacitance of vascular system
R	:	Distal resistance

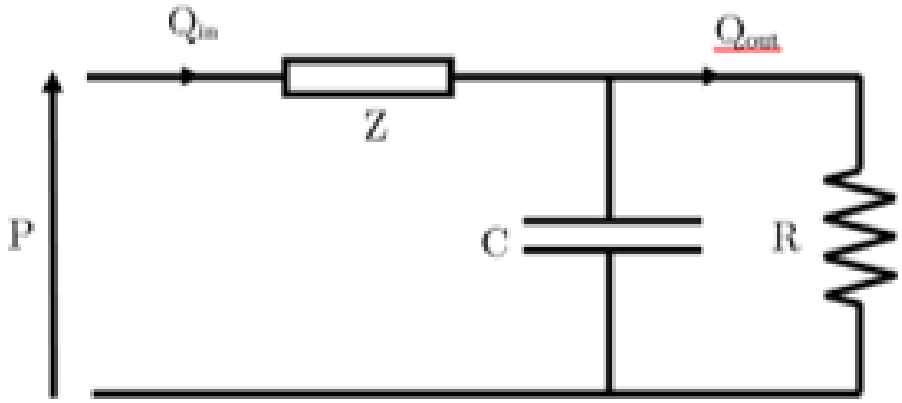

Figure 2.4: *Analog electrical system of the WK3*

This model allows for the variation of the outlet pressure using a simple differential equation (eq 2.3), in which P_{in} and Q_{in} are the pressure and flow at a node i, respectively. Basically, the gradient of pressure leads to the movement of the flow countering the hydraulic impedance. This impedance term corresponds to the friction losses, elasticity of the vessel as well as the blood inertia.

$$Q_{in} = C\frac{d}{dt}(P_{in} - Q_{in}Z) + \frac{P_{in} - Q_{in}}{R} \tag{2.3}$$

Solving (eq 2.3), by using a forward finite difference method, gives

$$P_n = (1 - \frac{\Delta t}{CZ})P_{n-1} + \frac{\Delta t}{CZ}(R + Z)Q_n + R(Q_n - Q_{n-1}) \tag{2.4}$$

Where:

n : Time step

Δt : Time step size

2.3.3.2 Adjustment of the Windkessel parameters

Although WK3 is the most common lumped model, the model parameters are patient specific and must be adjusted to match the patient data. The availability of flow data, through phase contrast MRI, as well as the pressure range, allows for the acquisition of adapted parameters. For that, a first pressure profile is obtained numerically by solving (eq 2.3).

The required inputs for solving (eq 2.3) are the flow data from 4D-MRI and the parameters of WK3 available in the literature [76]. The obtained pressure is then scaled to match the patient specific pressure range. Finally, a procedure of system identification for the pressure-flow transfer function is conducted in order to recover the adjusted Windkessel parameters. The new parameters are introduced into the 0-D model that is solved sequentially with the Navier-Stokes equations.

In order to solve the numerical form in (eq 2.4), the following inputs are needed:

- Flow rate profile of the internal and external carotid arteries acquired through PC-MRI (example of ECA flow Figure 2.1 A);
- Windkessel Initial parameters cited in the table below ;
- Time step size $\Delta t = 10^{-4}s$;
- Initial values $P_1 = 10.5kPa$ equivalent to diastolic pressure.

The pressure was then calculated for 8 cycles to ensure the stabilization of the resulting pressure. The profile of the last cycle is taken into consideration . The obtained pressure is then scaled in such a way that the maximum and minimum of the pressure are equivalent

	R ($[dyn][s][cm]^{-5}$)	C($[cm]^5[dyn]^{-1}$)	Z ($[dyn][s][cm]^{-5}$)
ICA	$2.35e^3$	$2.23e^{-5}$	$2.56e^4$
ECA	$5.49e^3$	$9.54e^{-6}$	$5.97e^4$

Table 2.2: *Initial Windkessel parameters for ICA and ECA*

to the corresponding systolic and diastolic pressures of the patient. In this case, the pressure ranges from 10.5 to 16kPa.

The relationship between the outflow and the pressure, as symbolized with the electrical circuit in Figure 2.4, can be written in the frequency domain as:

$$P_n = Z_{system} Q_n \tag{2.5}$$

where Z_{system} is the harmonic response of the system.

$$Z_{system} = Z + \frac{R}{1 + i2\pi f RC} \tag{2.6}$$

By expressing Z_{system} in the Laplace domain, we obtain

$$Z_{system} = Z + \frac{R}{1 + sRC} = Z + \frac{R + Z + sZRC}{1 + sRC} \tag{2.7}$$

$$Z_{system} = \frac{\frac{R+Z}{RC} + sZ}{\frac{1}{RC} + s} \tag{2.8}$$

To obtain the parameters R, Z and C, the transfer function estimation of the MATLAB system identification toolbox *(Mathworks System Identification Toolbox Release R2017b)* has been employed. It consists of an iterative algorithm for approximating the transfer function by loading the same length arrays of input and output of the TF and choosing a continuous time approximation, as well as an estimated initialization of the parameters. At the end of this procedure we obtain the result under the form (eq 2.9) and a fitting approximation percentage, which was around 90-98% for our data sets.

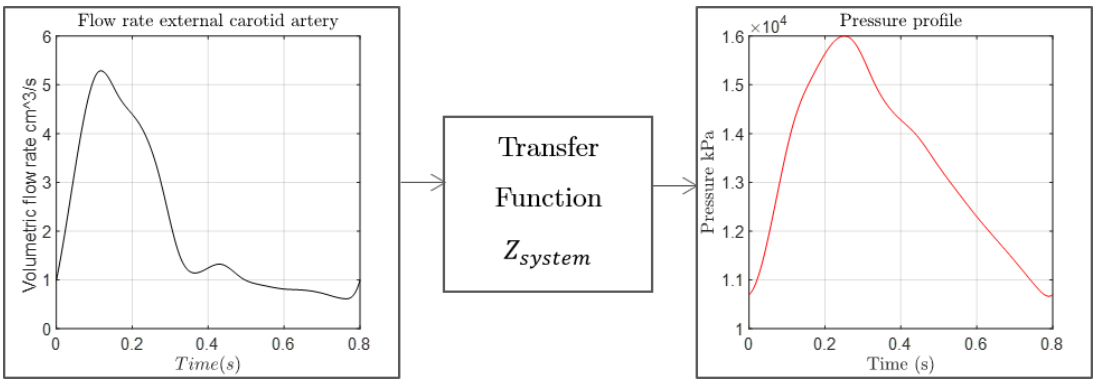

Figure 2.5: *Relation between flow rate and pressure*

$$Z_{system} = \frac{\alpha + s\beta}{\gamma + s} \tag{2.9}$$

The parameters obtained from solving the system of three unknowns and three equations are reported in Table 2.3.

	R ($[kg][m]^{-4}[s]^{-1}$)	C($[kg]^{-1}[m]^4[s]^2$)	Z ($[kg][m]^{-4}[s]^{-1}$)
ICA	$5.77E9$	$1.748E-11$	$3.11E9$
ECA	$5.735E9$	$8.05E-11$	$6.597E8$

Table 2.3: *Adjusted Windkessel parameters for ICA and ECA*

These parameters have been used to calculate sequentially the pressure boundary conditions during the CFD simulations, using a centered integration form through a UDF compiled with FLUENT (*ANSYS ®Academic Research Mechanical, Release 17.2*). The obtained pressure at the inlet was also compared to simulations where a constant pressure of 13 kPa and a ramped pressure profile between 10 and 16 kPa were imposed at the outlets (see section 3.1.5).

2.3.4 Meshing of the fluid domain

Because CFD calculations are sensitive to the employed grid, it is then very important to pay attention to the convergence with respect to the mesh relative quantities. Using structured meshes with complicated geometries, such as arteries, might lead to an over-

simplification of the problem and less efficient mesh distribution. Tetrahedral elements can describe more complex surfaces [99].

The ANSYS Meshing product is an automated, high performance tool that offers adapted analysis-specific meshing strategies. The models were meshed using a dominant tetra approach. Tetra elements are more keen to describe complex geometries such as arteries. The inputs are the geometry, the max element size, the meshing method, transition and desired quality. Since it is essential to compute the WSS, inflation layers are added to the mesh. They ensure small grid size at the boundary layer and smoother transition towards the main stream domain, located at the centerline of the geometrical models.

2.4 Computational Structural modeling

The arterial tissue has been modeled as a 1mm layer that covers the fluid domain. In the case of diseased artery, the plaque geometry was obtained by filling the stenosis area, so that the full model resembles a hypothetical healthy artery. The artery material is considered incompressible, isotropic and hyperelastic [35]. More specifications about the hyperelastic model are presented in subsection 2.4.1 below.

As for the mechanical properties of the atherosclerosis plaque, it is considered elastic with a young modulus of 0.9 GPa. This value can be modified according to the degree of calcification of the plaque. In this regard, Mouktadiri et al. [100] delivered a cartography of the elastic properties of arterial tissue, according to the calcification stage of the artery.

The structural geometry was meshed using ANSYS meshing tool with a mesh size of 0.3 mm3. This allows the observation of the propagation of the pulse wave in the arterial structure, which has a mean velocity of 9m/s [101].

2.4.1 Mooney-Rivlin 5-Parameters hyperelastic model

The arterial tissue was defined by the Mooney-Rivlin hyperelastic model, which adequately describe the strain-stress relationship in large arteries [23][102][54]. In the case of incompressible material, the 5 parameters Mooney-Rivlin Stain energy density function reads

$$W = \sum_{i+j\leq 2} C_{ij}(In_i - 3)^i.(In_j - 3)^j \tag{2.10}$$

The SEDF is a scalar function of the principle invariants of left Cauchy-Green deformation tensor (In_i, In_j) and material constants C_{ij}.

The material constants have been obtained from previous experimental tests and fitted by Gao et al. [74][82]. They are reported in Table **??**:

Parameter	Value[kPa]
C_{10}	50.445
C_{01}	30.491
C_{20}	40
C_{02}	120
C_{11}	10

Table 2.4: *Mooney Rivlin Parameters for the arterial tissue*

2.4.2 Structural boundary conditions

In the performed simulations the inlet and outlets of the structure were fixed and an elastic support was applied at the external wall of the geometry, representing the arterial tissue, in order to assimilate the surrounding environment of the carotid bifurcation (see Figure 2.7).

To the best of the author knowledge, there have been no studies that evaluated the

mechanical properties of surrounding tissue. Then, an elastic foundation of 0.001N.mm-3 has been introduced, which allowed procuring physiological values of artery displacement during the pulse.

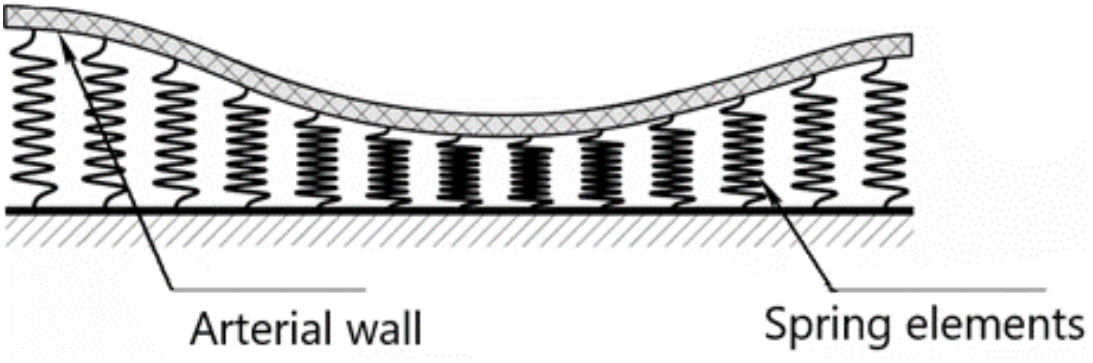

Figure 2.6: *Elastic foundation schematization*

2.4.3 Fluid-Structure coupling

The vascular system is under continuous stress because of blood pressure (Figure **??**). The natural cycles of inflations are an indicator of the state of the vascular system. From a mechanical point of view, the deformation of the arterial structure, in response to the pressure applied from the fluid, depends among other on the geometry and mechanical properties of the artery itself.

Most of the computation vascular biomechanical studies treat the vessel wall as rigid or use very simplified arterial models [103][104][105]. This is due, in large part, to the difficulty in computationally solving coupled fluid structural domains. This approximation might be valid when dealing with small arteries, where the deformation is very small due to the presence of the muscular tissue. On the other side, large arteries present deformations that cannot be neglected.

2.4.4 One-way Coupling

The mechanical stress distribution in the arterial wall is related to a multitude of physiological phenomena, e.g. the wall remodeling [99]. One approach to address the transient

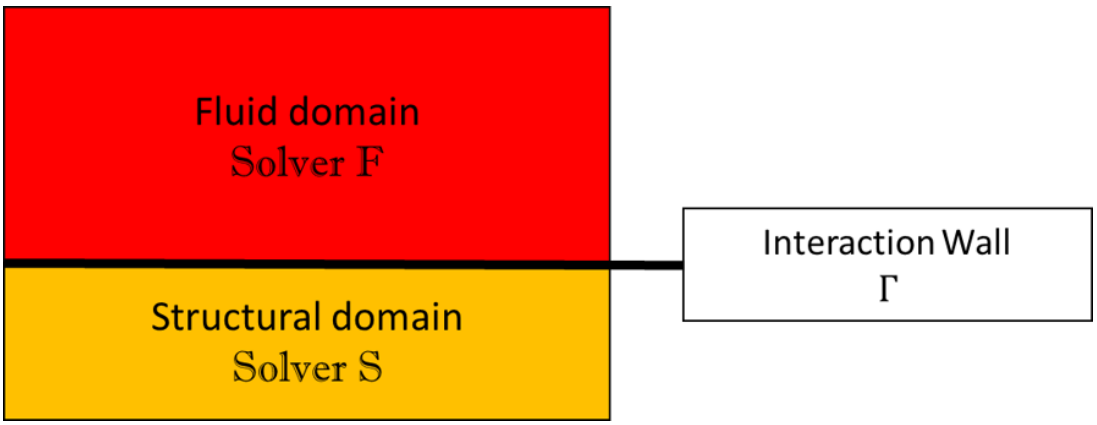

Figure 2.7: *Representation of the fluid-structure interaction problem*

behavior of CA, is to evaluate the stress and motion of the artery imposed by the blood pressure, as Dirichlet boundary condition at the internal wall of the structure geometry, without considering the change of volume in the fluid domain. This method is called the one-way fluid structure interaction.

2.4.5 Two-ways coupling

One of the main characteristics of the mechanical behavior of large arteries is the presence of large deformations. These deformations have certainly the biological role of maintaining a continuous blood flow, but might be problematic from computational mechanics point of view. When the main concern is studying the behavior of arteries, this enlargement of diameter, estimated to 10%, cannot be neglected. In fact, the deformation changes the blood flow, which questions the validity of calculations considering rigid wall hypothesis.

2.4.5.1 Partitioned approach in solving FSI problems

With the aim of investigating how the carotid artery reacts to the blood pulse, and how does the blood flow respond to the artery enlargement, it seemed necessary to conduct a fluid-structure interaction study to evaluate the overall behavior of the CA. This can be done through a partitioned approach, where the mechanics of both fields are solved separately, and then the respective data, i.e. pressure at the fluid wall and the displacement

of the structural nodes in contact with the fluid domain, are coupled. Compared to the monolith approach that uses the same solver for both fluid and structural domains, the staggered algorithm allows for more choice in the modeling of the separated parts and thus more accuracy [106][107].

To solve the strong coupling between the fluid and structure in an interaction problem, where the materials are incompressible and have comparable densities, which is the case for blood and arteries, it is necessary to perform multiple coupling iterations to reach convergence. In the case of large deformations, the convergence is hard to achieve, since the partitioned FSI iterations are explicit and suffer from instability issues. In this case, introducing partial implicit or relaxation to the FSI iterations might be a solution. Nevertheless, the results obtained should always be examined carefully. The algorithm for solving partitioned FSI is presented below.

$n = 0$	
$s^0 = s_p^{n+1}$	//Structural domain initialization
Do	
Solve $F(sn) = f^{n+1}$	//Solve fluid domain
Transfer $f^{n+1}\|\Gamma$ to S	//Transfer F pressure results at Γ as Neumann BC for S
Solve $S(f^{n+1}) = s^{n+1}$	//Solve structural domain
Transfer $s^{n+1}\|\Gamma$ to F	//Transfer S displacement at Γ as Dirichlet BC for F
$n = n + 1$	
While $n < nmax$ and $s^{n+1} > tolerance$	//Check convergence

2.4.5.2 Contact management and convergence criterion

To compute the fluid-structure coupling, the System-Coupling module by ANSYS was employed. It allows the transfer of data between the fluid and the structural solvers and the configuration of the coupling procedure. A time step of $10E-3s$ was used to compute one way coupling and 5.10^{-3} for the two ways coupling. An under-relaxation factor of 0,5

was imposed to the pressure transferred from the fluid to the structural part to facilitate the convergence. The maximum coupling iterations was set to 20 and the convergence criterion to 0,01.

Also, due to the change in volume, partial remeshing of the fluid area is generally needed to avoid the presence of extremely large or very small mesh cells. Fluent offers the possibility to configure the remeshing, through imposing cells merging and division conditions. The choice of these parameters was based on the minimum and maximum cell sizes for each mesh. Generally, the cell volume was limited between 0.1mm3 and 0.5mm3. A condition on the mesh quality was also added, so that the accuracy of the analysis is enhanced. A maximum of 0.8 cell skewness value was imposed as a condition of remeshing.

2.5 General organization of results

In the following chapters, the obtained results were distributed into two parts depending on the used computational model. First, the CFD results are presented, considering the rigid wall hypothesis. The focus is on the effect of boundary conditions and viscosity models on the obtained results. The wall shear stress in the different models is discussed. The effect of the plaque presence on the fluid behavior is addressed.

Then, the major FSI results are presented a special interest on the structural part as well as a comparison between the different models. Also the frequency response of healthy and diseased arterial models is compared with the aim of retrieving a marker of the presence of the plaque.

Chapter 3

Computational Fluid Dynamics in the Carotid Artery

The overall objective of this section is the formulation of the fluid flow model, for both simplified and patient specific geometries, and the presentation of the flow quantities of interest, with a higher focus on the near wall plaque and after-plaque regions. The flow quantities derived from CFD simulations are evaluated with the aim of understanding the effect of the plaque presence on the flow distribution.

An analysis of the near wall quantities is put forward by evaluating their behavior in the after-plaque areas.

3.1 Rigid wall modeling of blood flow

3.1.1 Introduction

Blood flow in the carotid bifurcation can be considered as time-dependent, laminar incompressible flow. Solving such a problem requires simultaneous numerical resolution of the momentum field and satisfying the continuity equation, which can be performed utilizing finite volume method. The accurate resolution of the flow field using this method is dependent on the proper choice of the grid and boundary conditions.

The aim of the work presented in this chapter is to quantify the local hemodynamics in both simplified CAD models and geometries derived from CT-scans of the CA, with an emphasis of how the presence of the plaque alters the near wall quantities.

3.1.2 Mesh sensitivity analysis

The grid size was refined until the variation of maximum and minimum values of WSS at the plaque area became less than 1% difference. Finally, a volume element size of 0.3 mm was chosen, resulting in $2.26e^6$ elements.

Many criteria can be used to evaluate the mesh quality. Table 6 reports the skewness of the elements as a mesh metric, which represents the deviation between the cell shape and the corresponding equilateral cell. Lower skewness values are correlated with a good mesh quality.

Type of element	Skewness			
	< 0.25	$0.25 - 0.5$	$0.5 - 0.75$	> 0.75
Tetrahedral	$1.31e^6$	$6.17e^5$	$2.81e^4$	195
Wedge shaped	$2.55e^5$	$4.79e^4$	$1.28e^3$	2
Pyramid	0	0	75	586
	69.2%	29.42%	1.30%	0.03%

Table 3.1: *The elements skewness of the adapted mesh*

3.1.3 Carreau-Casson models comparison

Results from rigid wall simulations in the simplified geometry model, with a variable pressure outlet, have been compared for both Casson and Carreau rheological models. The same boundary conditions and geometry are considered for both configurations, varying only the rheological law introduced in the fluid simulation. Figure 3.1 shows the obtained velocity profile at the outlet of the stenosed branch of the carotid bifurcation, ICA in this case. Only slight differences between the corresponding velocity curves can be observed. Henceforth the Carreau model was utilized since it has a better-defined low shear behavior.

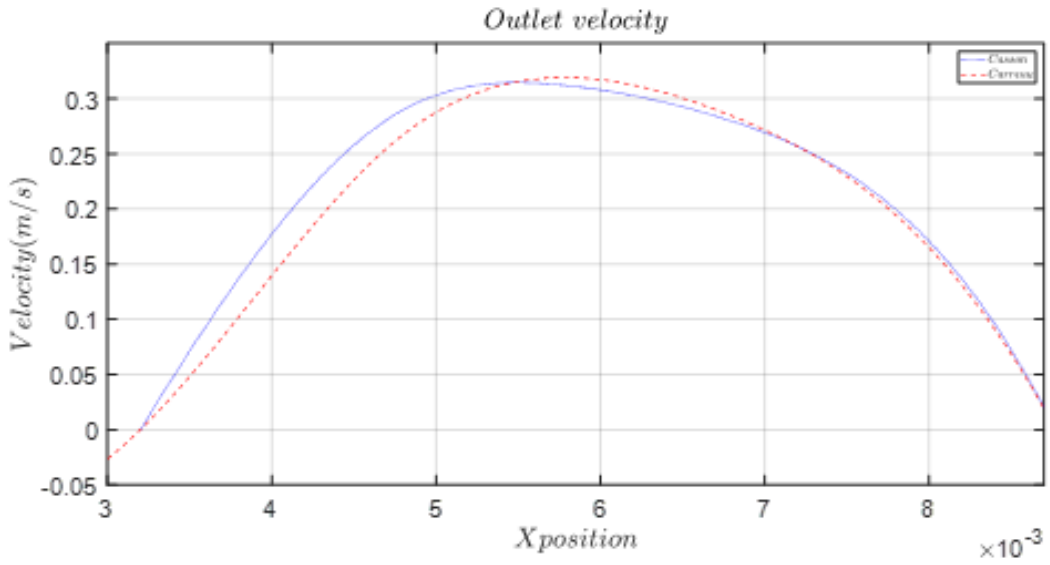

Figure 3.1: *Velocity profile at the outlet*

Nevertheless, the viscosity of blood changes from one person to another, due to hematocrits concentration and the shape of the red blood cells. In these cases, the generalized Newtonian models might not be the right choice for capturing the disturbance of blood flow. The viscoelastic MPTT model, developed by Amblard et al. and validated by Menut et al., offers the possibility to include the RBC concentration as a parameter of the blood viscosity [52][54]. It also appears to better capture the flow behavior during diastolic phase.

As for the WSS, a disparity in the results given by the different models and by the MRI data, makes it difficult to define a reference value for the shear component. The WSS

seems to be very sensitive to the employed model, andmodel and can only be compared to the results from similar models.

3.1.4 Inlet boundary condition

3.1.4.1 Formulation

The obtained velocity from MRI was approximated with a 5th order Fourier series. The time dependent peak velocity is described by the equation below:

$$V_{peak}(t) = a_0 + \sum_{k=1}^{5} a_k cos(kt\omega) + b_k sin(kt\omega) \tag{3.1}$$

whereω is the angular frequency of the cardiac pulse, which is equal to 7.85 rad/s, t is the simulation time and the values of the Fourier coefficients a_k and b_k are listed below:

a_0	a_1	a_2	a_3	a_4	a_5
0.4340	0.0712	-0.1204	-0.0462	-0.0398	-0.0296

b_1	b_2	b_3	b_4	b_5
0.3536	0.1394	0.0194	0.0329	-0.0088

Table 3.2: *Fourier-coefficients for the peak of velocity at the inlet BC*

The velocity condition defined as

$$U(x, z, t) = (1 - \frac{x^2 + z^2}{R^2})V_{peak}(t) \tag{3.2}$$

is applied at each nodal coordinate (x,0,z).

Prescribing a blunt or a parabolic blood distribution at the inlet, with an equivalent mass flow rate, leads to the same observed velocity profile at the outlets. Figure 3.2 reports the velocity along the diameter of the outlet section, corresponding to the ICA.

A previous study by Hoi et al. found that in the carotid bifurcation, the effect of the

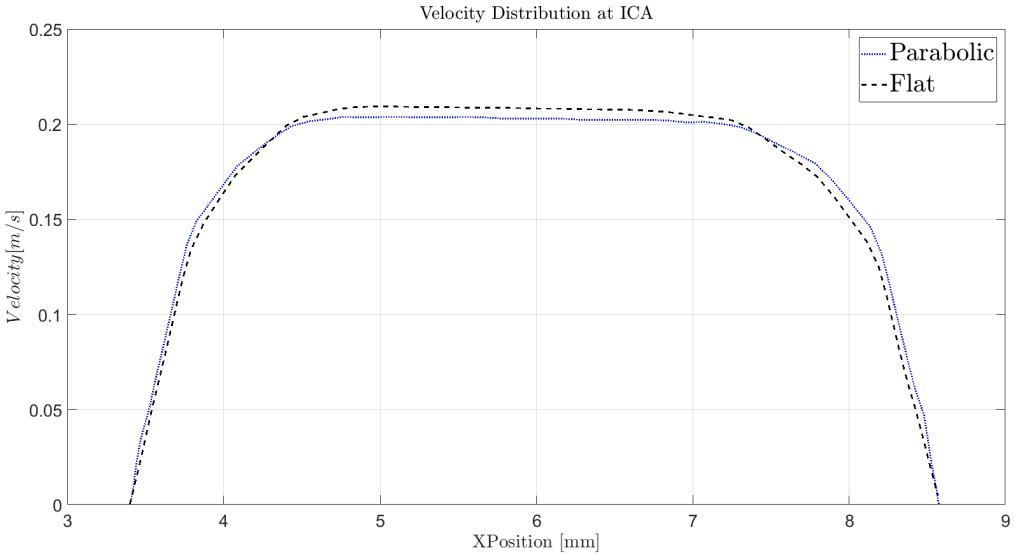

Figure 3.2: *Resulting velocity profile at ICA with parabolic and flat(plateau) velocity distributions at inlet*

inlet velocity distribution is minimal when the length of the CCA is larger than 3 times its dimeter [108]. This is the case in our simulations. As mentioned in Chapter 2, the Womersley number was about 4, closely approximating a Poiseuille flow solution. In the extended analysis by Campbell et al. [98], where Womersley, blunt and parabolic distributions were compared to patient specific data, the parabolic distribution produced the lowest mean error for both WSS and OSI.

An assumption that was made in this work, as well as in the Campbell study, is to consider an axial flow direction during the acquisition of data, through the PC-MRI and when applying the velocity as a boundary condition. Neglecting in-plane velocity components might underestimate the effect of the distribution of the flow on the WSS. Here again the distance between the inlet and the zones of interest is $90 \pm 5mm$, being 15 times larger than the CCA diameter, which is large enough to allow for the establishment of the flow.

3.1.5 Outlet boundary conditions

It is obvious that the pressure applied at the boundary is going to define the behavior of the flow. After testing three different pressure BC's at the outlet, the pressure profiles

have been obtained at the inlet section, which follow the shape of the corresponding pressure imposed at the outlet (Figure 3.3) .

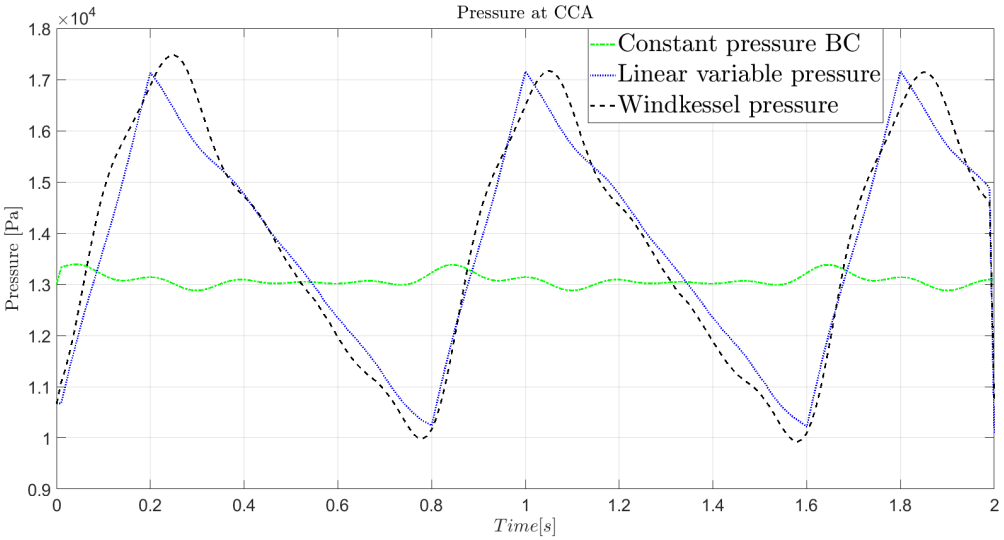

Figure 3.3: *Computed Pressure at inlet boundary during the cardiac cycle for different pressure BC's*

The prescribed pressure at the boundary reflects, as expected, on the flow distribution in terms of flow rate, going through the different branches. To further verify the effect of outlet BC, a comparison study has been performed between the three configurations in terms of mass flow rate in internal and external BCs (Figure 3 4) . The results from constant or linearly variable pressures show a similar distribution of blood flow between the two branches of the CA bifurcation, estimated to 45.5% for the ECA and 54.5% for the ICA. The mean mass flow rate through ICA is 57.87% according to the imagery data and 58.36% resulting from the simulation with Windkessel BC (see Figure 3.4).

In a normal artery, the flow distribution between ICA and ECA is of the ratio (70:30) [109][110]. In our case, due to the presence of the plaque, the normal flow distribution is changed, meaning that less blood is flowing through the ICA.

3.1.6 Summarizing of FLUENT fluid model

The results presented in the following sections were obtained by finite volume method simulations, with the parameters listed below Table 3.3:

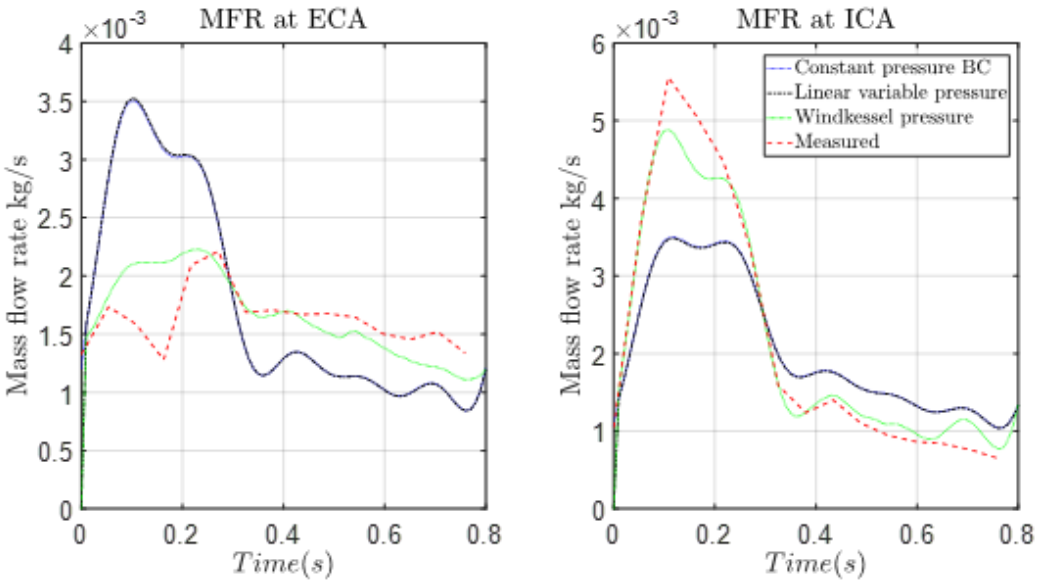

Figure 3.4: *Mass flow rate in internal and external carotid arteries during a cardiac cycle for different pressure BC's in comparison with the PC-MRI measure of mass flow rate*

3.2 Effect of the plaque on the circulation

3.2.1 Velocity

The blood flow rate reduces because of the presence of the atherosclerosis plaque. The Rigid wall simulations estimated a decrease in peak velocity at the ICA with plaque to 20% from the original value. Figure 3.5 presents the computed velocity magnitude at the section with maximum diameter narrowing, compared to the velocity in the same location for the model without the diameter narrowing. The Velocity streamlines in Figure 3.6show the presence of recirculation in the after-plaque area. These disturbances are also found in the bifurcation area, which is a typical location for tissue damage. It is well known that when separation occurs, it produces eddies and vortices.

Solver	Pressure-based		
Solution method	Scheme	PISO	
	Spacial discretization	Gradient	Least square cell based
		Pressure	Second order
		Momentum	Second order Upwind
	Transient formulation	Second order Implicit	
Under-relaxation	Pressure	0.3	
	Momentum	0.7	
Solution initialization	Gauge pressure	10665 Pa	
Time step	0.001s		
Blood model	Viscosity	Carreau model	
	Density	1060 kg/m3	
Inlet boundary condition	Parabolic distribution of the velocity in the inlet section		
	Time dependent		
Outlet boundary condition	0-D Windkessel		
Wall	No-Slip shear wall condition		

Table 3.3: *Recapitulation table of the Simulation configuration*

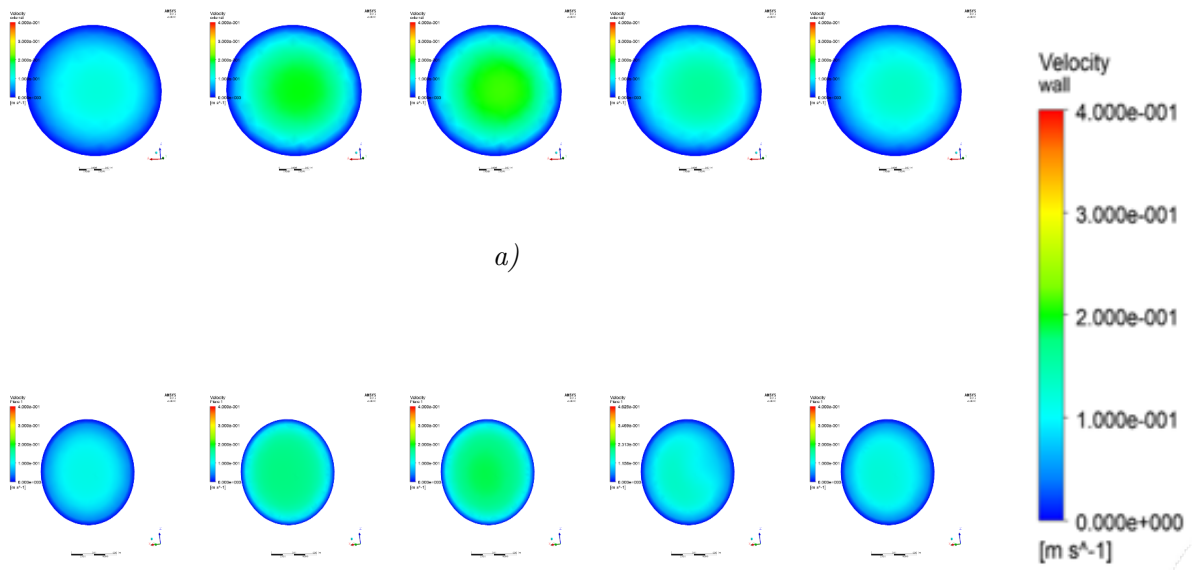

a)

b)

Figure 3.5: *Velocity magnitude distribution in a cross-section located in the plaque area for a) healthy and b) diseased models of the carotid artery at different instants of the cardiac cycle*

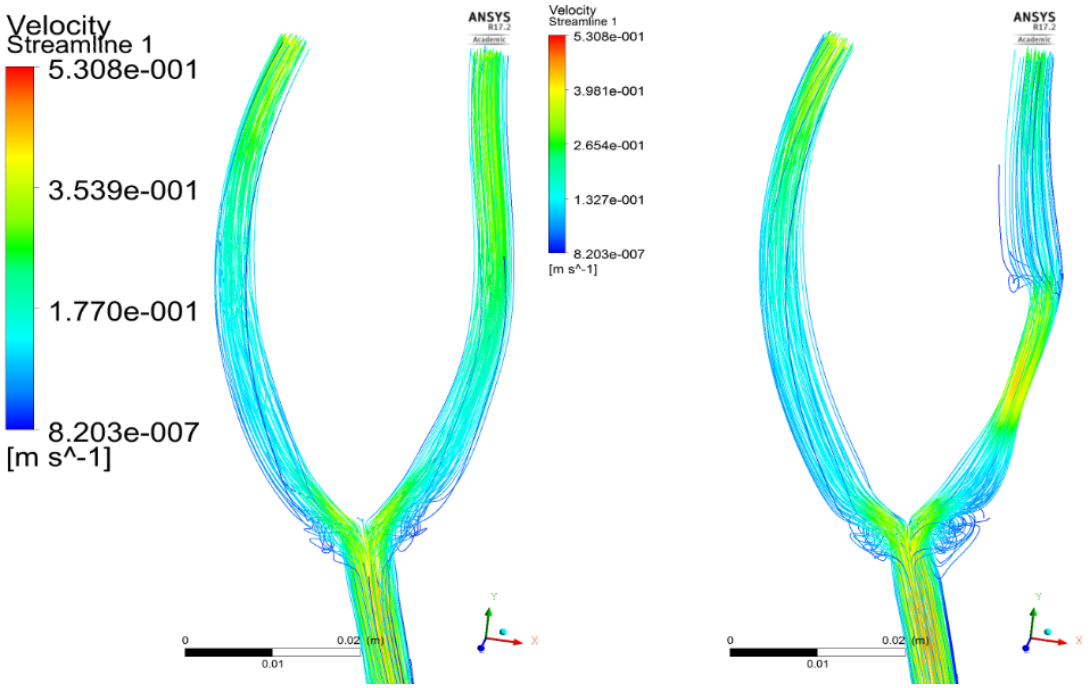

Figure 3.6: *Velocity streamlines during the systolic peak for healthy and diseased carotid models*

The computed velocity at the central section of the artery (Figure 3.6) shows how the fluid flow is disturbed in bending areas. The fluid becomes very slow at the outer walls of the bifurcation. An even slower flow develops at the inner bend of the after-plaque area in the ICA, as shown in Figure 3.7 below at the mid-diastole phase. Clearly, the stenosed artery shows more disturbance when compared with the general behavior of the no-plaque case. Nevertheless, the presence of the plaque in a branch causes higher velocity in the other branch, resulting in less low shear zones.

Keeping in mind the evolution of atherosclerosis plaques, it seemed important to focus on the flow behavior in the above-mentioned area. Figure 3.8 illustrates the behavior of velocity vectors in a section of this area of interest. The flow appears to be more disturbed during the diastolic phase with a very low velocity leading to low shear stresses at the inner bend of the diseased arterial branch.

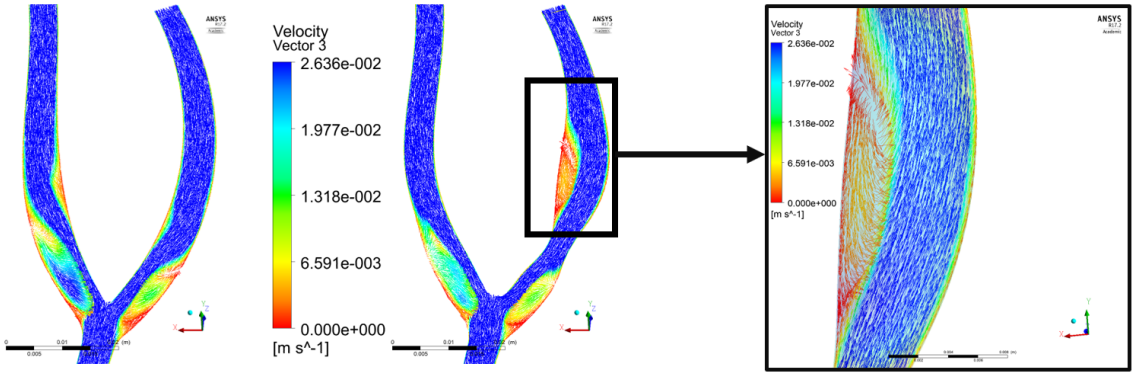

Figure 3.7: *Velocity vectors in the section along the longitudinal direction*

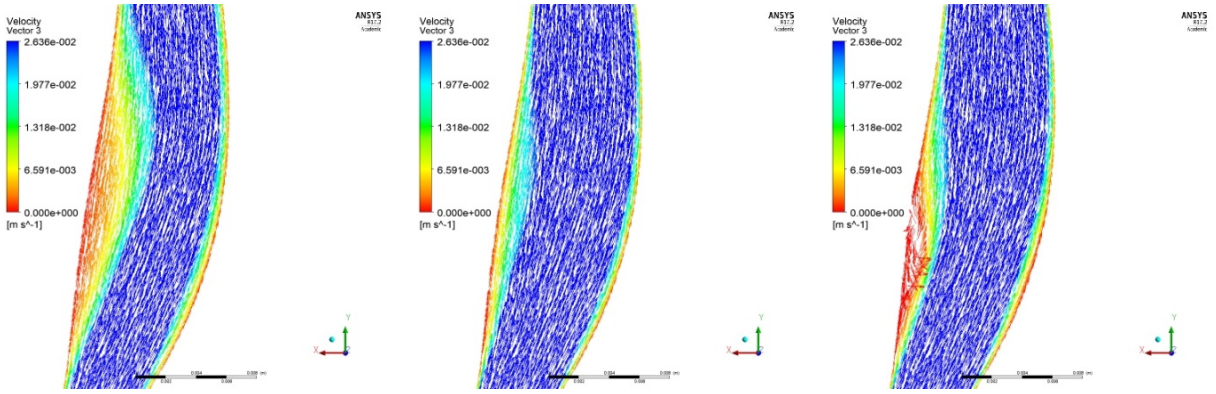

(a) t=0 (b) t=0.1 s (c) t=0.2 s

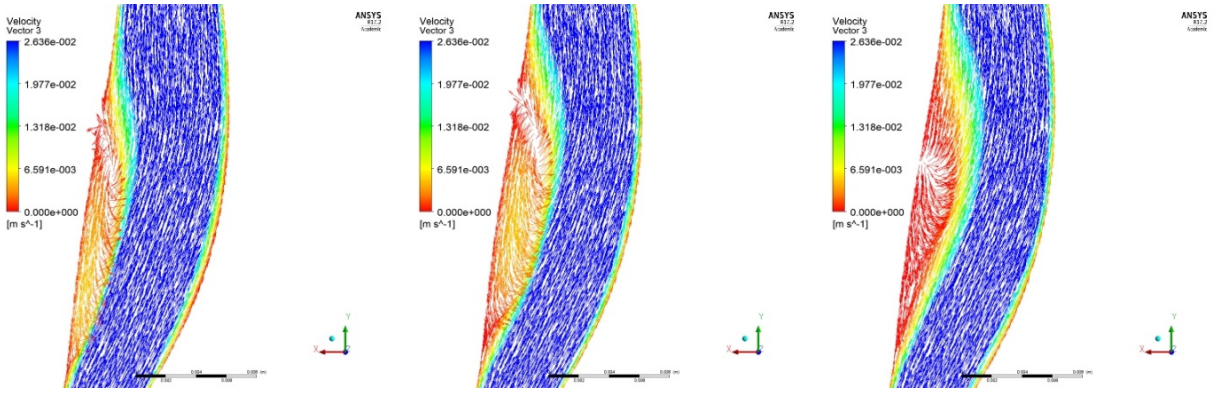

(d) t=0.3 s (e) t=0.4 s (f) t=0.5 s

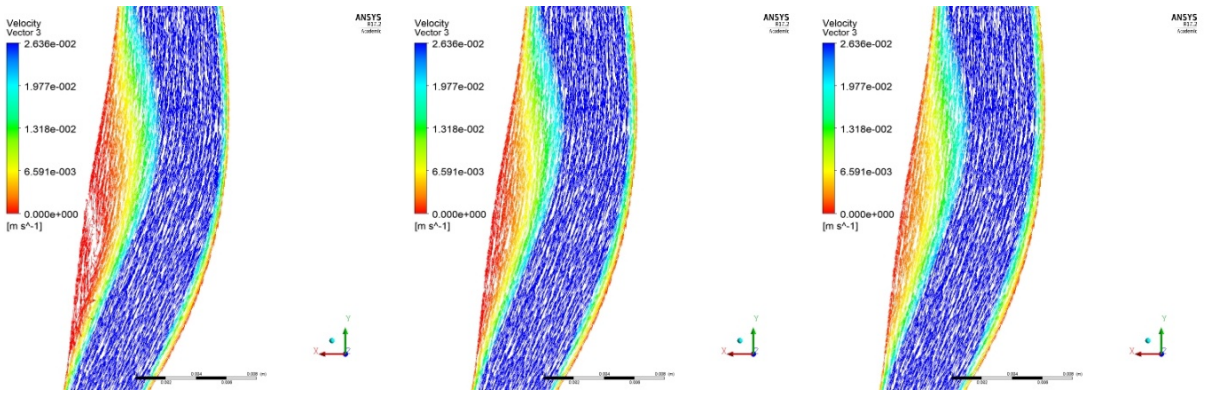

(g) t=0.6 s (h) t=0.7 s (i) t=0.8 s

Figure 3.8: *Velocity vectors in the longitudinal section plane of the after-plaque area for the selected 9 instants in different time points of the cardiac cycle*

Visualizing the in-plane velocities at this location, shows the establishment of a symmetric flow around the centerline of the arterial branch, which is a typical behavior of Poiseuille flows in bends. It means that particles leave the main stream flow to the low shear regions and rejoin afterwards. Figure 3.9 represents the in-plane velocity component in different moments of the cardiac cycle with a helicity value ranging from $0.2m/s^2$ in the mid-systolic phase to $1.5m/s^2$ in the diastolic phase.

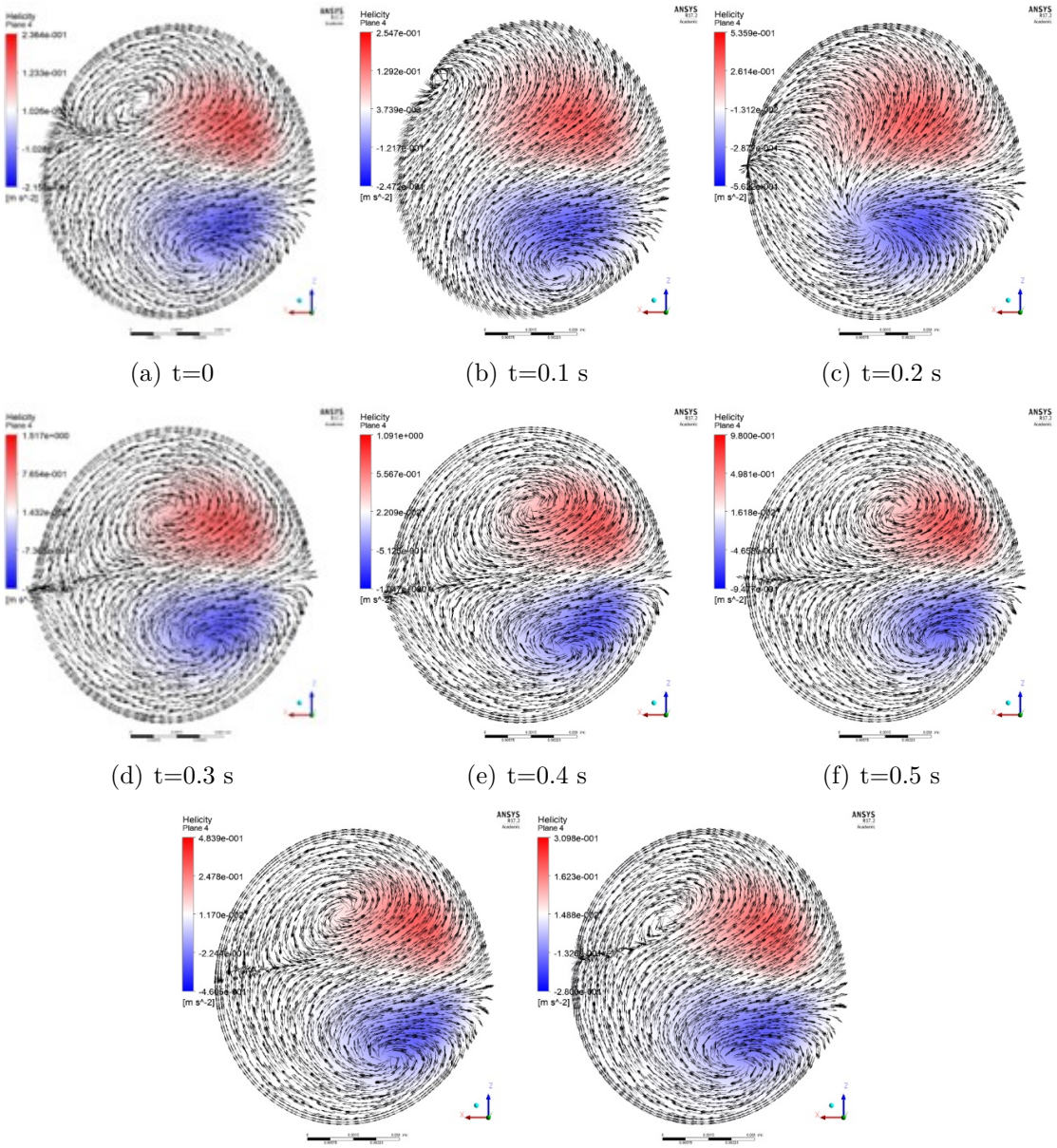

(a) t=0 (b) t=0.1 s (c) t=0.2 s

(d) t=0.3 s (e) t=0.4 s (f) t=0.5 s

(g) t=0.6 s (h) t=0.7 s

Figure 3.9: *Normalized in-plane velocity vectors and computed helicity distribution in the after-plaque region of the diseased CA model*

The presence of the plaque, which creates a very low shear zone, as mentioned before, allows for a higher residency time and makes it difficult for the particle to leave this area. The particles tendency to accumulate in the after-plaque area is enhanced by the presence of the bending and thus, express a higher risk of plaque growth.

3.2.2 Wall shear stress

The regular trend of a shear-thinning fluid flowing through a narrowing area under a pressure gradient effect is the augmentation of the flow velocity in this area, leading to an increase in the WSS. In the case of the CA, Figure 3.10 shows the distribution of WSS during the cardiac cycle and clearly demonstrates the elevated shear stress in the plaque area and low shear stress in the after-plaque area.

Compared to the no-plaque configuration, the WSS at the plaque was 5 times higher during the systolic peak (see Figure 3.11). On the other hand, this value was considerably lower in the after-plaque zone (see Figure 3.12). The profile of the WSS over time in that zone also indicates the presence of oscillations resulting from the flow recirculation.

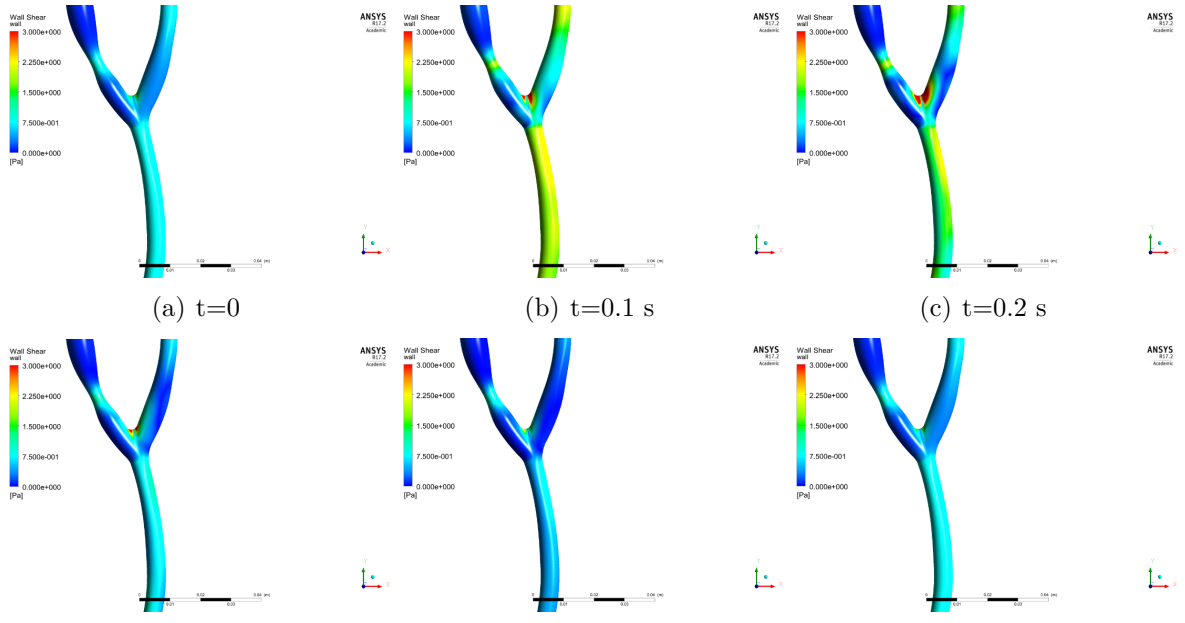

(a) t=0 (b) t=0.1 s (c) t=0.2 s

(d) t=0.4 s (e) t=0.6 s (f) t=0.8 s

Figure 3.10: *Wall shear stress distribution in the carotid bifurcation for different time points of the cardiac cycle*

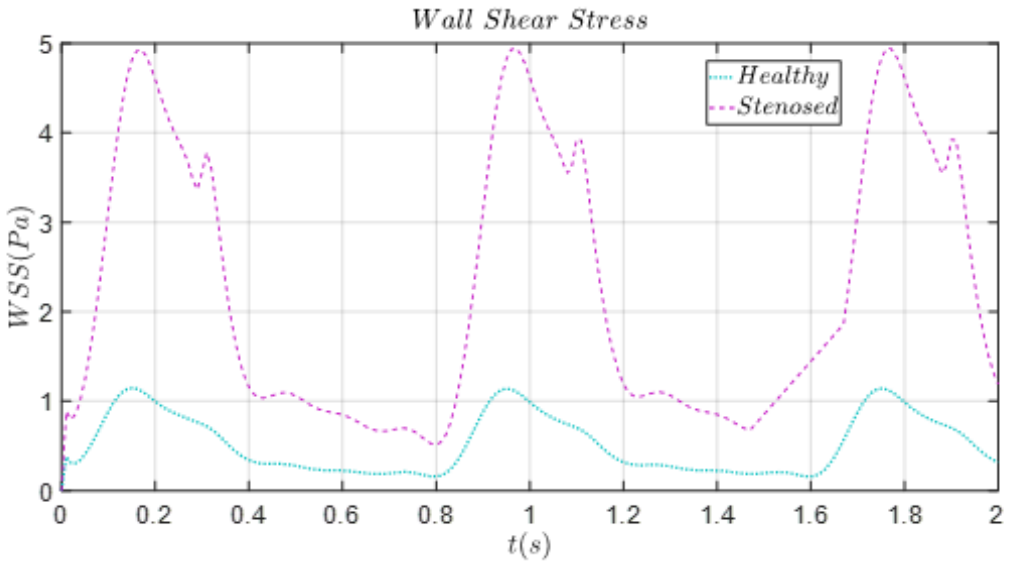

Figure 3.11: *WSS in healthy and stenosed arteries in the plaque region*

The oscillatory shear index (OSI) and the time averaged WSS (TAWSS) was calculated in several following the formulas

$$OSI = 0.5(1 - \frac{|\int_0^T \vec{\tau}|}{\int_0^T \vec{\tau}} \tag{3.3}$$

$$TAUSS = \frac{1}{T}\int_0^T \vec{\tau} \tag{3.4}$$

where $\vec{\tau}$ is the shear vector and T the period of a cardiac cycle. The location of these points is indicated in Figure 3.13.

According to the OSI values which are summarized in Table 3.4, clearly the regions of LWSS show a higher oscillating shear index, due to the recirculation in these areas.

	P1	P2	P3	P4	P5
OSI	9.155E-06	0.363	0.437	1.839E-04	3.634E-03
TAWSS	1.1923	0.0153	0.0078	0.1507	0.6771

Table 3.4: *OSI and TAWSS values at different locations of the CA*

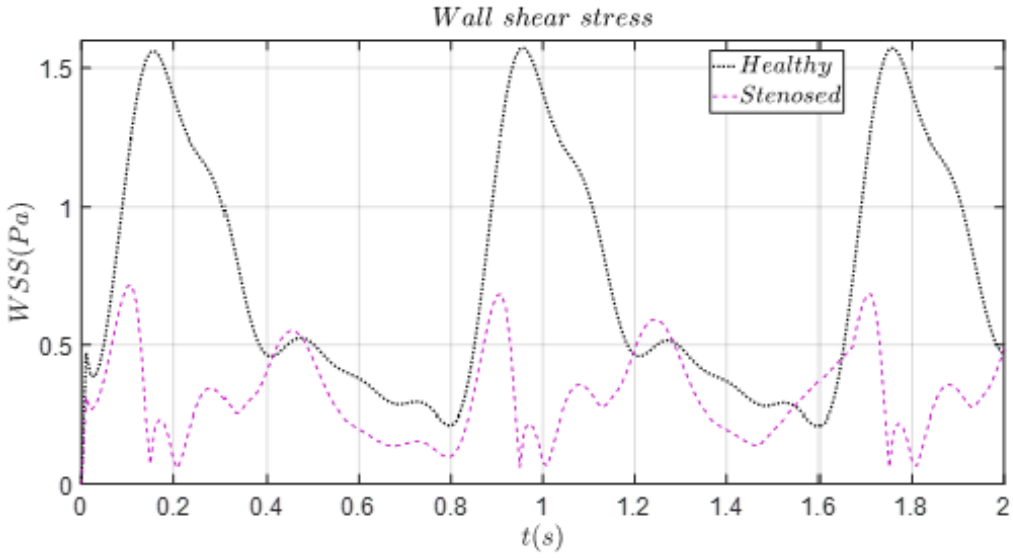

Figure 3.12: *WSS in healthy and stenosed arteries in the after-plaque region*

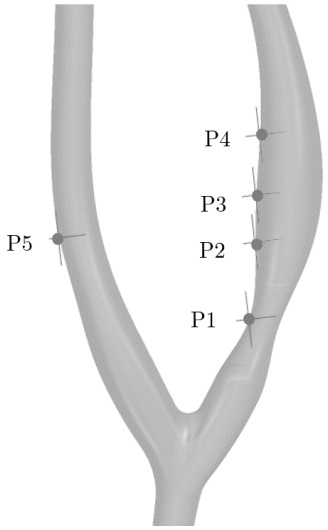

Figure 3.13: *Location of points of interest*

3.2.3 Effect of the diameter restriction on the near wall quantities

To assess the geometrical effect due to the size of the plaque on the variation of the WSS, CFD analysis on the simplified model were conducted varying the diameter of the plaque area from 1.2 to 1.8 mm. In Table 3.5, the values of the near wall quantities in the the plaque and after-plaque areas are reported.

Stenosed lumen	Plaque			After-plaque		
diameter [mm]	OSI	TAWSS	RRT	OSI	TAWSS	RRT
1.20	3.75E-04	3.80E+00	2.63E-01	2.87E-01	4.54E-02	5.16E+01
1.30	6.28E-04	4.00E+00	2.56E-01	2.52E-01	3.99E-02	5.10E+01
1.40	4.19E-04	3.54E+00	2.82E-01	2.50E-01	3.03E-02	6.60E+01
1.50	6.00E-04	2.00E+00	4.68E-01	1.91E-01	2.24E-02	7.20E+01
1.60	8.47E-04	1.67E+00	6.01E-01	1.32E-01	2.69E-02	5.05E+01
1.70	5.79E-04	1.32E+00	7.60E-01	4.67E-01	2.31E-02	6.59E+02
1.80	5.51E-04	1.00E+00	9.19E-01	6.39E-02	3.03E-02	3.80E+01

Table 3.5: *Near wall quantities for simplified model with different stenosed lumen sizes*

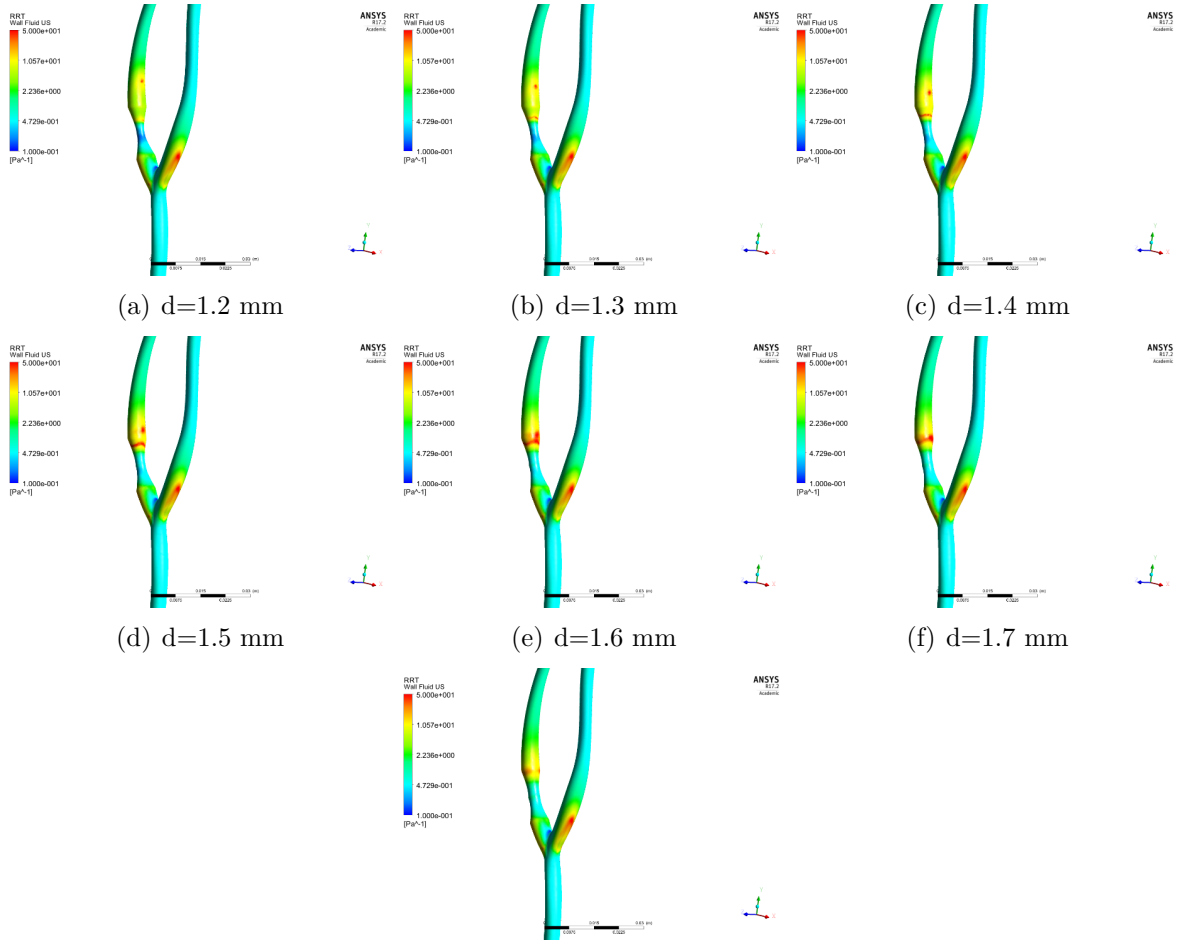

(a) d=1.2 mm (b) d=1.3 mm (c) d=1.4 mm

(d) d=1.5 mm (e) d=1.6 mm (f) d=1.7 mm

(g) d=1.8 mm

Figure 3.14: *Relative Residency Time Near wall quantities for simplified model with different stenosed lumen diameter (d)*

The distribution of the RRT in these cases showed the displacement of the most disturbed area in the after-plaque region. For the least stenosed cases (Figure 3.14 e, f and g) the highest RRT is observed in the plaque area located in the downstream of the branch whereas it is located further downstream the ICA. The presence of the disturbance in the limit of the plaque, an area which is already fragile might be the cause of further growth in cases where the stenosis is assumed less severe.

3.3 Application in the case of patient specific carotid bifurcation

3.3.1 Patient specific geometry and meshing

This section contains the application of the precedent procedure in the case of a patient specific geometry, obtained through the reconstruction of a neck CT-scans (see Figure 3.15). The patient had an atherosclerosis plaque located in the ECA. The degree of stenosis was estimated to 62.44% according to the lumen section narrowing (NASCET system).

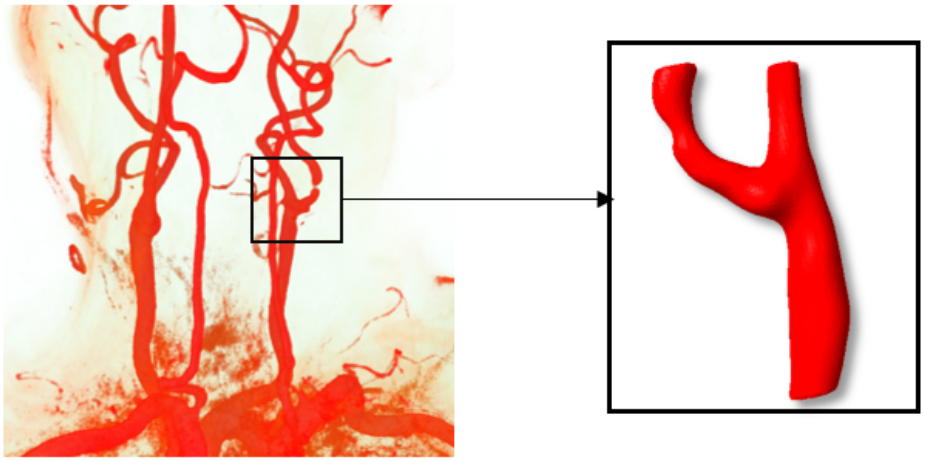

Figure 3.15: *Segmented geometry from CT scans*

At the inlet and outlets of the domain, the geometry was extended by 8 mm, to allow for a flow establishment during the simulation. The choice of tetrahedral mesh (Figure 3.16)

resulted in 1.02E6 elements. The skewness of the elements is reported in Table 3.6.

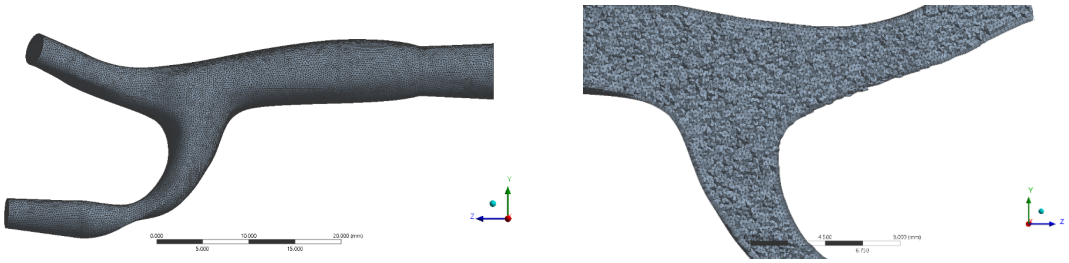

Figure 3.16: *Meshing of the fluid domain of the segmented geometry of the CA*

Type of element	Skewness			
	<0.25	0.25-0.5	0.5-0.75	>0.75
Tetrahedral	4.65E+05	3.01E+05	3.44E+04	495
Wedge shaped	1.55E+05	6.23E+04	1.27E+03	45
	60.78%	35.62%	3.49%	0.05%

Table 3.6: *Skewness of the mesh elements*

3.3.2 Computational fluid dynamics results for patient specific geometry

Blood flow was modeled according to the Table 8 and the vessel wall was assumed rigid. Computational simulation of three cardiac cycles was carried out with a time-step size of 0.001s. Figure 3 16 presents the obtained pressure distribution over the cardiac cycle.

In terms of mass flow distribution between the two branches of the artery during a cardiac cycle, the computed ratio is (0.244:0.756) i.e. a 20% decrease in blood flow going through the stenosed artery, compared to the typical ratio Figure 3.18. This number, which might seem low compared to the degree of stenosis, can be explained by the compliance effect of the downstream vasculature that helps maintaining the flow, but increasing the pressure in the vessel. In fact, the concerned population usually manifest a hypertension problem.

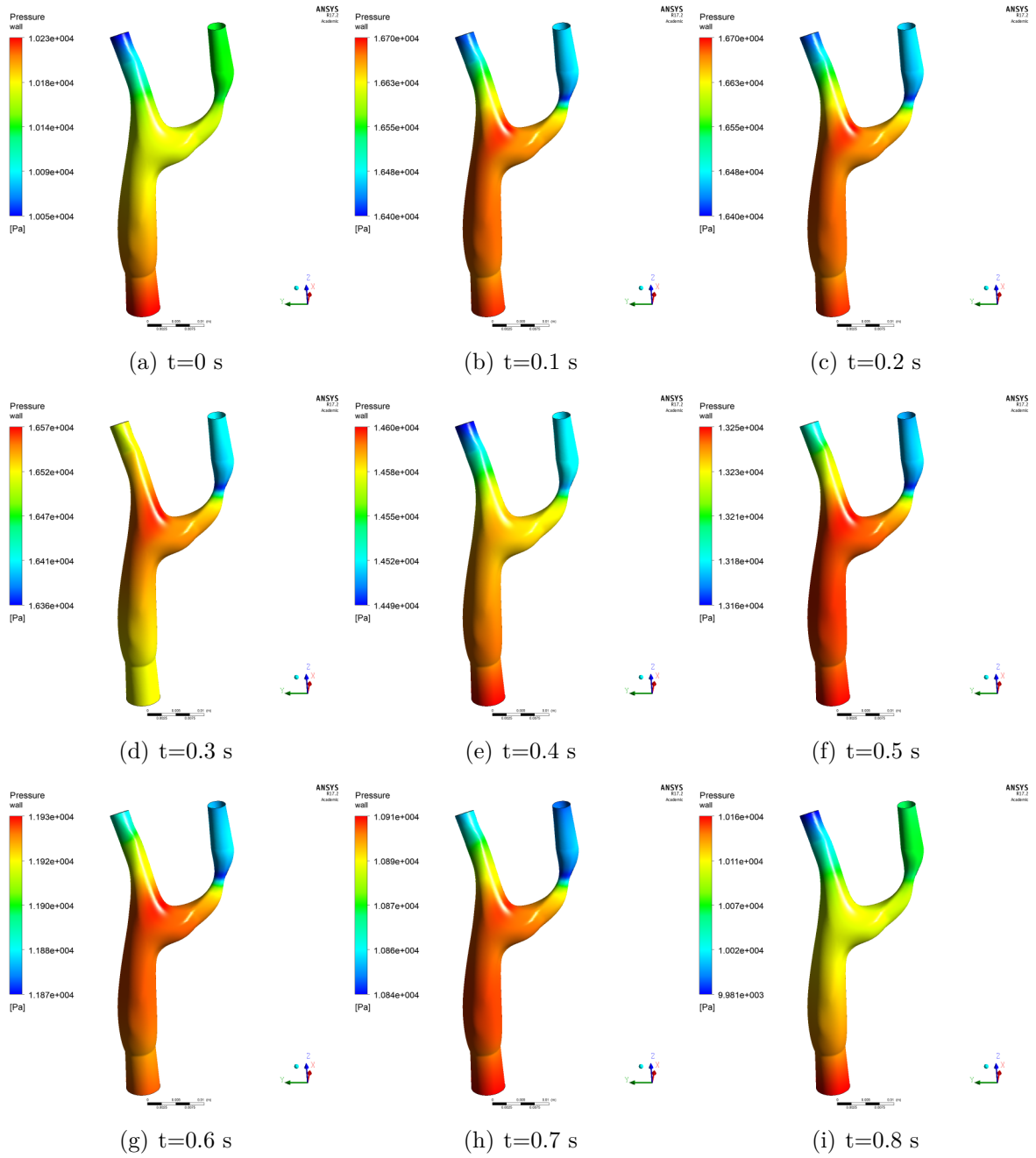

(a) t=0 s (b) t=0.1 s (c) t=0.2 s

(d) t=0.3 s (e) t=0.4 s (f) t=0.5 s

(g) t=0.6 s (h) t=0.7 s (i) t=0.8 s

Figure 3.17: *Pressure Distribution in the fluid domain wall in different time points for the segmented geometry of CA*

Regarding the flow disturbance in the after-plaque region, the in-plane velocities continue to exhibit the helical behavior as for the simplified geometry model. In Figure 3.19, the velocity magnitude is shown in black along with the normalized in-plane vectors of the velocity in red. Clearly, the velocity has lost the parabolic profile and the maximum velocity is in the near inner curvature wall region.

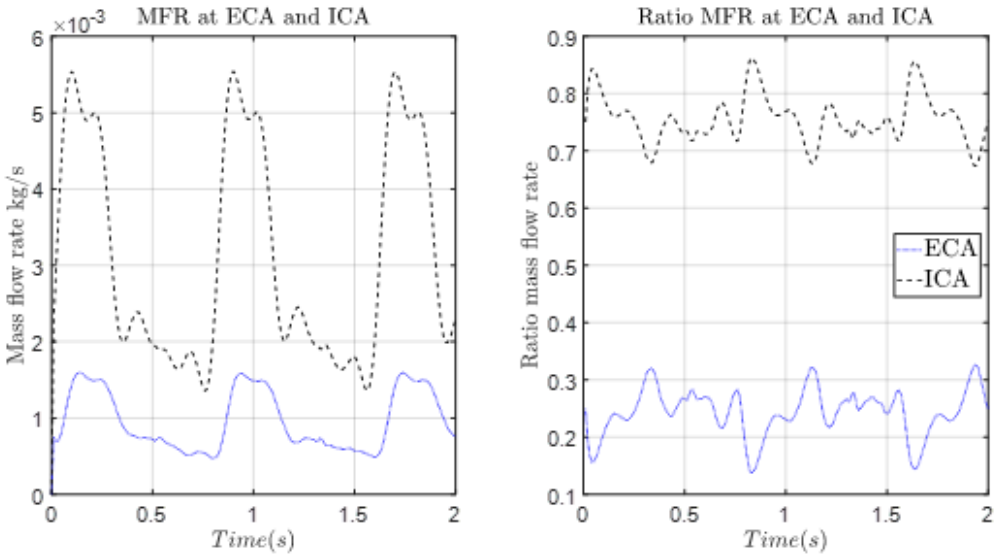

Figure 3.18: *Mass flow rate distribution between internal and external CAs*

3.3.3 Comparison between stenosed artery and a hypothetical healthy arterial model

To examine the effect of the plaque on the dynamics of fluid flow, another simulation was carried out considering a hypothetical healthy artery, obtained from the previous geometrical model by approximating the plaque area with a cylindrical section of the same diameter as the external outlet (Figure 3.20).

The averaged WSS values in the CCA, ranged from 0.01 to 1.02 Pa with an overall spatial and temporal mean value of 0.64 Pa in this area. The difference between both configurations is presented in terms of WSS behavior. The TAWSS index in Figure 3 21 and Figure 3 22 shows an average WSS of 11.9Pa in the plaque region of the diseased artery, compared to 6.9 Pa in the hypothetical healthy one. The value of the WSS during a cardiac cycle in the same region is shown in

Figure 3.21

Computing the time averaged wall quantities, for both stenosed (Figure 3.22) and healthy (Figure 3.23) geometrical models, shows higher oscillations in the after-plaque area and the relative residency time (RRT) 20 times higher in that same region.

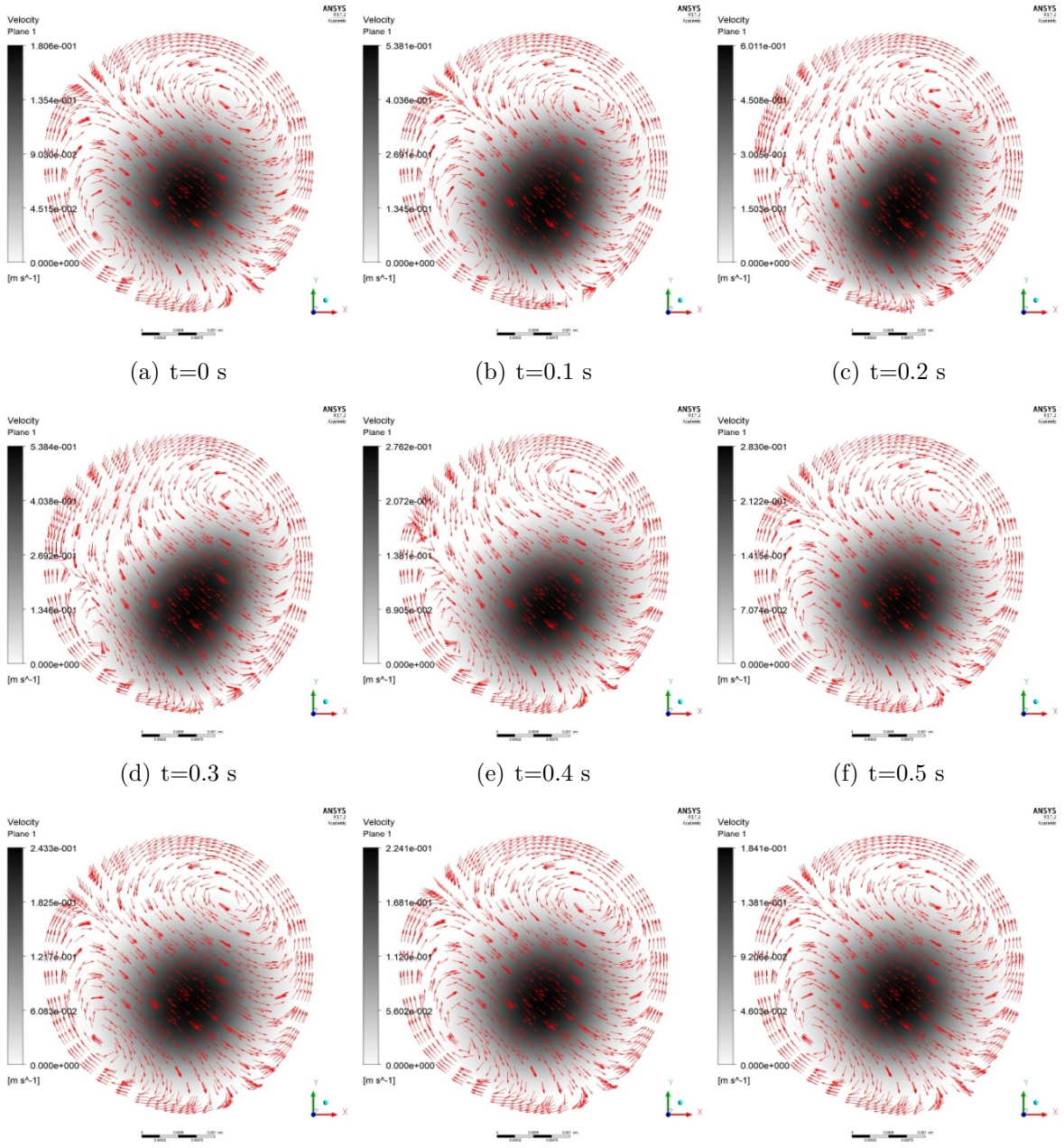

(a) t=0 s (b) t=0.1 s (c) t=0.2 s

(d) t=0.3 s (e) t=0.4 s (f) t=0.5 s

(g) t=0.6 s (h) t=0.7 s (i) t=0.8 s

Figure 3.19: *Velocity magnitude and normalized in plane velocity vectors in a section of the after-plaque region*

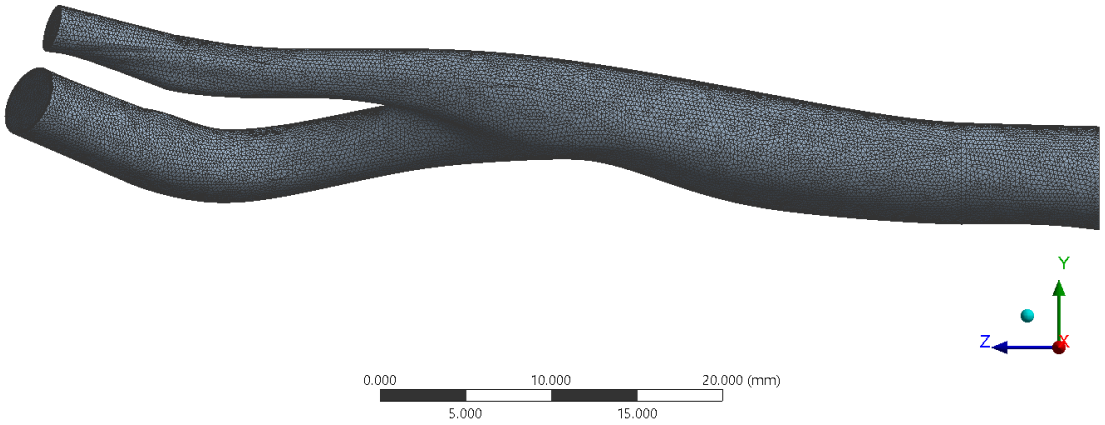

Figure 3.20: *Geometry and finite element mesh of the fluid domain of the hypothetical healthy CA*

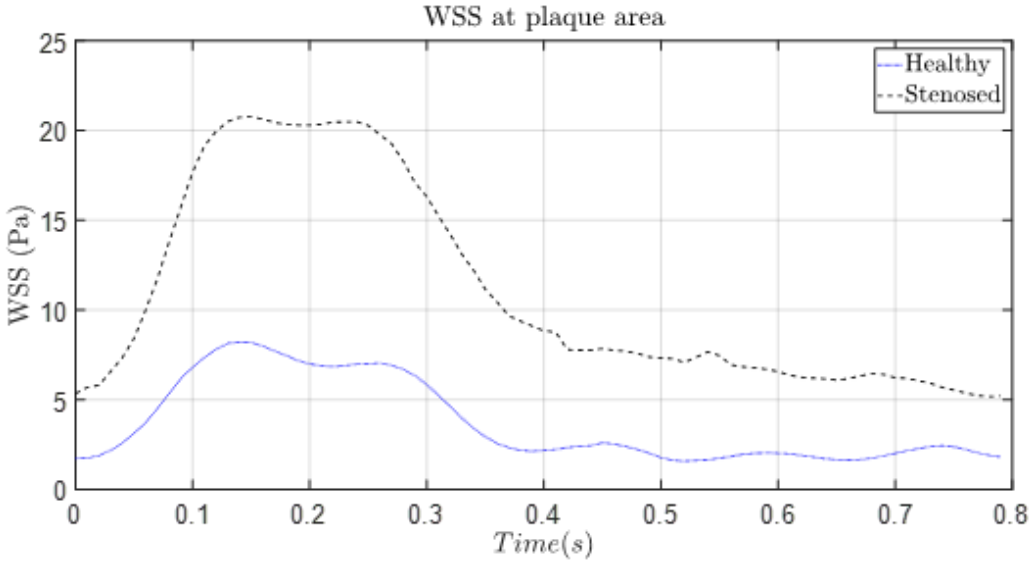

Figure 3.21: *WSS in the plaque region during a cardiac cycle for healthy and diseased carotid arteries*

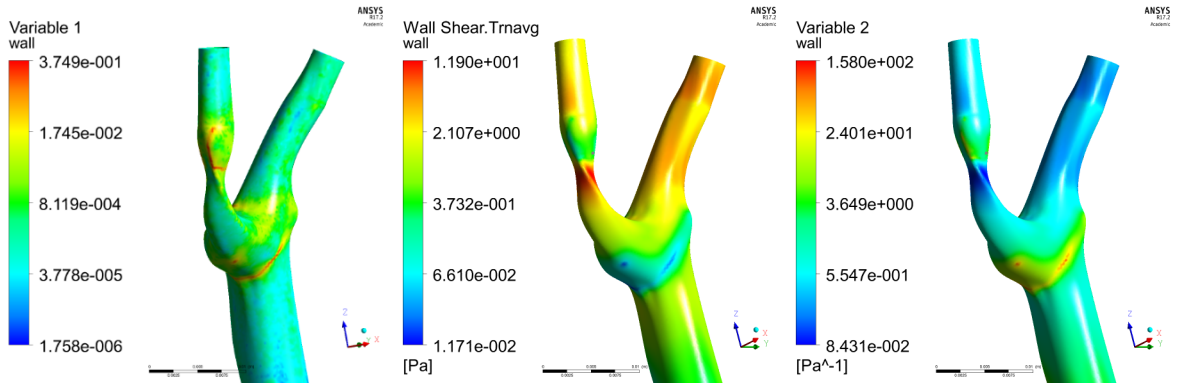

(a) OSI (b) TAWSS (c) RRT

Figure 3.22: *Averaged wall shear indexes for patient-specific carotid model*

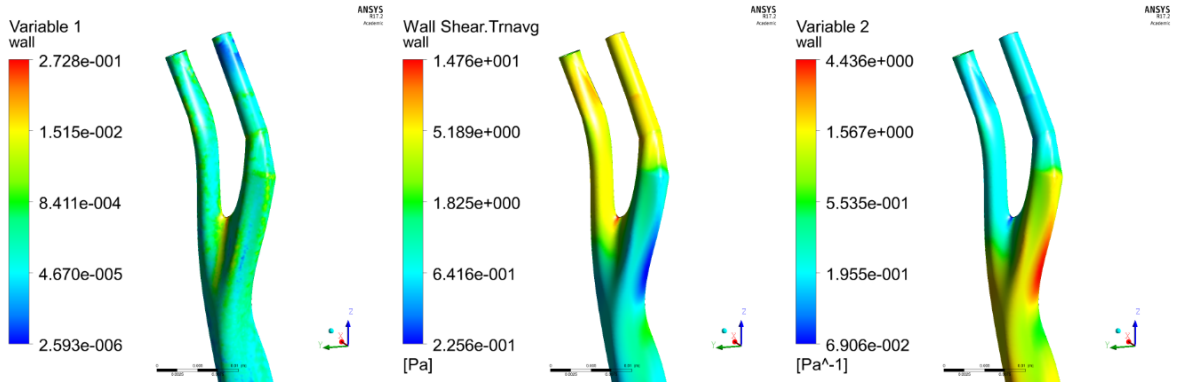

(a) OSI (b) TAWSS (c) RRT

Figure 3.23: *Averaged wall shear indexes for hypothetical healthy carotid model*

The RRT was calculated as following

$$RRT = \frac{1}{(1 - 2 * OSI) * TAWSS} \tag{3.5}$$

3.4 Conclusion and limitations

While using simplified models is a useful approach for having a control over the modeling parameters and analyze the effect of well-defined differences, imagery derived geometries results in more accurate quantitative results. The general behavior of blood flow for both cases shows the disturbance of the flow, due to the presence of plaques. In fact, the plaque causes the development of recirculation areas where the WSS loses its natural behavior by becoming low and oscillatory. This allows for a higher residency time and thus higher probabilities for flow particles to deposit and may cause plaque growth. The main limitation in the case of numerical solving of hemodynamics problems, is the unavoidable errors in obtaining in-vivo data. Actually, a great discrepancy in results of WSS is observed in the literature [111][68][112][113], due to the limited grid size and time step size in the available imagery systems and also due to the approximation in the calculations of the near wall quantities. The improvement of experimental methods or 3D particle tracking velocimetry techniques might offer a better validation tool for CFD studies. In all the models presented in this chapter, the rigid wall assumption was made. Such an analysis, even if it is the most common numerical method in computing blood flow in arteries, gives no indications about the structural behavior of the arterial tissue and its response to flow solicitations. The study of the behavior of the arterial tissue is presented in the next chapter by FSI simulations.

Chapter 4

Fluid Structure Interaction in the Carotid Artery

In this section, the behavior of the carotid artery is investigated. The results of the fully coupled simulations of carotid artery and blood flow are presented. Also, the effect of the plaque presence on the structural deformation, including a preliminary wave frequency analysis, is examined.

4.1 Introduction

Studies on the fluid dynamics of the carotid artery usually assume a rigid arterial wall. This assumption might drastically influence the conclusions about the blood behavior. While the blood pressure causes the artery to deform, the deformation of the artery also affects the fluid flow. To obtain accurate results about the flow condition, a full coupled analysis is necessary. The results from CFD and FSI analyses are here compared for the case of a simplified geometry. Also a study of feasibility in the case of patient-specific geometry was conducted. On the other hand, the presence of atherosclerosis plaque changes the mechanical properties of the artery [114] and thus changes the mechanical response of the system to the blood pressure oscillation. In other words, the transient response in terms of deformation changes when the mechanical properties are altered. In this chapter, the effect of the plaque presence is evaluated by studying the transient deformation of the simplified geometry for both healthy and diseased arteries, with the aim of investigating the possibility of identification of acoustic markers that characterize a diseased artery.

4.2 TWO-ways FSI

The main objective of this section is to evaluate the effect of the fluid-structure coupling on the hemodynamics of the carotid artery. To do so, strong coupling between the fluid and the structural domains is considered.

4.2.1 Simplified model

As explained in Chapter 2, the simplified geometry realized with CAD modeling is used. The fluid model is the same as in section 3.2 and the constitutive model for the structure is presented in section 2.4. For the structural boundary conditions, the extremities of the artery are clamped and an elastic support of 0.001 N/mm3 is applied at the external wall

of the structure. The following simulations was conducted at a time step of 0.01 s and for the duration of 2 s. The same fluid model as detailed in section 3.1.6 is used.

4.2.1.1 Blood flow in deformable simplified artery

Figure 4.1 shows the velocity distributions obtained when considering the artery deformable. The flow separation continues to occur in the bifurcation and after-plaque region as observed in the CFD results. Fluctuations of the flow, although of lower magnitude, remain at those regions, as presented in Figure 4.1.Because of the deformation of the artery we observe a decrease in magnitude velocity compared to the rigid case which over-estimate this flow characteristic.

4.2.1.2 Secondary flow

Secondary flows can be observed by visualizing the velocity distribution in the after-plaque region. This fact is shown in Figure 4.2, where the in-plane velocity vectors in a section perpendicular to mainstream flow is presented. During the first 0.2 s of the cardiac cycle, representing the systolic phase, the in-plane vectors are mainly directed outwards, following the arterial distension. On the other hand, during the diastolic phase the flow rejoins the mainstream. The helicity ranges from 0.015 m/s2 in the systolic phase to 0.318 m/s2 in the early diastole. Clearly the helicity value obtained with FSI simulations is lower compared to the one corresponding to CFD analysis (Chapter 3). This is a consequence of the diminution in the blood flow velocity due to the enlargement of the section.

The obtained WSS in this case is lower than the case with rigid wall (see Figure 4 3). The mean WSS over time in the plaque region is 0.93 Pa, compared to 1.19 Pa obtained using CFD. Thus the ratio WSS-FSI/WSS-CFD is 78% in the high shear regions.

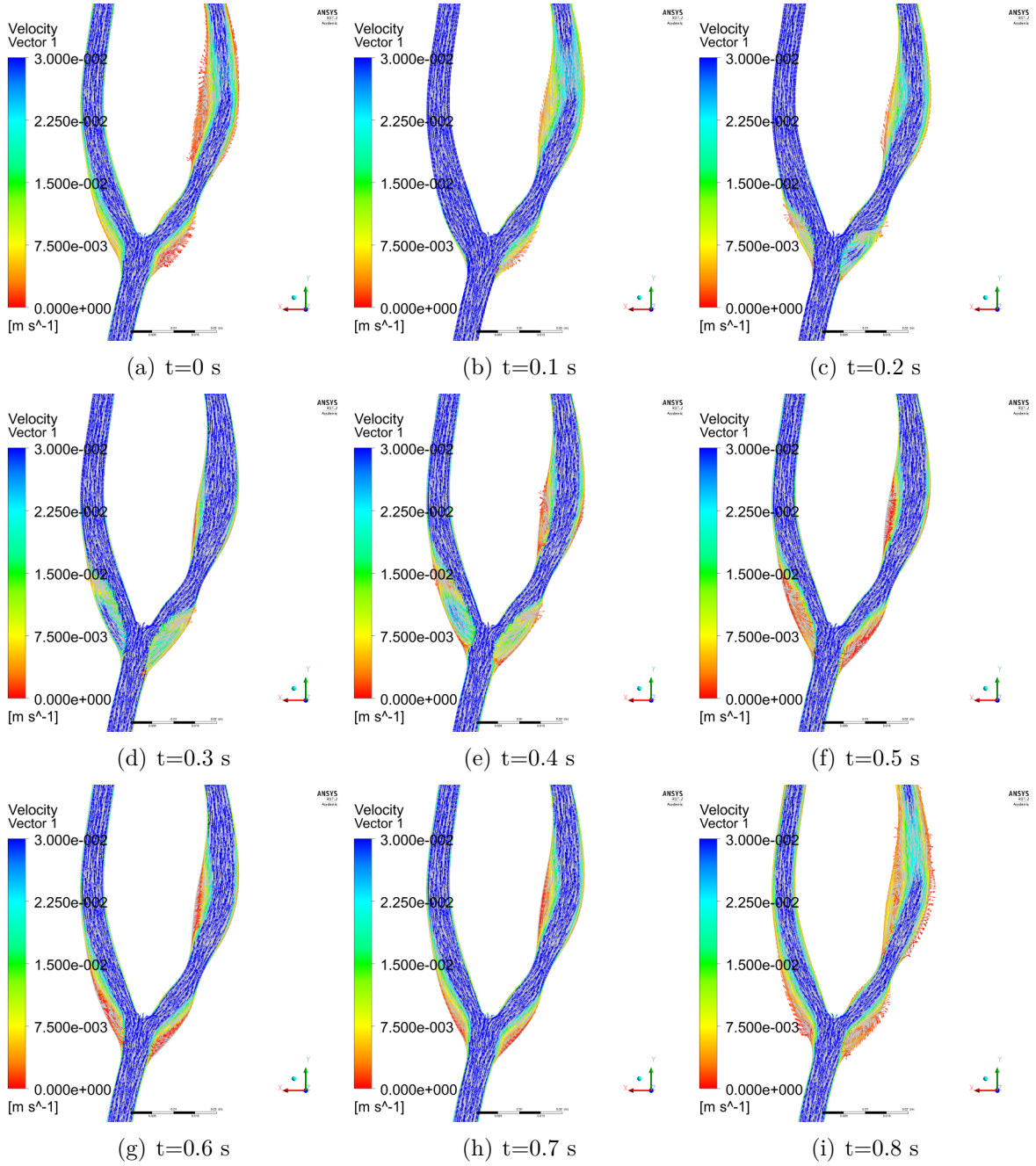

(a) t=0 s (b) t=0.1 s (c) t=0.2 s

(d) t=0.3 s (e) t=0.4 s (f) t=0.5 s

(g) t=0.6 s (h) t=0.7 s (i) t=0.8 s

Figure 4.1: *Velocity distribution in the median plan of the simplified carotid artery during the cardiac cycle*

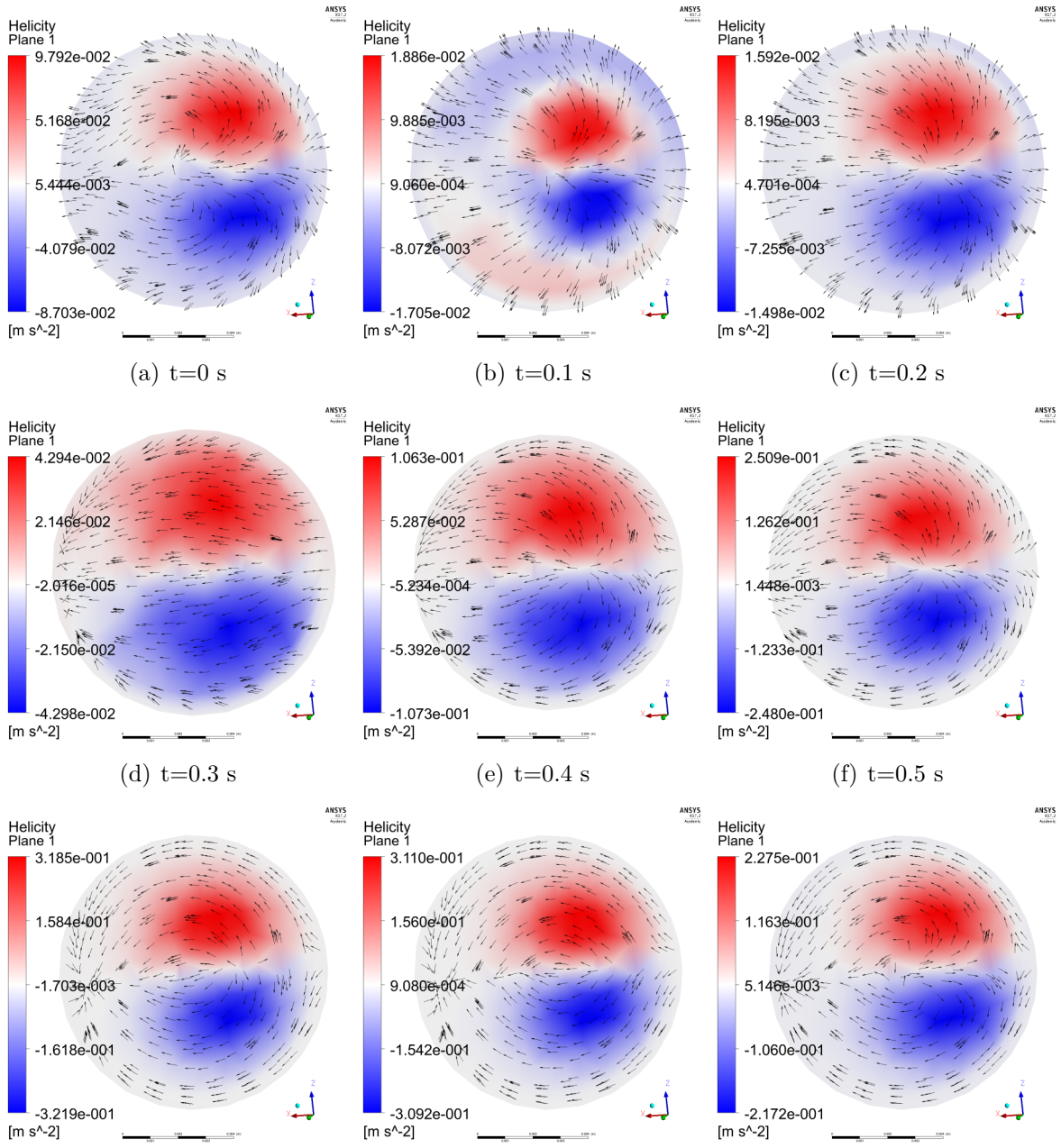

(a) t=0 s (b) t=0.1 s (c) t=0.2 s

(d) t=0.3 s (e) t=0.4 s (f) t=0.5 s

(g) t=0.6 s (h) t=0.7 s (i) t=0.8 s

Figure 4.2: *Secondary flow in the after-plaque area during the cardiac cycle*

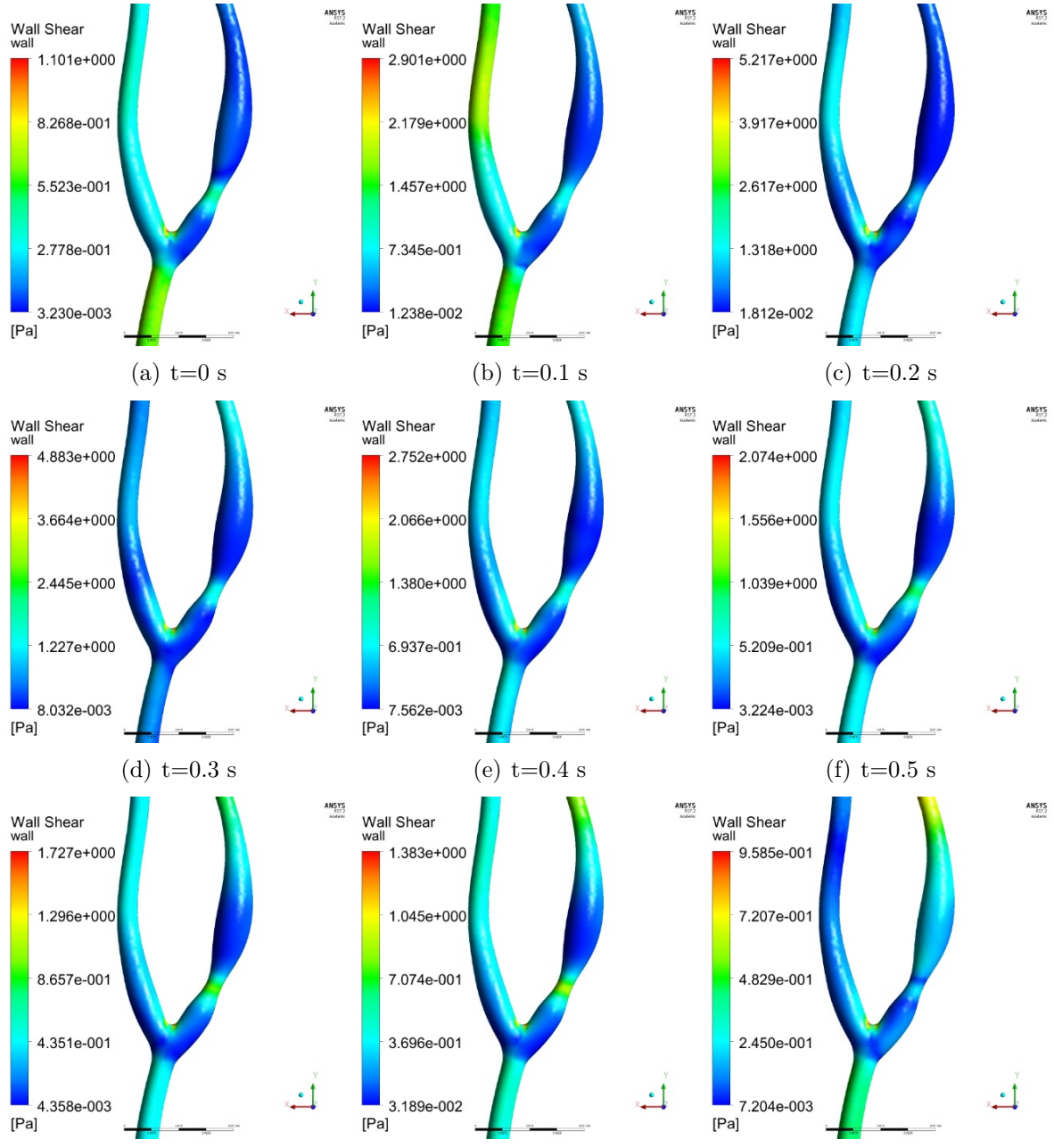

(a) t=0 s (b) t=0.1 s (c) t=0.2 s

(d) t=0.3 s (e) t=0.4 s (f) t=0.5 s

(g) t=0.6 s (h) t=0.7 s (i) t=0.8 s

Figure 4.3: *Wall shear stress distribution in the simplified model of the CA (FSI)*

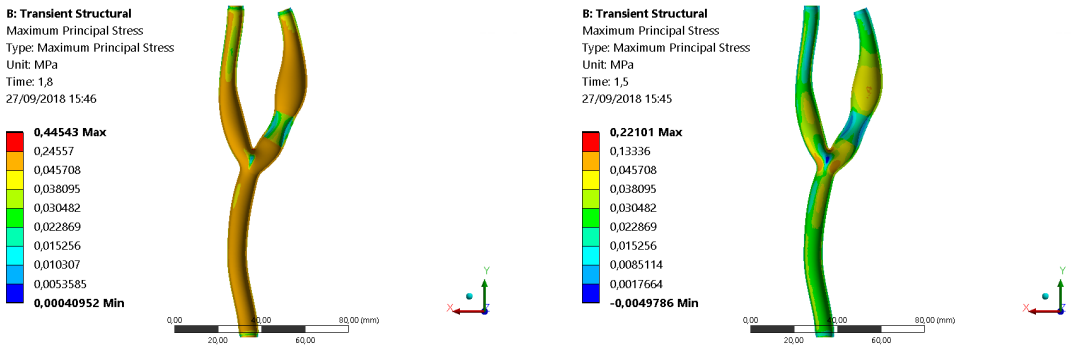

Figure 4.4: *Maximum principal stress of the simplified carotid artery during systole (left) and diastole (right)*

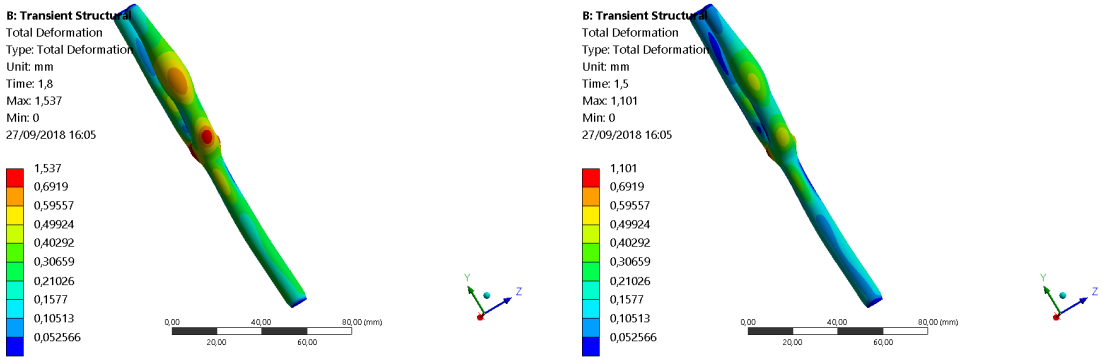

Figure 4.5: *Total deformation of the simplified carotid artery during systole (left) and diastole (right)*

4.2.1.3 Structural response of the simplified arterial model

Conducting FSI simulations provide details about the behavior of the arterial structure. In Figure 4.4, the maximum principal stress distribution during systolic peak and diastolic phase are presented. The arterial wall deformation at the same instants (Figure 4.5) shows an enlargement ranging from 8% to 15% compared to diastolic phase. At the plaque region this ratio falls to 5% due to the stiffening of the artery. This local stiffening could then bring to local higher stress gradients at the plaque borders, for each cardiac cycle.

4.2.2 Applicability of FSI in the case of patient specific models

Lumped Windkessel model has proven to be more accurate for simulating blood flow in the arterial system. Nevertheless, it is a time-consuming method, especially for coupled approaches. To minimize the computational cost, while preserving the realistic pressure

waveform provided by the Windkessel model, the pressure profile obtained using Windkessel model in CFD analysis is applied as a transient pressure outlet in FSI simulations.

The results in this section are obtained using the patient-specific geometry and following the same procedure in section 4.2.1.

4.2.2.1 WSS comparison between rigid and deforming wall configurations

Preliminary FSI simulations in a patient-specific geometry showed similar WSS trends compared to CFD simulations (Figure 4 6). Nevertheless, a tangible difference was observed in the higher shear areas. Many research works were interested in evaluating the comparison between WSS obtained through imagery and the one obtained by finite volume simulations (see Table 4.1). Generally, PC-MRI derived WSS is lower than CFD derived WSS, with highest difference in HWSS zones. This behavior is compatible with the difference observed between FSI and CFD in our model (Figure 4 6 and Figure 4 7).

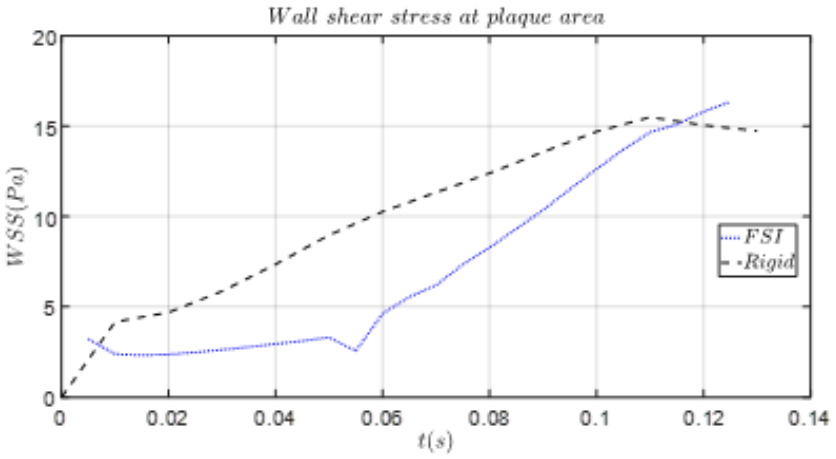

Figure 4.6: *Comparison between CFD and FSI simulations: WSS in the plaque area*

While imagery systems suffer from a limited resolution which affects the estimated near wall velocities, CFD models overestimate the WSS by ignoring the volume change in the fluid domain. Results obtained from FSI simulations can overcome both these drawbacks.

Study	Subject	MRI mean WSS (Pa)	CFD mean WSS (Pa)
Cibis et al. (2014)[68]	14 patients	0.50 ±0.13	0.73±0.25
Cibis et al. (2014)[114]	9 young Volunteers	0.62±0.18	High resolution 0.88±0.30 Low resolution 0.56±0.18
Kohler et al. (2001)[113]	1 in-vitro model	0.66	0.68
Papathanasopoulou et al. (2003)[112]	1 in-vitro model	2.14 (Systole) 0.93 (Diastole)	1.99 (Systole) 0.93 (Diastole)

Table 4.1: *MRI vs CFD comparison studies*

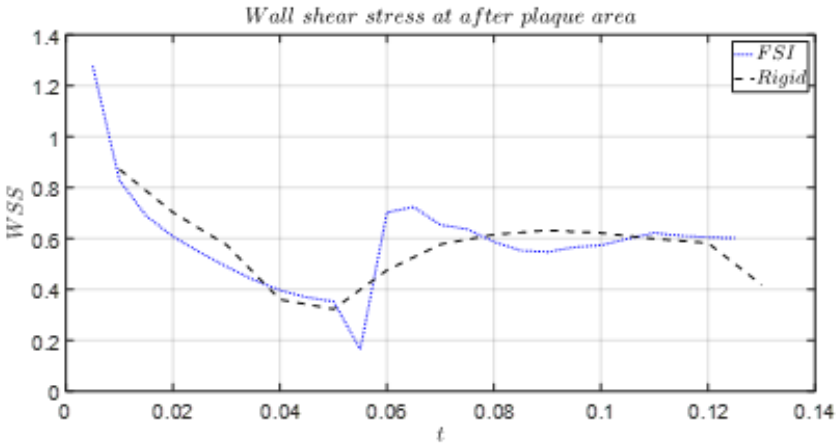

Figure 4.7: *Comparison between CFD and FSI simulations: WSS in the after-plaque area*

4.2.2.2 Structural behavior of the patient-specific geometry

Figure 4.8 shows the total deformation obtained by the simulation with the patient specific geometry based on MRI imagery. Figure 4.9 shows the presence of stress concentration at the upstream region of the plaque, which is usually the area of plaque rupture. This is a direct consequence of both the fluid response and the material property gradients. The highest stress concentration appears at the internal surface of the arterial wall, with a strong stress gradient toward the inside of the wall, where the local stretching of the tissues can favorite the appearing and growth of the plaque.

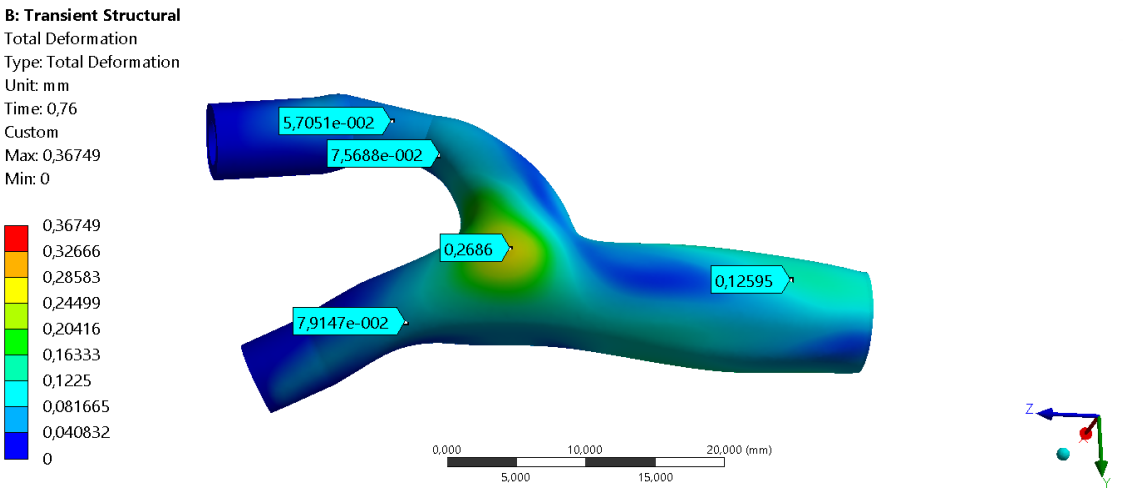

Figure 4.8: *Total deformation of the patient specific geometry*

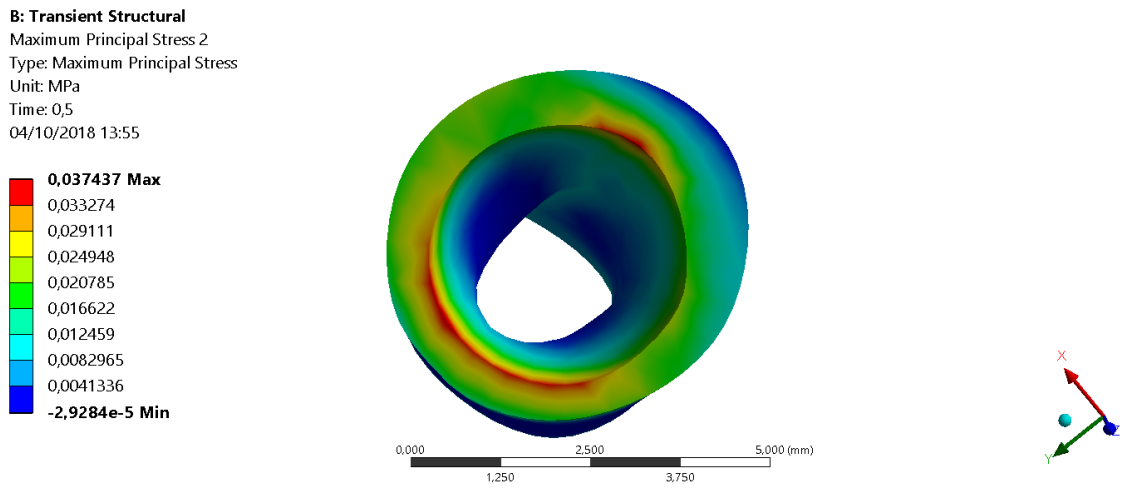

Figure 4.9: *Maximum principal stress distribution in the plaque*

4.3 Assessment of structural vibration

One of the most common approaches in engineering for detecting modifications or defects in structures is the transient response to external excitations. In the case of plaque detection, either an external excitation or the pulse can be exploited for promoting acoustic wave propagation, which, interacting with the structure, can reveal the presence of the plaque. At this aim, the analysis of the vibrational response of the artery, with and without plaque, is here investigated, looking for the acoustic footprint of the plaque within the arterial system. Because the vibrational response is directly related to the geometrical and material properties of the artery, and its interaction with the blood flows, the FSI simulations are needed for the analysis. The 2-way FSI simulations, presented in the previous section, allowed for investigating the role of the quasi-static structural deformation on the simulated flows and WSS. Nevertheless, because of the computational efforts needed for the transient coupled simulations, this section presents preliminary results obtained conducting simulations with 1-way fluid structure interaction, which are a first attempt to verify differences in the vibrational response of the artery, due to the presence of the plaque.

4.3.1 Structural model description

The arterial wall was modeled as a 1mm thick layer starting from the fluid geometrical models cited in Chapter 2. Besides, the atherosclerosis plaque was modeled by subtracting the fluid geometry of a diseased artery from the healthy one, performing a basic Boolean operation. The use of CAD geometry is useful to pin the geometrical effects down.

The material of the arteria wall has been considered as isotropic and homogeneous. In order to decouple geometrical and material effects, as for the mechanical properties, three configurations were taken into account:

- Carotid without plaque: in this case the arterial tissue is considered hyperelastic.
- Carotid with hyperelastic plaque: In this case the plaque is supposed to be of the same material as the arterial tissue. In other words, the structural model is considered homogenous.
- Carotid with elastic plaque: in this configuration, the plaque is considered elastic and the arterial wall hyperplastic.

Following the procedure explained in Chapter 2, the blood flows are simulated numerically. The obtained pressure at the wall of the fluid domain is then applied to the structural inner wall.

In this case, to evaluate the behavior of the arterial wall, the deformation of the wall is simulated under the effect of the blood pressure, without considering the impact of volume changes on the pressure distribution. To this end, the displacement of 14 nodes uniformly distributed along the wall as shown in Figure 4.10 was investigated. Figure 4.11 shows the time variation of the radial displacement of the selected nodes during the simulated cardiac pulse. All the signals have been plotted, from the bottom to the up of the figure, in order to follow the time response of the artery along its length. The bold curve corresponds to the vibrational signal calculated at the position of the plaque.

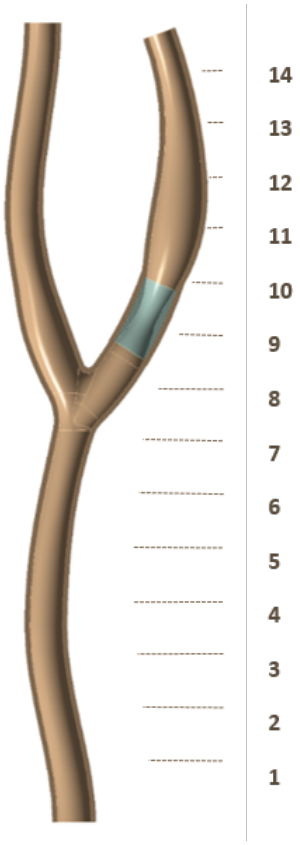

Figure 4.10: *Position of the nodes of interest*

A difference in the displacement amplitude is observed between 'before' and 'after' the bifurcation. While a comparable systolic displacement of 0.25 mm is observed for healthy and diseased carotids in sections located before the bifurcation corresponding to a diameter enlargement of 0,5 mm (9%), the after-plaque area shows a lower displacement for arteries with occlusion (see Figure 4.12). The presence of the plaque, either elastic or hyperelastic, seems to decrease the deformation energy (amplitude) of the artery wall over the plaque position. This variation could be due either to a variation of the blood flows inside the artery or to a diffractive effect of the plaque on the propagation of the wall deformation.

When looking at the signals in Figure 4.12, higher frequency components can be observed within the deformation signals. These components are due to the structural and fluid response of the artery to the pulse, and could give meaningful information on the presence of the plaque, which is a modification of the structure itself. For this reason, the signal have been filtered with an high pass filter, in order to filter the pulse and highlight the

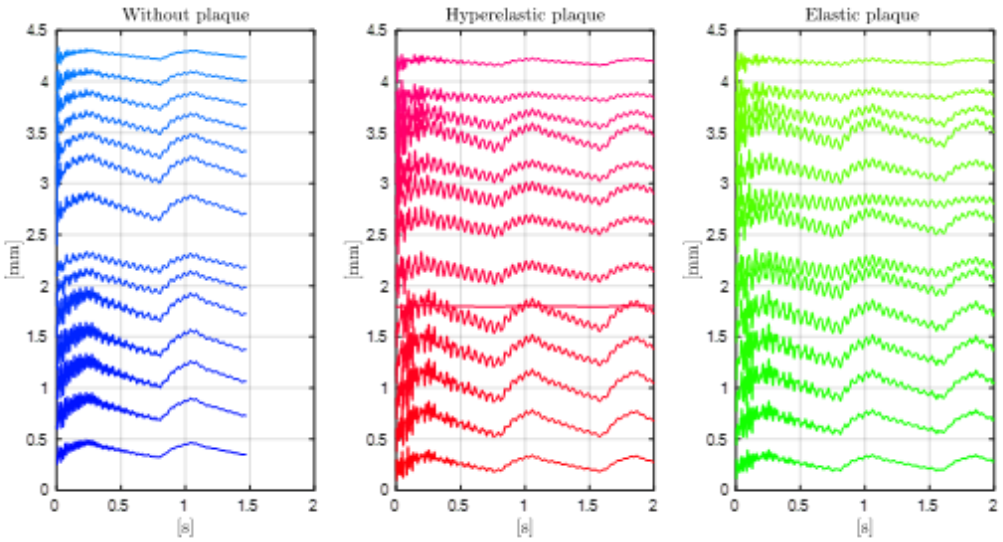

Figure 4.11: *Displacement of the nodes of interest during the cardiac cycle*

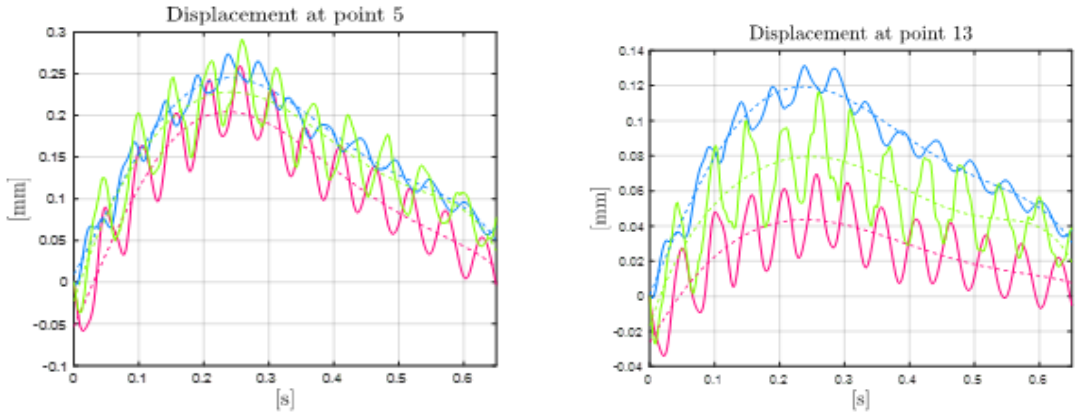

Figure 4.12: *Displacement of CCA(node 5) and ICA(node 13)*

higher frequency content of the signals.

Then, after applying a 30 Hz filter for the displacement signal (see Figure 4.13), beats of the signals can be observed in the case of diseased artery, for both hyperelastic and elastic plaque. The presence of beats can be associated to the appearance of further frequency components in the deformation signals, due to the presence of the plaque.

In order to investigate modification of the frequency content of the signals, due to the presence of the plaque, the FFT of the signals have been performed. Figure 4.14 shows the FFT of the deformation signals calculated in the three different configurations. The analysis of the spectra highlights four main frequencies (see Figure 4.14):

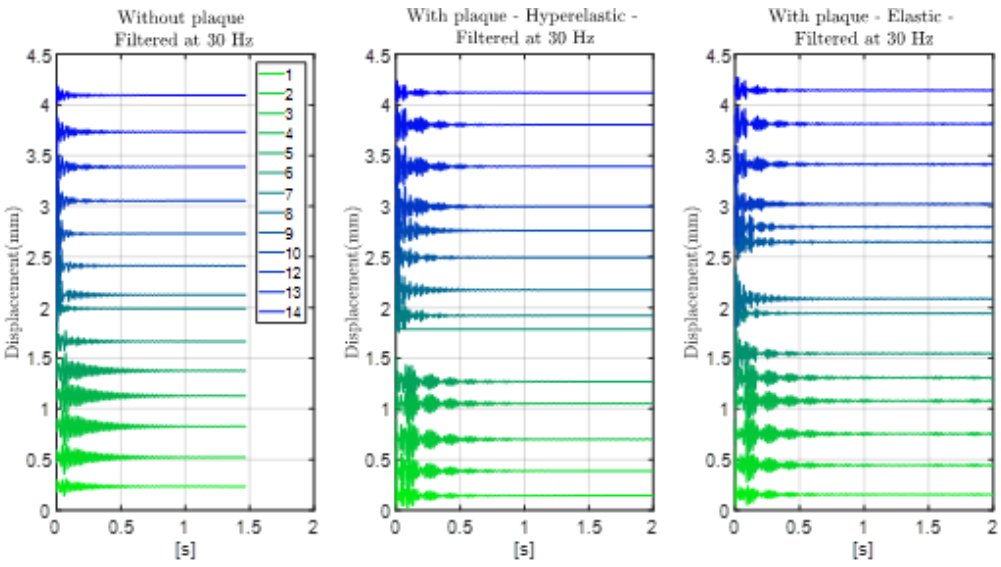

Figure 4.13: *Filtered displacement at 30Hz for the three configurations*

- 1 Hz: corresponding to the pulse wave frequency
- 18-22 Hz: Corresponding to the first mode of vibration of the structure
- 42-50 Hz: Corresponding the second mode of vibration of the structure
- 60 Hz: This mode can only be distinguished in the case of occlusion

The role of the structural dynamic response on the transient deformation of the artery is evident. The appearance of higher frequency content over 50 Hz is observable with the presence of the plaque, both elastic and hyperelastic. The higher frequency contributions explain the occurrence of the beating in the time signals in Figure 4.13.

Figure 4.15 shows the spectrogram of the radial transient deformation of the artery calculated after the plaque area, at point 12 in Figure 4.10. On the left, the signal calculated without plaque; while on the right is the one calculated with the presence of the plaque.

In order to highlight the frequency content of the signals, Figure 4.16 shows the same spectrograms, where each FFT (vertical line) has been normalized with respect to the maximum of the FFT calculated at each time interval (x axis). In such a way the frequency content during the whole time interval is highlighted.

The normalized spectrogram of the signal with plaque reveals the presence of further fre-

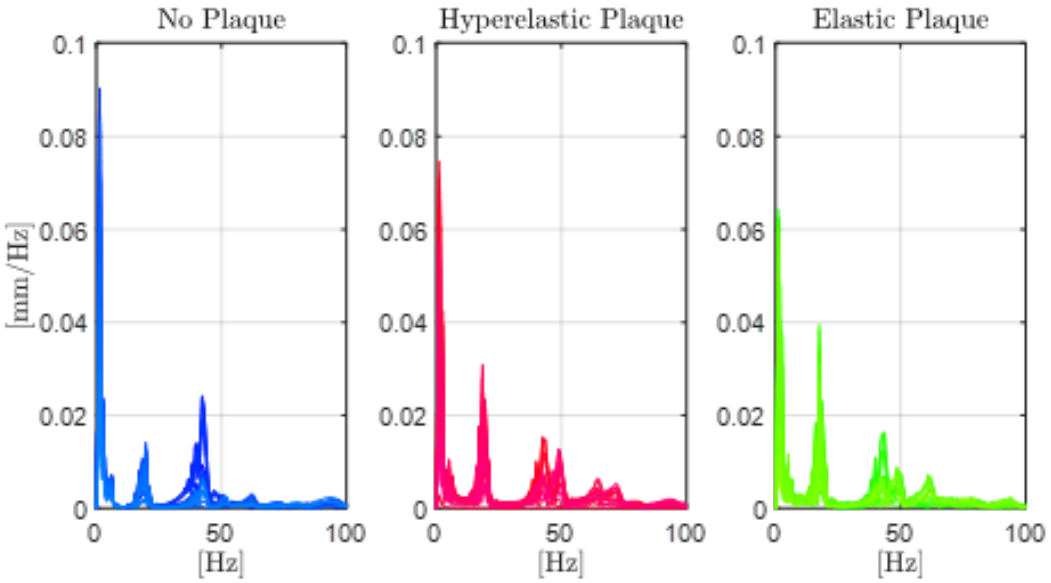

Figure 4.14: *Fourier transform of the total displacement for the different configurations*

quency components, which are at the origin of the beating in the time signals with plaque of Figure 4.13. Looking at the normalized spectrograms calculated for a point before the plaque area (point 4 in Figure 4.10), it is possible to notice as well the appearance of a further frequency content when the plaque is present on the artery (right plot in Figure 4.17).

It is interesting to notice that while the reduction of the amplitude of the low frequency oscillations due to the pulse (Figure 4.13) is appreciated only after the plaque, the further frequency content is observed both before and after the plaque. This difference could be related to the origin of the variations observed in the signal components with and without plaque:

- the reduction of the pulse amplitude, noticed after the plaque (Figure 4.13), is probably related to the modification of the blood flows due to the plaque presence;
- on the contrary, the further frequency components observed in the spectrograms (Figure **??**) are due to the structural response of the artery to the pulse excitation, and irradiate both before and after the plaque.

From the results of the simulations, it is clear that the transient response of the artery

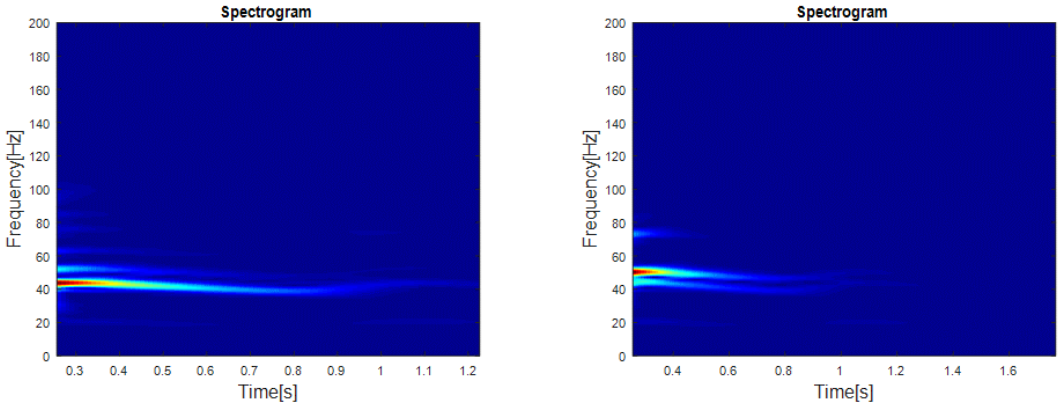

Figure 4.15: *Spectrogram of the deformation of a point AFTER the plaque area (point 12 in Figure 4.12), calculated WITH (left) and WITHOUT (right) plaque*

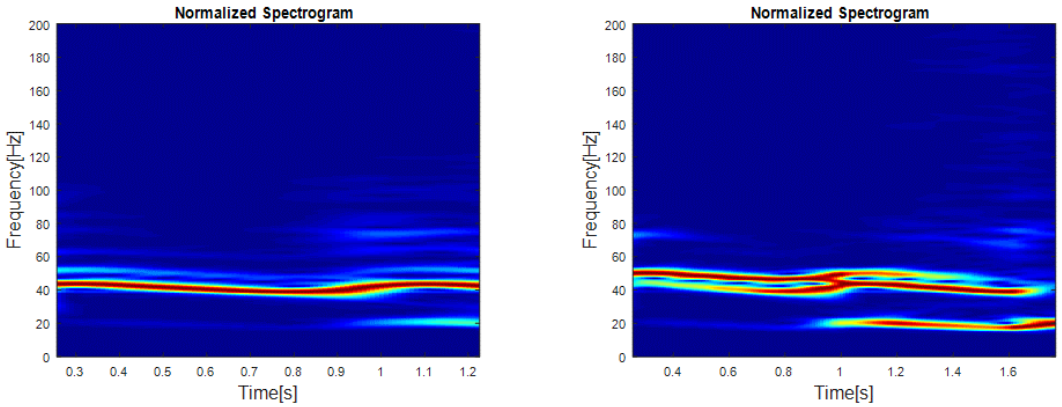

Figure 4.16: *Normalized spectrogram of the deformation of a point AFTER the plaque area (point 12 in Figure 4.10), calculated WITH (left) and WITHOUT (right) plaque. The spectrum is normalized at the maximum of each time FFT*

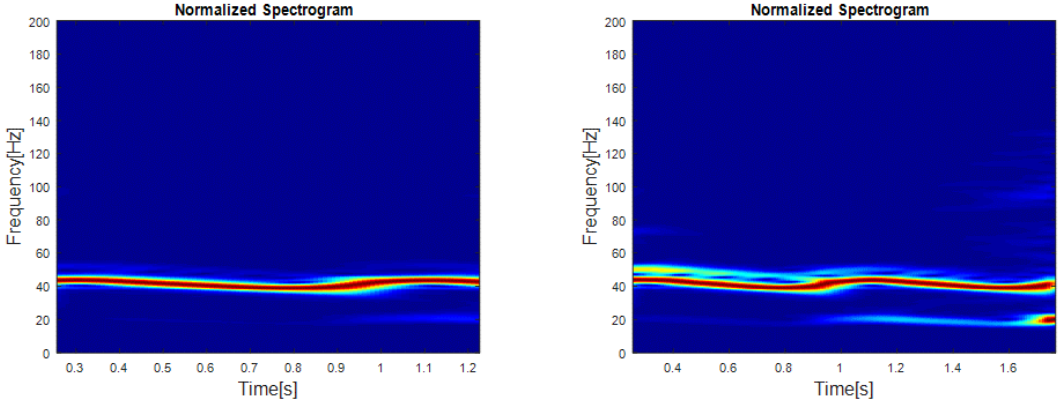

Figure 4.17: *Normalized spectrogram of the deformation of a point BEFORE the plaque area (point 12 in FiFigure 4.10), calculated WITH (left) and WITHOUT (right) plaque. The spectrum is normalized at the maximum of each time FFT*

changes when the plaque is introduced. The vibrational response and its frequency content varies as well when the mechanical properties of the plaque are altered.

The strength of this model resides in its flexibility. By varying the Young modulus of the plaque we can simulate the effect of plaques with different calcification levels. With the appearance of studies that correlate the grey scale and the mechanical properties of the atheroma, and with the increasing availability of PC-MRI data, the present model offers then the possibility to provide full patient specific results.

4.3.2 Effect of the Elastic support

From the showed results, the role of the structural dynamic response of the artery on the carotid behavior is evident. This means that a correct simulation needs the introduction of realistic structural boundary conditions as well as correct mechanical properties of the tissue.

In order to investigate the role of the surrounding media in the carotid vibrational(acoustic) response, an elastic support of 0.001 N/mm3 was added as a boundary condition at the outer layer of the carotid structure. In Figure 4.18 and Figure 4.19, the radial displacement of certain nodes at the outer wall of the diseased branch is presented, with and without elastic support respectively. Considering the elastic support allows for suppressing some frequencies of the artery acoustic response, which were linked to different boundary conditions of the artery itself.

In fact, the investigation of the modal response of both configurations, i.e. with and without elastic support, shows the presence of modes at low frequencies in the case of artery with no external support (Figure 4.19 and Figure 4.21).

Another point to be established is the effect of the boundary conditions at the outlets and inlets, and the length of the considered artery section. The modal response is sensitive to the boundary conditions applied to the arterial extremities. Considering clamped BC's rigidifies the structures leading to higher modal frequencies. This was observed while

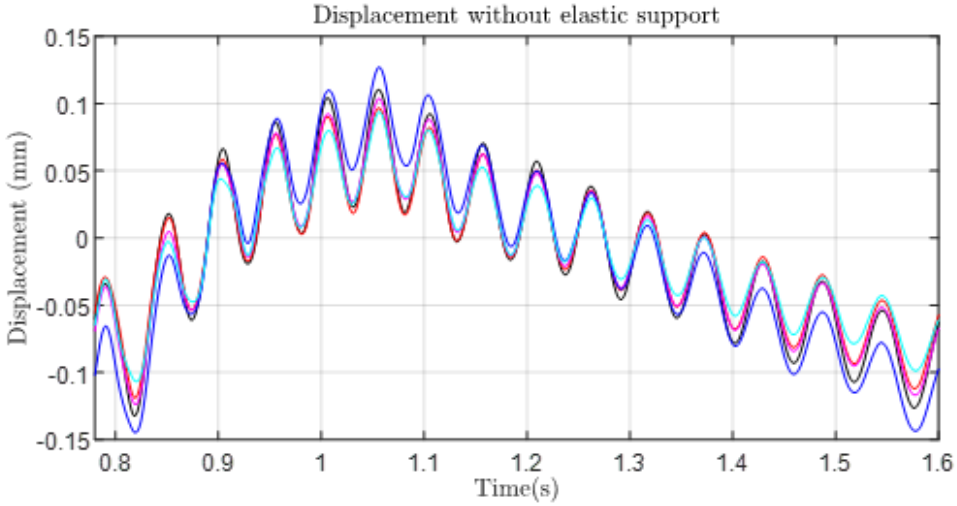

Figure 4.18: *Displacement of specific nodes of the carotid model without elastic support*

-8 9 -10 -1 -12

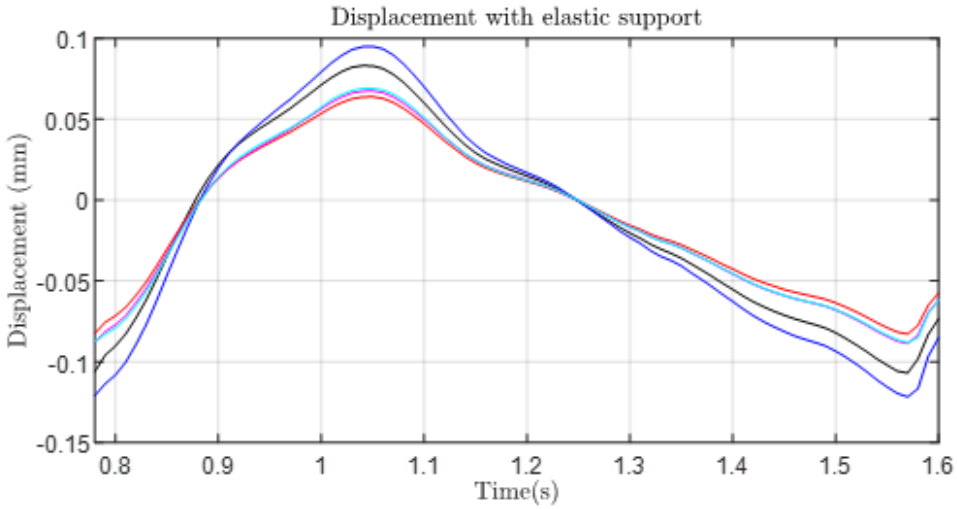

Figure 4.19: *Displacement of specific nodes of the carotid model with elastic support*

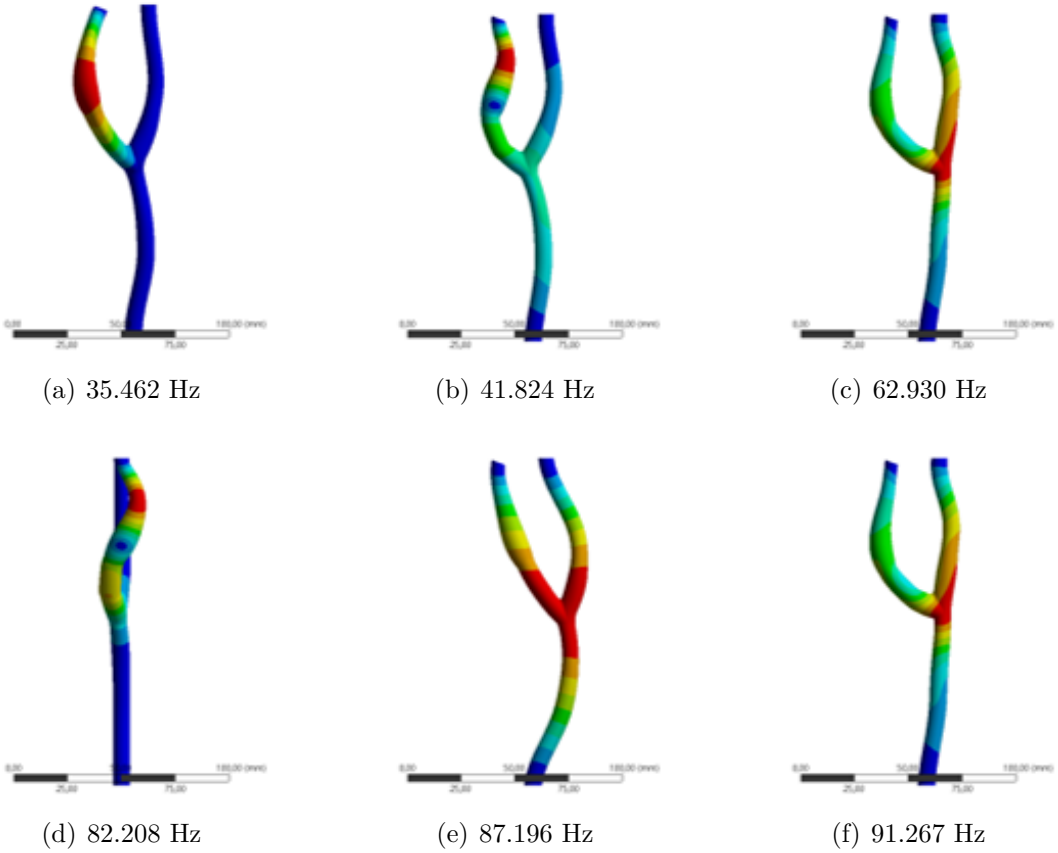

(a) 35.462 Hz (b) 41.824 Hz (c) 62.930 Hz

(d) 82.208 Hz (e) 87.196 Hz (f) 91.267 Hz

Figure 4.20: *Diseased artery mode shapes (Configuration 3 with elastic support)*

evaluating the modal response for the real artery. In fact, the length of the arterial branches, which was reduced compared to the simplified geometrical model, leaded to higher modal frequencies ranging from 100 to 400 Hz for the 30 first modes, compared to the 30-200 Hz frequency range for the previous configurations.

These results highlight the need for identifying and modelling realistic boundary conditions when simulating the transient vibrational response of the artery.

In the previous sections, the transient deformation (vibrations) of the artery wall (Figure 4.12) has been shown to be affected by the presence of the plaque. Moreover, the frequency content of the signal is affected by the material properties of the plaque (Figure 4.14). The plaque induces certainly different effect:

i) a localized mass on the artery wall;

ii) a localized modification of the artery stiffness;

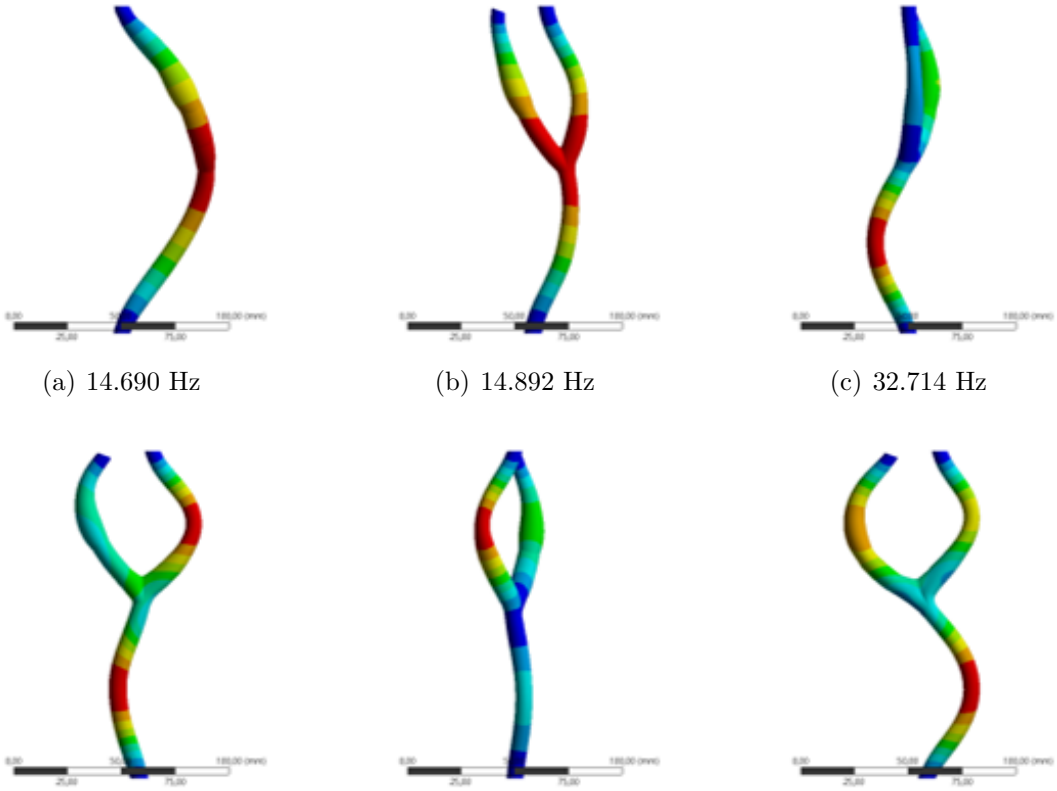

(a) 14.690 Hz (b) 14.892 Hz (c) 32.714 Hz

(d) 36.444 Hz (e) 37.549 Hz (f) 44.126 Hz

Figure 4.21: *Diseased artery mode shapes (Configuration 3 without elastic support)*

iii) localized modification of the artery geometry, leading to local perturbations in the blood flows.

The idea here is to evaluate the role of the plaque in modifying the structural response of the artery, analyzing the difference between the vibrational modes of the artery structure in the case of healthy and diseased arteries, considering different material properties for the plaque itself. In fact, the presence of distinguishable mode shapes and frequencies for the case with plaque might allow for a direct diagnosis of atherosclerosis.

Then, to investigate further the structural response of the simplified model, a modal analysis of the pre-stressed simplified structure in systolic and diastolic peaks was conducted. The table 4.2 below is a summary of the configurations considered for the parametrical modal analysis.

As illustrated in Figure 4.22, for high frequencies, all configurations recover the same number of modes, with the modal frequencies that decrease or increase slightly as a function of the introduced local stiffness and mass in each considered modal shape. Nevertheless, the appearance of modes at low frequencies (30-80Hz), due to the concentrated mass introduced by the plaque, are an indication of the presence of the plaque. This confirms the previous assumption that specific vibrational frequencies could appear because of the added mass, i.e. an atherosclerosis plaque.

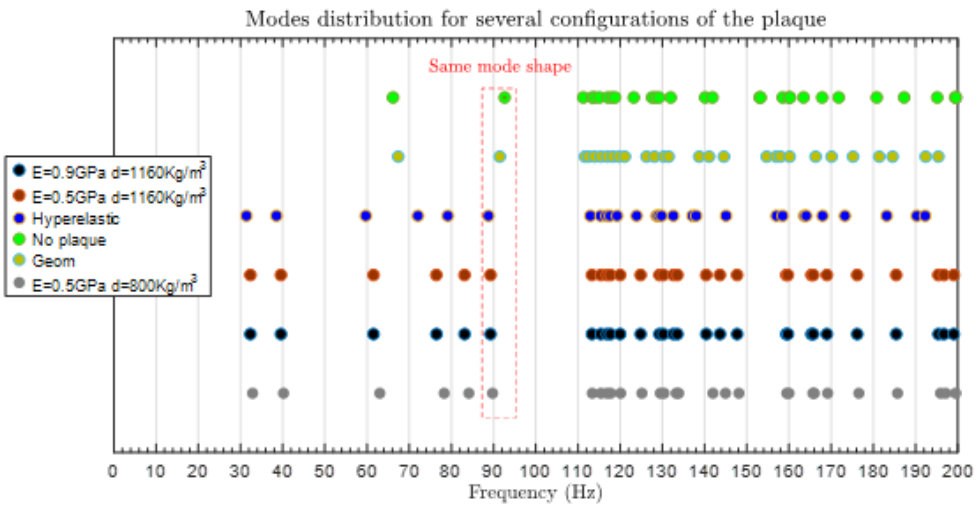

Figure 4.22: *Mode corresponding frequencies for several configurations of plaque*

Configuration	Description
1- No plaque	The simplified healthy model of the artery is utilized
2- Geom	Only the geometric effect is studied here. The structural geometry is obtained directly from the fluid geometry of the simplified diseased arterial geometric model by adding 1mm layer. Thus, no added mass of the plaque is present.
3- Hyperelastic	Diseased artery where the plaque is considered of the same material as the artery.
4- E = 0.9 GPa d = 1160 kg/m3	Diseased artery where plaque is considered elastic with a density of 1160kg/m3 and a Young modulus of 0.9 GPa.
5- E = 0.5 GPa d = 1160 kg/m3	The same as configuration 4 changing Young modulus 0.5 GPa
6- E = 0.5 GPa d = 800 kg/m3	Same as configuration changing the density of the plaque to 800 kg/m3.

Table 4.2: *Considered configurations for modal analysis*

Nevertheless, the applicability of this assumption needs to be validated through in-vivo measurements. The analysis of the displacement obtained using high resolution MRI can allow for the determination of vibration frequencies. Moreover, the CA being a peripheral artery, it could be conceivable to evaluate the displacement of the artery through high-resolution pulse palpation.

Even if the body movements as well as respiration affect the carotid deformations, these disturbances occur at low frequencies (c. 12-18 breaths per minute for adults), and it is possible to filter them from the potential measured signal of displacement.

The analysis of acoustic signals measured on patients could then contain the frequencies identified by a numerical model and characteristic of the plaque presence and its structural

properties.

4.4 Conclusions

The aim of this section was to investigate the arterial structure response to blood flow. The comparison between CFD and 2 ways FSI results showed that the CFD overestimates the WSS distribution along the arterial wall. The obtained values of WSS are closer to the imagery based ones, but still higher. The presence of in-plane velocity components suggests that it is important to consider them while imposing velocity BCs.

The time and frequency analysis of the transient deformation of the wall, during the pulse, showed interesting differences in the acoustic footprint of the artery with and without plaque, with the appearance of specific vibrational frequencies.

Concerning the structural response of the artery, the modal analysis showed the appearance of mode shapes at low frequencies correlated with the mass concentration due to plaque formation. Accounting for these preliminary results, the analysis of peripheral arterial motion might offer a new diagnosis tool for atherosclerosis at early stages.

Chapter 5

Summary and Reflections

Both CFD and FSI models for the CA has been presented in this project using simplified and patient specific geometries. Variation of the parameters for the hemodynamic simulations, i.e. rheological model and outlet boundary conditions, have been investigated to verify their accuracy.

The comparison between healthy and stenosed arteries showed a diversity of flow disruptions near the stenosis area leading to a higher shear stress in the plaque zone and lower shear stress in the after-plaque area. This result was observed both in the generic simplified geometry and in the patient specific geometry.

Along with all other involved factors, the plaque vulnerability depends on the local WSS and the local strength of the tissue. On one hand LWSS zones are areas of vivid proliferation of atherosclerosis plaques, on the other hand the HWSS can promote inflammations and cause plaque instability. A considerable difference between the FSI and CFD results has been obtained. The WSS is undeniably higher for the rigid wall simulation. The difference in the WSS results between FSI and CFD simulations actually support the choice of the coupled method. Moreover, the coupled approach gives access to the structural stress distribution and gradients in the artery wall, due to both fluid flow alteration and gradients in the structural properties.

The presence of the plaque also influences the behavior of the arterial tissue in terms of vibrational (acoustic) response. In fact, it is accompanied by a decrease in value of frequencies corresponding to each specific mode for all considered cases. Moreover, the appearance of localized modes, due to the localized increase of the mass due to the plaque and with characteristic frequencies, could allow for the detection of the plaque and its structural properties.

Although CFD is the most common method, the presented results showed that it tends to overestimate the WSS, especially in high shear rate regions. The FSI simulations, on the other hand, present a more realistic appreciation of the shear rate. The accuracy of those methods is still unknown and depend highly on the considered boundary conditions. With the promising advancement in MRI resolution and the decrease in scanning time, the potential of improving the boundary conditions and having a reliable validation method is increasing.

The possibility of using patient specific imagery data allowed for obtaining personalized details concerning the behavior of the vascular system, in order to categorize the patients. Nevertheless, the segmentation of the images is usually user-dependent and sometimes even time consuming due to the poor contrast with adjacent tissue. Besides, high quality images are necessary to obtain details about the wall thickness and, in the case of atherosclerosis, to identify clearly the composition of the plaque in terms of calcification, the size of the lipid core and the fibrous cap. This is necessary to study the plaque rupture. Here, the micro constituents of the plaque were not considered due to the unavailability of the specific data, in addition to the time consuming 3-D simulations for multiscale models. Thus, the problem of validation of imagery-based geometries persists. Further advances in the imagery techniques along with multiscale modeling might allow for better accuracy, improving computational based-results.

While comparing CFD and FSI results, rigid walls simulations are, without any doubt, more stable. Coupling the two domains using segregated methods is a great challenge. The convergence is not easy to achieve and the simulations are very expensive in computational

efforts. Nevertheless, they provide clarifications about the structural behavior and stress distribution. There is certainly a long way to achieve efficient and validated coupled methods, which can be utilized as a decision-making tool. However, FSI simulations can be employed to statistically categorize patients who share similar disease patterns.

Computational simulations are highly dependent on the external environment of the artery. Taking the existence of external tissue can stabilize the coupled simulations and damp the vibration of arteries. One other important consideration is the perivascular support. In fact, the boundary condition imposed on the structure have an impact on the wave propagation within the vessel and fixing the carotid ends might cause a reflection of the pressure wave which could affect the deformation of the artery.

There were several limitations in this study. Time consuming calculations reduces the possibility of running multiple patient specific simulations. Nevertheless, the aim of this work was to develop a numerical model accounting for patient specific data in order to investigate the effect of the plaque presence on both the blood flows and the acoustic response of the artery. The material properties considered for the plaque, corresponding to a purely elastic material, as well as the assumption of uniform wall thickness might influence the results.

Another main step will consist in a full acoustic analysis on a 2-way FSI simulation. While the analysis provided in this work, by a 1-way approach, gives main information of the structural contribution of the plaque in the acoustic signals from the artery, the same analysis by a 2-way model will allow to account for the acoustic contribution due to the modification of the blood flows.

The method proposed in this dissertation is aimed to provide useful information for the future assessments of the dynamic response of carotid artery when more patient specific data is available and in-vivo experimental investigations are carried out.

Bibliography

[1] Y. Robert Li. *Cardiovascular diseases: from molecular pharmacology to evidence-based therapeutics*. John Wiley & Sons, 2015, p. 512.

[2] V Kundel et al. "Measuring Carotid Plaque Inflammation in Moderate to Severe Sleep Apnea Using Hybrid Positron Emission Tomography/Magnetic Resonance Imaging (PET/MRI)". In: *Fundamentals In Sleep And Respiratory Neurobiology*. American Thoracic Society, 2019, A4462–A4462.

[3] Tomas Vaisar et al. "Common Pathways of Protease-Induced Plaque Rupture Identified by Parallel Analyses of Unstable Human Carotid Artery Plaques and Mouse Model of Plaque Rupture". In: *Arteriosclerosis, Thrombosis, and Vascular Biology* 39.Suppl_1 (2019), A736–A736.

[4] Lloyd E Chambless et al. "Risk factors for progression of common carotid atherosclerosis: the Atherosclerosis Risk in Communities Study, 1987–1998". In: *American journal of epidemiology* 155.1 (2002), pp. 38–47.

[5] Elizabeth Wilkins et al. "European cardiovascular disease statistics 2017". In: (2017).

[6] MO Pentikäinen et al. "Modified LDL–trigger of atherosclerosis and inflammation in the arterial intima". In: *Journal of internal medicine* 247.3 (2000), pp. 359–370.

[7] Gabriel A. Adelmann. *cardiology essentials in clinical practice*. Springer Science & Business Media, 2010.

[8] Moritz Wildgruber, Filip K Swirski, and Alma Zernecke. "Molecular imaging of inflammation in atherosclerosis". In: *Theranostics* 3.11 (2013), p. 865.

[9] Paul Butler, Adam WM Mitchell, and Harold Ellis. *Applied radiological anatomy*. Cambridge University Press, 1999.

[10] Amir Manbachi et al. "On the shape of the common carotid artery with implications for blood velocity profiles". In: *Physiological measurement* 32.12 (2011), p. 1885.

[11] *Carotid artery Disease*. `https://www.nhlbi.nih.gov/health-topics/carotid-artery-disease`. Accessed: 2019.

[12] Litao Ruan et al. "Correlates of common carotid artery lumen diameter in black and white younger adults: the Bogalusa Heart Study". In: *Stroke* 40.3 (2009), pp. 702–707.

[13] *Lam Vascular Associates*. `www.lamvascular.com`. Accessed: 2018.

[14] Stenting Trial. "Stenting versus Endarterectomy for Treatment of Carotid-Artery Stenosis". In: *50 Studies Every Surgeon Should Know* (2017), p. 37.

[15] Ivan P. Casserly et al. "Slow-flow phenomenon during carotid artery intervention with embolic protection devices: predictors and clinical outcome". In: *Journal of the American College of Cardiology* 46.8 (2005), pp. 1466–1472. ISSN: 0735-1097. DOI: `10.1016/j.jacc.2005.05.082`.

[16] Stefan Kiechl and Johann Willeit. "The natural course of atherosclerosis: part II: vascular remodeling". In: *Arteriosclerosis, thrombosis, and vascular biology* 19.6 (1999), pp. 1491–1498.

[17] Christopher K Zarins et al. "Carotid bifurcation atherosclerosis. Quantitative correlation of plaque localization with flow velocity profiles and wall shear stress." In: *Circulation research* 53.4 (1983), pp. 502–514.

[18] Toshiyasu Miura et al. "Plaque vulnerability in internal carotid arteries with positive remodeling". In: *Cerebrovascular diseases extra* 1.1 (2011), pp. 54–65.

[19] Frank JH Gijsen et al. "Strain distribution over plaques in human coronary arteries relates to shear stress". In: *American Journal of Physiology-Heart and Circulatory Physiology* 295.4 (2008), H1608–H1614.

[20] Zuzana Macek Jilkova et al. “CCM proteins control endothelial β1 integrin dependent response to shear stress”. In: *Biology open* 3.12 (2014), pp. 1228–1235.

[21] D. J. Patel, D. L. Fry, and J. S. Janicki. “The Elastic Symmetry of Arterial Segments in Dogs”. In: *Circulation Research* 24 (1969), pp. 1–8.

[22] R. H. Cox, A. Fronek, and L. H. Peterson. “Effects of carotid hypotension on aortic hemodynamics in the unanesthetized dog”. In: *American journal of Physiology* 229.5 (1975), pp. 1376–1380.

[23] C. Lally, A. J. Reid, and P. J. Prendergast. “Elastic Behavior of Porcine Coronary Artery Tissue Under Uniaxial and Equibiaxial Tension”. In: *Annals of Biomedical Engineering* 32.10 (2004), pp. 1355–1364.

[24] G. A. Holzapfel. “Structural and Numerical Models for the (Visco)elastic Response of Arterial Walls with Residual Stresses”. In: vol. 441. 2003, pp. 109–184. DOI: 10.1007/978-3-7091-2736-0_4.

[25] R. W. Ogden. “Nonlinear Elasticity, Anisotropy, Material Stability and Residual Stresses in Soft Tissue”. In: vol. 441. 2003, pp. 65–108.

[26] G. A. Holzapfel, T. C. Gasser, and R. W. Ogden. “A New Constitutive Framework for Arterial Wall Mechanics and a Comparative Study of Material Models”. In: *Journal of elasticity and the physical science of solids* 61.1-3 (2000), pp. 1–48.

[27] G. A. Holzapfel. “Collagen in Arterial Walls: Biomechanical Aspects”. In: *Collagen: Structure and Mechanics* 12 (2008), pp. 285–324. ISSN: 1742-5689. DOI: 10.1098/rsif.2015.0188.

[28] P. Kalita and R. Schaefer. “Mechanical Models of Artery Walls”. In: *Archives of Computational Methods in Engineering* 15.1 (2008), pp. 1–36.

[29] C. J. Chuong and Y. C. Fung. “Compressibility and constitutive equation of arterial wall in radial compression experiments.” In: *Journal of biomechanics* 17.1 (1984), pp. 35–40.

[30] Lambros S Athanasiou, Dimitrios I Fotiadis, and Lampros K Michalis. *Atherosclerotic Plaque Characterization Methods Based on Coronary Imaging*. Academic Press, 2017.

[31] Hector M Garcia-Garcia, Marco A Costa, and Patrick W Serruys. "Imaging of coronary atherosclerosis: intravascular ultrasound". In: *European heart journal* 31.20 (2010), pp. 2456–2469.

[32] AK Chin et al. "A physical measurement of the mechanisms of transluminal angioplasty." In: *Surgery* 95.2 (1984), pp. 196–201.

[33] Martin Kaltenbach et al. "Prolonged application of pressure in transluminal coronary angioplasty". In: *Catheterization and cardiovascular diagnosis* 10.3 (1984), pp. 213–219.

[34] Gustav VR Born and Peter D Richardson. "Mechanical properties of human atherosclerotic lesions". In: *Pathobiology of the human atherosclerotic plaque*. Springer, 1990, pp. 413–423.

[35] G. A. Holzapfel et al. "Computational approaches for analyzing the mechanics of atherosclerotic plaques: a review." In: *Journal of biomechanics* 47.4 (2014), pp. 859–869.

[36] Michael G Lawlor et al. "Experimental determination of circumferential properties of fresh carotid artery plaques". In: *Journal of biomechanics* 44.9 (2011), pp. 1709–1715.

[37] CL Lendon et al. "Testing of small connective tissue specimens for the determination of the mechanical behaviour of atherosclerotic plaques". In: *Journal of biomedical engineering* 15.1 (1993), pp. 27–33.

[38] Howard M Loree et al. "Static circumferential tangential modulus of human atherosclerotic tissue". In: *Journal of biomechanics* 27.2 (1994), pp. 195–204.

[39] Eoghan Maher et al. "Tensile and compressive properties of fresh human carotid atherosclerotic plaques". In: *Journal of biomechanics* 42.16 (2009), pp. 2760–2767.

[40] JJ Mulvihill et al. “Mechanical, biological and structural characterization of in vitro ruptured human carotid plaque tissue”. In: *Acta biomaterialia* 9.11 (2013), pp. 9027–9035.

[41] SRH Barrett et al. “Experimental measurement of the mechanical properties of carotid atherothrombotic plaque fibrous cap”. In: *Journal of biomechanics* 42.11 (2009), pp. 1650–1655.

[42] Chen-Ket Chai et al. “Local axial compressive mechanical properties of human carotid atherosclerotic plaques—characterisation by indentation test and inverse finite element analysis”. In: *Journal of biomechanics* 46.10 (2013), pp. 1759–1766.

[43] Richard T Lee et al. “Structure-dependent dynamic mechanical behavior of fibrous caps from human atherosclerotic plaques.” In: *Circulation* 83.5 (1991), pp. 1764–1770.

[44] Richard T Lee et al. “Prediction of mechanical properties of human atherosclerotic tissue by high-frequency intravascular ultrasound imaging. An in vitro study.” In: *Arteriosclerosis and thrombosis: a journal of vascular biology* 12.1 (1992), pp. 1–5.

[45] Eoghan Maher et al. “Inelasticity of human carotid atherosclerotic plaque”. In: *Annals of biomedical engineering* 39.9 (2011), pp. 2445–2455.

[46] NV Salunke et al. “Compressive stress-relaxation of human atherosclerotic plaque”. In: *Journal of Biomedical Materials Research: An Official Journal of The Society for Biomaterials, The Japanese Society for Biomaterials, and The Australian Society for Biomaterials and the Korean Society for Biomaterials* 55.2 (2001), pp. 236–241.

[47] LDT Topoleski et al. “Composition-and history-dependent radial compressive behavior of human atherosclerotic plaque”. In: *Journal of Biomedical Materials Research: An Official Journal of The Society for Biomaterials and The Japanese Society for Biomaterials* 35.1 (1997), pp. 117–127.

[48] Ali C Akyildiz, Lambert Speelman, and Frank JH Gijsen. "Mechanical properties of human atherosclerotic intima tissue". In: *Journal of biomechanics* 47.4 (2014), pp. 773–783.

[49] Jiyuan Tu, Kiao Inthavong, and Kelvin Kian Loong Wong. *Computational Hemodynamics–Theory, Modelling and Applications*. Springer, 2015.

[50] Pijush K. Kundu, Ira M. Cohen, and David R. Dowling. *Fluid Mechanics*. 2011, p. 920. ISBN: 9780123821003. DOI: 10.1016/b978-0-12-405935-1.00013-7.

[51] Michel-Yves Jaffrin and Francis Goubel. *Biomécanique des fluides et des tissus*. Masson, 1998.

[52] Anne Amblard et al. "Analysis of type I endoleaks in a stented abdominal aortic aneurysm". In: *Medical Engineering & Physics* 31.1 (2009), pp. 27–33. ISSN: 1350-4533. DOI: 10.1016/j.medengphy.2008.03.005.

[53] P. R. S. Vijayaratnam et al. "The Impact of Blood Rheology on Drug Transport in Stented Arteries: Steady Simulations". In: *PLoS One* 10.6 (2015), e0128178.

[54] M. Menut et al. "Comparison between a generalized Newtonian model and a network-type multiscale model for hemodynamic behavior in the aortic arch: Validation with 4D MRI data for a case study". In: *Journal of Biomechanics* 73 (2018), pp. 119–126.

[55] MlNEO Motomiya and Takeshi Karino. "Flow patterns in the human carotid artery bifurcation." In: *Stroke* 15.1 (1984), pp. 50–56.

[56] Charles R White and John A Frangos. "The shear stress of it all: the cell membrane and mechanochemical transduction". In: *Philosophical Transactions of the Royal Society of London B: Biological Sciences* 362.1484 (2007), pp. 1459–1467.

[57] N. Resnick et al. "Platelet-derived growth factor B chain promoter contains a cis-acting fluid shear-stress-responsive element". In: *Proceedings of the National Academy of Sciences of the United States of America* 90.10 (1993), pp. 4591–4595.

[58] O. Traub and B. C. Berk. “Laminar shear stress: mechanisms by which endothelial cells transduce an atheroprotective force.” In: *Arteriosclerosis, Thrombosis, and Vascular Biology* 18.5 (1998), pp. 677–685.

[59] David N Ku et al. “Pulsatile flow and atherosclerosis in the human carotid bifurcation. Positive correlation between plaque location and low oscillating shear stress.” In: *Arteriosclerosis: An Official Journal of the American Heart Association, Inc.* 5.3 (1985), pp. 293–302.

[60] Andrew R Williams et al. “Local hemodynamic changes caused by main branch stent implantation and subsequent virtual side branch balloon angioplasty in a representative coronary bifurcation”. In: *Journal of applied physiology* 109.2 (2010), pp. 532–540.

[61] C.K. Zarins et al. “Carotid bifurcation atherosclerosis. Quantitative correlation of plaque localization with flow velocity profiles and wall shear stress.” In: *Circulation Research* 53.4 (1983), pp. 502–514.

[62] Ilko L Maier et al. “Carotid artery flow as determined by real-time phase-contrast flow MRI and neurovascular ultrasound: A comparative study of healthy subjects”. In: *European journal of radiology* 106 (2018), pp. 38–45.

[63] Andreas Hjelm Brandt et al. “A comparison study of vector velocity, spectral doppler and magnetic resonance of blood flow in the common carotid artery”. In: *Ultrasound in medicine & biology* 44.8 (2018), pp. 1751–1761.

[64] Wouter V Potters et al. “Volumetric arterial wall shear stress calculation based on cine phase contrast MRI”. In: *Journal of Magnetic Resonance Imaging* 41.2 (2015), pp. 505–516.

[65] E Doutel et al. “Experimental and numerical methodology to analyze flows in a coronary bifurcation”. In: *European Journal of Mechanics-B/Fluids* 67 (2018), pp. 341–356.

[66] Valérie Deplano, Carine Guivier-Curien, and Eric Bertrand. "3D analysis of vortical structures in an abdominal aortic aneurysm by stereoscopic PIV". In: *Experiments in Fluids* 57.11 (2016), p. 167.

[67] Merih Cibis et al. "Wall shear stress calculations based on 3D cine phase contrast MRI and computational fluid dynamics: a comparison study in healthy carotid arteries". In: *NMR in Biomedicine* 27.7 (2014), pp. 826–834.

[68] Merih Cibis et al. "Relation between wall shear stress and carotid artery wall thickening MRI versus CFD". In: *Journal of biomechanics* 49.5 (2016), pp. 735–741.

[69] Abdul SM Khader et al. "Effect of increased severity in patient specific stenosis of common carotid artery using CFD—a case study". In: *World Journal of Modelling and Simulation* 7.2 (2011), pp. 113–122.

[70] A. Campbell et al. "Retrospective analysis of outcomes after IVF using an aneuploidy risk model derived from time-lapse imaging without PGS". In: *Reproductive BioMedicine Online* 27.2 (2013), pp. 140–146.

[71] C. M. Schirmer and A. M. Malek. "Computational fluid dynamic characterization of carotid bifurcation stenosis in patient-based geometries". In: *Brain and behavior* 2.1 (2012), pp. 42–52.

[72] Michele Conti et al. "Carotid artery hemodynamics before and after stenting: A patient specific CFD study". In: *Computers & Fluids* 141 (2016), pp. 62–74.

[73] Yuri Bazilevs, Kenji Takizawa, and Tayfun E Tezduyar. "Challenges and directions in computational fluid–structure interaction". In: *Mathematical Models and Methods in Applied Sciences* 23.02 (2013), pp. 215–221.

[74] D. Tang et al. "3D MRI-Based Multicomponent FSI Models for Atherosclerotic Plaques". In: *Annals of Biomedical Engineering* 32.7 (2004), pp. 947–960.

[75] Z. Y. Li et al. "How Critical Is Fibrous Cap Thickness to Carotid Plaque Stability? A Flow–Plaque Interaction Model". In: *Stroke* 37 (2006), pp. 1195–1199.

[76] I. E. Vignon-Clementel et al. “Outflow boundary conditions for 3D simulations of non-periodic blood flow and pressure fields in deformable arteries”. In: *Computer Methods in Biomechanics and Biomedical Engineering* 13.5 (2010), pp. 625–640.

[77] S. Avril. “Hyperelasticity of Soft Tissues and Related Inverse Problems”. In: vol. 34. 2017, p. 36 66. DOI: 10.1002/cnm.2901.

[78] Z. Teng et al. “3D Critical Plaque Wall Stress Is a Better Predictor of Carotid Plaque Rupture Sites Than Flow Shear Stress: An In Vivo MRI-Based 3D FSI Study”. In: *Journal of Biomechanical Engineering* 132.3 (2010).

[79] Peter D Richardson, MJ Davies, and GVR Born. “Influence of plaque configuration and stress distribution on fissuring of coronary atherosclerotic plaques”. In: *The Lancet* 334.8669 (1989), pp. 941–944.

[80] George C Cheng et al. “Distribution of circumferential stress in ruptured and stable atherosclerotic lesions. A structural analysis with histopathological correlation.” In: *Circulation* 87.4 (1993), pp. 1179–1187.

[81] H. Gao and Q. Long. “Effects of varied lipid core volume and fibrous cap thickness on stress distribution in carotid arterial plaques”. In: *Journal of Biomechanics* 41.14 (2008), pp. 3053–3059.

[82] H. Gao et al. “Carotid arterial plaque stress analysis using fluid–structure interactive simulation based on in-vivo magnetic resonance images of four patients”. In: *Journal of biomechanics* 42.10 (2009), pp. 1416–1423.

[83] D. Tang et al. “A negative correlation between human carotid atherosclerotic plaque progression and plaque wall stress: In vivo MRI-based 2D/3D FSI models”. In: *Journal of biomechanics* 41.4 (2008), pp. 727–736.

[84] Sang-Wook Lee et al. “Geometry of the carotid bifurcation predicts its exposure to disturbed flow”. In: *Stroke* 39.8 (2008), pp. 2341–2347.

[85] S. M. Abdul Khader et al. “Haemodynamic study of Flow in concentric and eccentric stenosed carotid Artery”. In: *MATEC Web of Conferences* 144.3 (2018).

[86] M. Cilla et al. “A parametric model for analysing atherosclerotic arteries: On the FSI coupling”. In: *International Communications in Heat and Mass Transfer* 67 (2015), pp. 29–38.

[87] Sang Hyuk Lee et al. “A fluid-structure interaction analysis on hemodynamics in carotid artery based on patient-specific clinical data”. In: *Journal of Mechanical Science and Technology* 26.12 (2012), pp. 3821–3831.

[88] D Lopes et al. “Influence of arterial mechanical properties on carotid blood flow: comparison of CFD and FSI studies”. In: *International Journal of Mechanical Sciences* (2019).

[89] A Abbas Nejad et al. “Pulsatile flow of non-Newtonian blood fluid inside stenosed arteries: Investigating the effects of viscoelastic and elastic walls, arteriosclerosis, and polycythemia diseases”. In: *Computer methods and programs in biomedicine* 154 (2018), pp. 109–122.

[90] Frank JH Gijsen, Frans N van de Vosse, and JD Janssen. “The influence of the non-Newtonian properties of blood on the flow in large arteries: steady flow in a carotid bifurcation model”. In: *Journal of biomechanics* 32.6 (1999), pp. 601–608.

[91] Ian Marshall et al. “MRI and CFD studies of pulsatile flow in healthy and stenosed carotid bifurcation models”. In: *Journal of biomechanics* 37.5 (2004), pp. 679–687.

[92] Young I Cho and Kenneth R Kensey. “Effects of the non-Newtonian viscosity of blood on flows in a diseased arterial vessel. Part 1: Steady flows”. In: *Biorheology* 28.3-4 (1991), pp. 241–262.

[93] N Casson. “A flow equation for pigment-oil suspensions of the printing ink type”. In: *Rheology of disperse systems* (1959).

[94] Z. Stankovic et al. “4D flow imaging with MRI”. In: *Cardiovascular diagnosis and therapy* 4.2 (2014), pp. 173–192.

[95] JR Womersley. “Oscillatory flow in arteries: the constrained elastic tube as a model of arterial flow and pulse transmission”. In: *Physics in Medicine & Biology* 2.2 (1957), p. 178.

[96] John R Womersley. “Method for the calculation of velocity, rate of flow and viscous drag in arteries when the pressure gradient is known”. In: *The Journal of physiology* 127.3 (1955), pp. 553–563.

[97] O. San and A. E. Staples. “An improved model for reduced-order physiological fluid flows”. In: *Journal of Mechanics in Medicine and Biology* 12 (2012).

[98] I. C. Campbell et al. “Effect of Inlet Velocity Profiles on Patient-Specific Computational Fluid Dynamics Simulations of the Carotid Bifurcation”. In: *Journal of Biomechanical Engineering* 134.5 (2012).

[99] C. Wang, X. Guo, and G. S. Kassab. “A New Observation on the Stress Distribution in the Coronary Artery Wall”. In: *Journal of Biomechanical Engineering* 131.11 (2009).

[100] G. Mouktadiri, B. Bou-Saïd, and H. W. Berre. “Aortic endovascular repair modeling using the finite element method”. In: *Journal of Biomedical Science and Engineering* 6 (2013), pp. 917–927.

[101] MA Marcos Gómez et al. “The increase in the speed of the pulse wave is not associated with elevated central blood pressure in hypertensive patients with kidney disease”. In: *Nefrologia: publicacion oficial de la Sociedad Espanola Nefrologia* 30.5 (2010), pp. 578–583.

[102] A. Karimi et al. “Study of plaque vulnerability in coronary artery using Mooney-Rivlin model: A combination of finite element and experimental method”. In: *Biomedical Engineering Applications Basis and Communications* 26.01 (2014).

[103] C. A. Taylor, T. J. R. Hughes, and C.K. Zarins. “Finite element modeling of blood flow in arteries”. In: *Computer Methods in Applied Mechanics and Engineering* 158.1-2 (1998), pp. 155–196.

[104] M. Oshima et al. “Finite element simulation of blood flow in the cerebral artery”. In: *Computer Methods in Applied Mechanics and Engineering* 191.6-7 (2001), pp. 661–671.

[105] K. Perktold and G. Rappitsch. “Computer simulation of local blood flow and vessel mechanics in a compliant carotid artery bifurcation model”. In: *Journal of Biomechanical Engineering* 28.7 (1995), pp. 845–856.

[106] U. Langer and H. Yang. “Numerical simulation of fluid–structure interaction problems with hyperelastic models: A monolithic approach”. In: *Mathematics and Computers in Simulation* 145 (2018), pp. 186–208.

[107] U. Langer and H. Yang. “Partitioned solution algorithms for fluid–structure interaction problems with hyperelastic models”. In: *Journal of Computational and Applied Mathematics* 276 (2015), pp. 47–61.

[108] Yiemeng Hoi et al. “Effect of common carotid artery inlet length on normal carotid bifurcation hemodynamics”. In: *Journal of biomechanical engineering* 132.12 (2010), p. 121008.

[109] M. F. O’Rourke and W. W. Nichols. “Aortic diameter, aortic stiffness, and wave reflection increase with age and isolated systolic hypertension”. In: *Hypertension* 45.4 (2005), pp. 652–658.

[110] K. Sato et al. “The distribution of blood flow in the carotid and vertebral arteries during dynamic exercise in humans”. In: *The Journal of physiology* 589 (2011), pp. 2847–2856.

[111] Loic Boussel et al. “Phase-contrast magnetic resonance imaging measurements in intracranial aneurysms in vivo of flow patterns, velocity fields, and wall shear stress: comparison with computational fluid dynamics”. In: *Magnetic Resonance in Medicine: An Official Journal of the International Society for Magnetic Resonance in Medicine* 61.2 (2009), pp. 409–417.

[112] Panorea Papathanasopoulou et al. “MRI measurement of time-resolved wall shear stress vectors in a carotid bifurcation model, and comparison with CFD predictions”. In: *Journal of Magnetic Resonance Imaging* 17.2 (2003), pp. 153–162.

[113] Uwe Köhler et al. "MRI measurement of wall shear stress vectors in bifurcation models and comparison with CFD predictions". In: *Journal of Magnetic Resonance Imaging: An Official Journal of the International Society for Magnetic Resonance in Medicine* 14.5 (2001), pp. 563–573.

[114] Merih Cibis et al. "Wall shear stress calculations based on 3D cine phase contrast MRI and computational fluid dynamics: a comparison study in healthy carotid arteries". In: *NMR in Biomedicine* 27.7 (2014), pp. 826–834.

[115] Heinrich Blasius. *Grenzschichten in Flüssigkeiten mit kleiner Reibung*. Druck von BG Teubner, 1907.

Appendix A

Solver characteristics

Pressure-based segregated algorithm

The pressure-based solver uses a projection method where the velocity field is obtained by solving the equation for the pressure. On the other hand, the pressure equation is obtained from the velocity field in order to satisfy the continuity. The segregated algorithm solves sequentially the Navier-Stokes equations through multiple iterations, where the pressure is corrected at the end of each iteration till the solutions for momentum and continuity equations converge. To this end, each governing equation is decoupled from others. Although this algorithm converges at a slower rate, as compared to coupled algorithm, this way of solving problems is memory efficient. For a laminar incompressible flow, which is the case in this study, the steps of the pressure-based segregated algorithm are shown in the Figure A.1.

Spatial discretization

ANSYS Fluent stores the values of variables at the cell centers. However, the values on the faces are necessary for calculating the convection terms. The used second-order Upwind scheme evaluates the face quantities Φ_f from the adjacent upstream cell center quantities, using a multidimensional linear reconstruction approach. This is computed using a Taylor series expansion of the cell centered solution (eq. A.1).

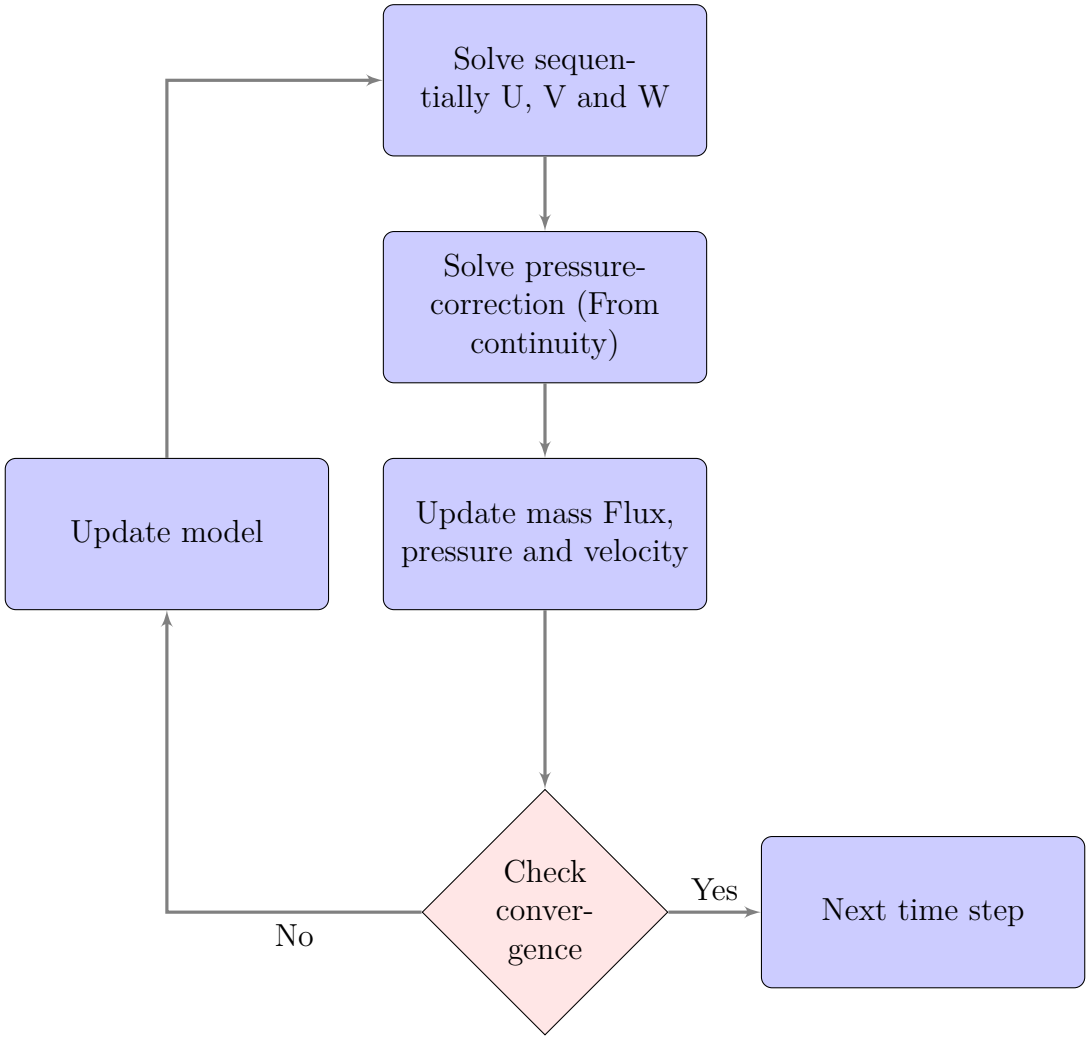

Figure A.1: *Steps of pressure based segregated algorithm in the case of laminar incompressible flow*

$$\Phi_f = \Phi_c + \bigtriangledown\Phi_c.\vec{r} \tag{A.1}$$

The momentum equation is discretized as following (eq. A.2)

$$a_k u_k = \sum_{nb} a_{nb} u_{nb} + \sum p_f A.\hat{k} + S \tag{A.2}$$

Shear stress calculations

In the case of laminar flow, the wall shear stress (WSS)in the case of Newtonian fluid is defined by the normal velocity gradient at the wall (eq. 3), where μ is the dynamic viscosity, ν the velocity along the boundary and n the height above the boundary:

$$\tau = \mu \frac{\partial \nu}{\partial n} \tag{A.3}$$

To obtain accurate values of the WSS, the boundary layers must be solved correctly. For that, the adjacent grid should meet the condition (eq. 4), based on Blasius solution for a laminar flow over a flat plate [115]:

$$y_p = \sqrt{\frac{u_\infty}{\gamma.x}} \tag{A.4}$$

where:

- y_p : Distance from the wall
- u_∞ : Free stream velocity
- γ : Kinematic viscosity
- x : Distance along the wall

FOLIO ADMINISTRATIF

THESE DE L'UNIVERSITE DE LYON OPEREE AU SEIN DE L'INSA LYON

NOM : ZOUGGARI **DATE de SOUTENANCE** : 06/12/2019

Prénoms : Lina

Titre : BIOMECHANICAL BEHAVIOR OF CAROTID ATHEROSCLEROSIS: A NUMERICAL APPROACH

NATURE : Doctorat Numéro d'ordre : 2019LYSEI116

Ecole doctorale : Mécanique, Energétique, Génie Civil et acoustique (MEGA)

Spécialité : Biomécanique

Résumé : L'athérosclérose est une maladie qui atteint le système vasculaire. Elle se manifeste par la formation d'une plaque d'athérome au niveau de la couche intima de tissu artérielle causant la rigidification et la paroi. La majorité des décès cardiovasculaire en Europe sont une conséquence de cette pathologie. En effet, une plaque d'athérome non stable, qu'on appelle aussi vulnérable, peut évoluer vers un stade avancé appelé sténose ou la lumière artérielle est réduite à un tel niveau que le sang ne peut plus irriguer les organes en aval. Dans le cas où la formation de la plaque a lieu au niveau des artères coronaires, il s'agit d'un risque d'arrêt cardiaque. Une autre conséquence de la présence d'une plaque dans le système vasculaire est sa possibilité de rupture et donc le relâchement de débris qui, transporté par le flux sanguin, sont capables d'obstruer les plus petits vaisseaux au niveau du cerveau causant des accidents cérébraux et par conséquent paralysie ou mort cérébrale.
Le processus de formation de la plaque est très long et renforcé par la présence de substances telles que la nicotine ou Cholestérol LDL dans le sang. Quand ces substances s'introduisent dans le tissu artériel, elles peuvent causer une réaction inflammatoire en chaine provoquant la génération et l'évolution de l'athérome. En général, l'athérosclérose est une maladie asymptomatique, ceci rend son diagnostic difficile au premiers stades. En effet, le diagnostic s'effectue suite à un malaise ou urgence médicale à l'aide d'outils d'imagerie médicale tels que IRM ou Echo-doppler.
Pour toutes les raisons invoquées précédemment, cette pathologie ne cesse de susciter la curiosité de la communauté scientifique dans le but de la comprendre tout d'abord les phénomènes qui conduisent à l'occurrence et au développement de cette maladie ainsi que d'améliorer le diagnostic et le traitement.
Dans ce sens, notre projet consiste à étudier les phénomènes mécaniques qui accompagnent la présence de la plaque au niveau de la bifurcation carotidienne, un site fréquent de formation d'athéromes. Afin d'effectuer cela, nous évaluons le comportement du fluide et de la structure artérielle par les méthodes volumes finis et éléments finis. Dans un premier temps, nous étudions la dynamique du sang pour des modèles simplifiés et réels avec et sans plaque. Ensuite, nous nous intéressons à l'effet de la déformation de la paroi sur l'hémodynamique. Finalement, nous étudions la réponse vibratoire de la structure artérielle afin de vérifier l'effet la présence de la plaque sur la déformation de la carotide.

MOTS-CLÉS : Carotide, Athérosclérose, FSI, CFD

Laboratoire (s) de recherche : Laboratoire de Mécanique des Contacts et des Structures (LaMCoS)

Directeur de thèse : Benyebka BOU-SAID, Antonio CULLA

Président de jury :

Composition du jury : Valérie DEPLANO, John TICHY, Patrick LERMUSIAUX, Francesco MASSI